

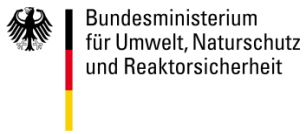
ProBIRD report

Weather-dependence of nocturnal bird migration and cumulative collision risk at offshore wind farms in the German North and Baltic Seas

Jorg Welcker, Raúl Vilela



Funded by



Bundesministerium für Umwelt, Naturschutz und nukleare Sicherheit (BMU)
Stresemannstraße 128-130
10117 Berlin, Germany

Coordinated and supported by



Bundesamt für Seeschifffahrt und Hydrographie (BSH)
Federal Maritime and Hydrographic Agency
Bernhard-Nocht-Straße 78
20359 Hamburg, Germany

The research project “ProBIRD” (FKZ UM15 86 2000) is funded by BMU (Ressortforschungsplan 2015).

Responsibility for the content of this report lies entirely with the authors.

Authors



Dr. Jorg Welcker and Dr. Raúl Vilela
BioConsult SH GmbH & Co. KG
Schobüller Str. 36
25813 Husum, Germany

Citation

Welcker, J. & Vilela, R. 2019. Weather-dependence of nocturnal bird migration and cumulative collision risk at offshore wind farms in the German North and Baltic Seas. Technical report. Bio-Consult SH, Husum. 70 pp.

© Bundesamt für Seeschifffahrt und Hydrographie

Image (Title): Kai Gauger

Contents

1	SUMMARY.....	1
2	INTRODUCTION.....	3
3	MATERIALS & METHODS	5
3.1	Data collection	5
3.2	Data analysis	6
3.2.1	Radar data.....	6
3.2.2	Weather data and models	6
3.2.3	Coincidence of high migration intensities and unfavorable weather	8
3.2.4	Collision risk models (CRM)	9
4	RESULTS	12
4.1	Weather models	12
4.2	Prediction of migration intensities	31
4.3	Coincidence of high migration intensities and unfavorable weather	35
4.4	Collision risk models	36
5	DISCUSSION	41
5.1	Weather models	41
5.2	Prediction of migrating intensities	45
5.3	Collision risk.....	46
6	LITERATURE.....	49
A	APPENDIX.....	54
A.1	Weather models	54
A.2	Coincidence of high migration intensities and unfavorable weather	66
A.3	Collision risk models	67

List of figures

Figure 3-1 Location of the study sites in the EEZ of the German North and Baltic Sea.....6

Figure 3-2 Monthly flight height distribution based on radar data from all available sites in the German EEZ. Lines represent cubic smoothing splines fitted to the raw data. 10

Figure 4-1 Standardized Error Variable Importance of Random Forest models on migration intensities (up to 1,000 m altitude, upper panels) and flight height (lower panels). Results for spring and fall migration are shown in left and right panels, respectively. 13

Figure 4-2 Partial dependence plots of TWC for RF models on migration intensities (MTR up to 1,000 m, upper panels) and flight height (lower panels). Results for spring and fall migration are shown in left and right panels, respectively. 14

Figure 4-3 Partial dependence plots of CWC for RF models on migration intensities (MTR up to 1,000 m, upper panels) and flight height (lower panels). Results for spring and fall migration are shown in left and right panels, respectively. 15

Figure 4-4 Partial dependence plots of barometric pressure for RF models on migration intensities (MTR up to 1,000 m, upper panels) and flight height (lower panels). Results for spring and fall migration are shown in left and right panels, respectively..... 16

Figure 4-5 Partial dependence plots of relative humidity for RF models on migration intensities (MTR up to 1,000 m, upper panels) and flight height (lower panels). Results for spring and fall migration are shown in left and right panels, respectively..... 17

Figure 4-6 Partial dependence plots of ambient temperature for RF models on migration intensities (MTR up to 1,000 m, upper panels) and flight height (lower panels). Results for spring and fall migration are shown in left and right panels, respectively..... 18

Figure 4-7 Partial dependence plots of the variable “accumulation unfavorable wind” for RF models on migration intensities (MTR up to 1,000 m, upper panels) and flight height (lower panels). Results for spring and fall migration are shown in left and right panels, respectively..... 19

Figure 4-8 Partial dependence plots of the 24h-change variables δ TWC, δ relative humidity and δ ambient temperature for RF models on migration intensities (MTR up to 1,000 m). Results for spring and fall migration are shown in left and right panels, respectively. 20

Figure 4-9 Partial dependence plots of 24h-change in barometric pressure for RF models on migration intensities (MTR up to 1,000 m). Results for spring and fall migration are shown in left and right panels, respectively. 21

Figure 4-10 Partial dependence plots of the 24h-change variables δ TWC, δ relative humidity and δ ambient temperature for RF models on flight height. Results for spring and fall migration are shown in left and right panels, respectively..... 22

Figure 4-11 Partial dependence plots of 24h-change in barometric pressure for RF models on flight height. Results for spring and fall migration are shown in left and right panels, respectively. 23

Figure 4-12 Partial dependence plots migration intensity for RF models on flight height. Results for spring and fall migration are shown in left and right panels, respectively. 23

Figure 4-13 Partial dependence plots of Julian day for RF models on migration intensities (MTR up to 1,000 m, upper panels) and flight height (lower panels). Results for spring and fall migration are shown in left and right panels, respectively.....	24
Figure 4-14 Partial dependence plots of the proportion of night for RF models on migration intensities (MTR up to 1,000 m, upper panels) and flight height (lower panels). Results for spring and fall migration are shown in left and right panels, respectively.	25
Figure 4-15 Interaction plots of TWC with Julian day for RF models on migration intensities (MTR up to 1,000 m, upper panels) and flight height (lower panels). Results for spring and fall migration are shown in left and right panels, respectively.	26
Figure 4-16 Interaction plots of TWC with CWC for RF models on migration intensities (MTR up to 1,000 m, upper panels) and flight height (lower panels). Results for spring and fall migration are shown in left and right panels, respectively.....	27
Figure 4-17 Interaction plots of ambient temperature with Julian day for RF models on migration intensities (MTR up to 1,000 m, upper panels) and flight height (lower panels). Results for spring and fall migration are shown in left and right panels, respectively.	28
Figure 4-18 Partial dependence plots of the factor “year” for RF models on migration intensities (MTR up to 1,000 m, upper panels) and flight height (lower panels). Results for spring and fall migration are shown in left and right panels, respectively.	29
Figure 4-19 Partial dependence plots of the factor “project” for RF models on migration intensities (MTR up to 1,000 m, upper panels) and flight height (lower panels). Results for spring and fall migration are shown in left and right panels, respectively.	29
Figure 4-20 Partial dependence plots of the factor “phase” for RF models on migration intensities (MTR up to 1,000 m, upper panels) and flight height (lower panels). Results for spring and fall migration are shown in left and right panels, respectively.	30
Figure 4-21 Partial dependence plots of the factor “lab” for RF models on migration intensities (MTR up to 1,000 m, upper panels) and flight height (lower panels). Results for spring and fall migration are shown in left and right panels, respectively.	30
Figure 4-22 Observed and predicted migration intensities (MTR) for spring, fall and both seasons combined. Data from all study years are included.	31
Figure 4-23 Scatterplots of observed and predicted migration intensities (MTR) in spring for all study years separately.	32
Figure 4-24 Scatterplots of observed and predicted migration intensities (MTR) in fall for all study years separately.	32
Figure 4-25 Observed and predicted migration intensities (MTR) in spring (upper panels) and fall (lower panels) for all study years with bars indicating the observed and open symbols the predicted values. In addition, the performance of the model in predicting nights with high migration intensities (>250 MTR) is indicated (FN = false negatives, FP = false positives, TN = true negatives, TP = true positives). The dashed blue line represents the threshold for observed values (250 MTR), the dashed red line is the optimized threshold for predicted values (157.7 MTR (spring) and 185.4 MTR (fall), see chap. 3.2.2).	33

Figure A 1 Standardized Error Variable Importance of Random Forest models on migration intensities up to 200 m altitude). Results for spring and fall migration are shown in left and right panels, respectively. 54

Figure A 2 Standardized Error Variable Importance of Random Forest models on migration intensities up to 1,000 m altitude (upper panels), up to 200 m (mid panels) and flight height (lower panels) including the explanatory variables “year”, “project”, “phase” and “lab”. Results for spring and fall migration are shown in left and right panels, respectively. 55

Figure A 3 Partial dependence plots of TWC for RF models on migration intensities (MTR up to 200 m). Results for spring and fall migration are shown in left and right panels, respectively. 56

Figure A 4 Partial dependence plots of CWC for RF models on migration intensities (MTR up to 200 m). Results for spring and fall migration are shown in left and right panels, respectively. 56

Figure A 5 Partial dependence plots of barometric pressure for RF models on migration intensities (MTR up to 200 m). Results for spring and fall migration are shown in left and right panels, respectively. 56

Figure A 6 Partial dependence plots of relative humidity for RF models on migration intensities (MTR up to 200 m). Results for spring and fall migration are shown in left and right panels, respectively. .. 57

Figure A 7 Partial dependence plots of ambient temperature for RF models on migration intensities (MTR up to 200 m). Results for spring and fall migration are shown in left and right panels, respectively. 57

Figure A 8 Partial dependence plots of variable “accumulation unfavorable wind” for RF models on migration intensities (MTR up to 200 m). Results for spring and fall migration are shown in left and right panels, respectively..... 58

Figure A 9 Partial dependence plots of δ TWC for RF models on migration intensities (MTR up to 200 m). Results for spring and fall migration are shown in left and right panels, respectively. 58

Figure A 10 Partial dependence plots of δ relative humidity for RF models on migration intensities (MTR up to 200 m). Results for spring and fall migration are shown in left and right panels, respectively. 59

Figure A 11 Partial dependence plots of δ ambient temperature for RF models on migration intensities (MTR up to 200 m). Results for spring and fall migration are shown in left and right panels, respectively. 59

Figure A 12 Partial dependence plots of δ barometric pressure for RF models on migration intensities (MTR up to 200 m). Results for spring and fall migration are shown in left and right panels, respectively. 60

Figure A 13 Partial dependence plots of Julian day for RF models on migration intensities (MTR up to 200 m). Results for spring and fall migration are shown in left and right panels, respectively. 60

Figure A 14 Partial dependence plots of the proportion of night for RF models on migration intensities (MTR up to 200 m). Results for spring and fall migration are shown in left and right panels, respectively. 61

Figure A 15 Interaction plots of TWC with Julian day for RF models on migration intensities (MTR up to 200 m). Results for spring and fall migration are shown in left and right panels, respectively. .. 61

Figure A 16 Interaction plots of TWC with CWC for RF models on migration intensities (MTR up to 200 m). Results for spring and fall migration are shown in left and right panels, respectively. 62

Figure A 17 Interaction plots of ambient temperature with Julian day for RF models on migration intensities (MTR up to 200 m). Results for spring and fall migration are shown in left and right panels, respectively. 62

Figure A 18 Partial dependence plots of the factor “year” for RF models on migration intensities (MTR up to 200 m). Results for spring and fall migration are shown in left and right panels, respectively... 63

Figure A 19 Partial dependence plots of the factor “project” for RF models on migration intensities (MTR up to 200 m). Results for spring and fall migration are shown in left and right panels, respectively. 63

Figure A 20 Partial dependence plots of the factor “phase” for RF models on migration intensities (MTR up to 200 m). Results for spring and fall migration are shown in left and right panels, respectively... 63

Figure A 21 Partial dependence plots of the factor “lab” for RF models on migration intensities (MTR up to 200 m). Results for spring and fall migration are shown in left and right panels, respectively... 64

Figure A 22 Observed and predicted migration intensities (MTR) in spring for all study years with bars indicating the observed and open symbols the predicted values. In addition, the performance of the model in predicting nights with high migration intensities (>250 MTR) is indicated (FN = false negatives, TN = true negatives, TP = true positives). The dashed blue line represents the threshold for observed and predicted values (250 MTR). 64

Figure A 23 Observed and predicted migration intensities (MTR) in fall for all study years with bars indicating the observed and open symbols the predicted values. In addition, the performance of the model in predicting nights with high migration intensities (>250 MTR) is indicated (FN = false negatives, FP = false positives, TN = true negatives, TP = true positives). The dashed blue line represents the threshold for observed and predicted values (250 MTR). 65

List of tables

Table 3.1 Study sites and sample sizes of the data sets used in this study. 5

Table 3.2 Bird related parameters used in Collision Risk Models 10

Table 3.3 Turbine related parameters used in Collision Risk Models. For hub height, rotor radius and maximum blade width the range of the used values is given; the wind farm specific values were used in the models. Values of mean rotation speed, mean blade pitch angle and mean monthly operational time were based on information from a limited number of offshore wind farms (see text for details). The same values were used in all models. 11

Table 4.1 Summary of results of random forest models (full model and weather only model) by season. Models were based on migration intensities for the whole altitude range (up to 1,000 m), on altitude range up to 200 m, and on flight height. N hours is the number of hours observed, % Var. explained is the percentage of variance explained by the model. 12

Table 4.2	Confusion matrices of the observed and predicted classification of migration intensity exceeding the threshold of 250 MTR for spring (left) and fall (right). The cells represent true negatives (upper left), false positives (upper right), true positives (lower right) and false negatives (lower left).	34
Table 4.3	Confusion matrices of the observed and predicted classification of migration intensity exceeding the threshold of 250 MTR for spring (left) and fall (right). The threshold for predictions was optimized by maximizing Cohen’s Kappa (see chap. 3.2.2). The cells represent true negatives (upper left), false positives (upper right), true positives (lower right) and false negatives (lower left).	34
Table 4.4	Coincidence of high migration intensities and unfavorable weather. Given is the number and percentage of hours in which migration intensity was above three different thresholds for “high migration intensities” and in which three different levels of unfavorable weather conditions prevailed. Results are based on data from all available radar sites.	35
Table 4.5	Total estimated number of collisions of nocturnal migrants for all OWFs currently in operation or under construction in the German EEZ. Numbers reflect estimated collisions during the migration periods (spring and fall) per year (see text for details). In addition, mean collisions per turbine [\pm SE, range] is given.....	36
Table 4.6	Total estimated number of collisions of nocturnal migrants and mean collisions per turbine for OWFs in the German EEZ of the North Sea and Baltic Sea. Numbers reflect estimated collisions during the migration periods (spring and fall) per year (see text for details). The wind farms included in each region are given in Tab. A 3.....	37
Table 4.7	Monthly estimated number of collisions of nocturnal migrants and mean collisions per turbine per month combined for all OWFs currently in operation or under construction in the German EEZ.	37
Table 4.8	Total number of collisions and collisions per turbine for different thresholds of migration traffic rates (MTR). In addition, the proportion of collisions that occur when MTR was above different thresholds, the proportion of time and the absolute number of hours that MTRs were above thresholds is given. Except for the total number of collisions the mean \pm SE [range] of all single wind farms is given.....	38
Table 4.9	Effect of variation of the different input parameters of the Band model on estimated collisions. The values of input parameters used in the models for this report are given as well as alternative values and the deviation of estimated collision numbers [%] for the whole year. In addition, the range of deviation with respect to estimates for single months and wind farms is given.....	40
Tab. A 1	Coincidence of high migration intensities and unfavorable weather based on radar data from platforms only. Given is the number and percentage of hours in which migration intensity was above three different thresholds for “high migration intensities” and in which three different levels of unfavorable weather conditions prevailed.	66
Tab. A 2	Number of night hours per month used in the Collision Risk Models. Night hours were calculated based on latitude 54.4°N and Civil Twilight as the start and end point of the night. Night hours for July contain only the nights from the 15 th of July onwards (see chap.3.2.4 for details).	67

Tab. A 3	Offshore wind farms in the German North and Baltic Sea for which collision risk models were constructed. The number of turbines, hub height and rotor radius is given for each wind farm.	67
Tab. A 4	Total number of collisions and collisions per turbine for different thresholds of migration traffic rates (MTR) separately for the North and Baltic Sea. In addition the proportion of collisions that occur when MTR was above different thresholds, the proportion of time and the absolute number of hours that MTRs were above thresholds is given.	69

1 SUMMARY

During their migration, millions of birds cross the North and Baltic Sea each year, most of them during the night. With the rapid development of offshore wind farms in recent years collision risk of nocturnal migrants and the potential impairment of bird migration has increasingly come into focus. Yet, due to the difficulty of obtaining direct evidence of collisions or the avoidance behavior of nocturnal migrants at offshore wind farms, little is known with respect to their collision risk and associated number of fatalities. This is particularly true for the cumulative collision risk as no comprehensive data from multiple offshore sites was available yet.

Typically, bird migration shows high temporal variability at least part of which is driven by the prevailing weather conditions. Information on atmospheric variables can therefore be used to model and predict future migration intensities. Migration forecasts could then potentially be used to implement mitigation measures such as turbine curtailment in order to prevent bird collisions.

We used data on bird migration collected by marine surveillance radar over a period of nine years at 10 sites in the German Exclusive Economic Zone (EEZ) of the North and Baltic Sea to determine the relationship of migration intensity and flight height with atmospheric parameters and to construct a forecast model predicting migration intensities in the German EEZ. Further, we applied a collision risk model (SOSS Band model) to estimate the cumulative number of collisions of nocturnal migrants at all German offshore wind farms that are operational or currently under construction.

Our models explained up to 80% of the variance in migration intensities in our multi-year, multi-site dataset. Meteorological and time-related variables accounted for more than 70% of the variance alone. There was strong temporal variation in flux rates which varied across study years, within seasons and within the course of the night. Other factors such as study site, stage of the wind farm (baseline, construction, operation) and the company responsible for data collection were of minor importance.

Wind regime was the most important atmospheric driver of offshore migration. Flux rates increased with increasing tailwinds and, to a lesser degree, with seaward crosswinds indicating partial drift of birds to offshore locations. Our results also suggest that accumulation of migrants at the departure sites due to unfavorable wind conditions during previous nights affected migration activity.

Furthermore, nocturnal migrants generally preferred weather conditions characterized by low relative humidity and high barometric pressure which are usually associated with clear skies, moderate winds and no precipitation. The relationship with ambient temperature contrasted between spring and fall. Spring migration intensities increased with increasing temperature while during fall migration intensities increased with decreasing temperature.

Variation in mean flight height was less well explained by meteorological variables with models accounting for approx. 50-60% of the variance. Migration intensity was the most important predictor of flight height indicating a strong positive correlation between the two variables. The relationships between atmospheric variables and flight height corresponded well with results from migration intensity with one noticeable exception. In contrast to flux rates, flight height increased with increasing headwinds. A possible explanation may be related to our meteorological data reflecting wind conditions at sea level with no information on variation of conditions with altitude.

Mean flight height also showed strong temporal patterns. It decreased in the course of the night presumably indicating an increasing proportion of birds preparing to land. Additionally, flight height increased during spring migration but decreased throughout fall. Systematic seasonal changes in weather (wind) conditions or seasonality in the species composition and variation in their preferred flight height may account for this pattern.

Predictive models were based on mean migration intensity per night for altitudes up to 200 m, the height range most relevant for offshore wind farms and explained about 40% of the variation in validation datasets. However, the accuracy of our models to predict nights in which a threshold of 250 MTR (migration traffic rate) was exceeded was relatively low (30-60%) due to a tendency of the model to underpredict high migration intensities. Even though optimization procedures increased accuracy of predictions to about 85%, the predictive performance seems insufficient for an application of the model to regulate potential turbine curtailment directly.

The cumulative number of collisions of nocturnal migrants at offshore wind turbines in the German EEZ during spring and fall migration was estimated at approx. 35,000; 16,000 and 8,000 birds assuming an avoidance rate of 0.956; 0.980 and 0.990, respectively. This illustrates the pivotal effect of the assumed avoidance rate on model outcome. Uncertainty and variation in other bird-related and turbine-related input parameters resulted in additional uncertainty of the model outcome though sensitivity analysis indicated that their potential impact was minor in comparison to avoidance rate.

The total number of collisions estimated for the North Sea was higher compared to the Baltic Sea reflecting the higher number of turbines in the North Sea, yet the number of collisions per turbine was on average about 50% higher in the Baltic Sea. With respect to seasonal variation, 36% of all collisions can be expected to occur in October alone. In relation to the total estimated number of migrants crossing the North and Baltic Sea, about 0.03% and 0.002% of these birds were estimated to collide each year, respectively.

Due to the high temporal variation of migration intensities, estimated collisions were also aggregated in time. By calculating the proportion of collisions that theoretically occur when migration intensity exceeds a certain threshold, we assessed the efficacy of potential turbine curtailment. For example, our data suggest that if turbine shutdown were implemented when flux rates exceeded 500 MTR, 27% of collisions could theoretically be prevented with turbine shutdown amounting to approx. 30 h per annum.

These considerations assume that collisions are strictly proportional to the number of birds migrating. However, it has been suggested that nocturnal migrants are particularly prone to collisions during unfavorable weather conditions and poor visibility. Occasions where high migration intensities concur with inclement weather may therefore have a strong impact on overall collision risk. Our data indicate that such events occur only rarely (0.5-8 h per year depending on the definition of poor weather and high migration intensity). If collisions were strongly aggregated by these events, turbine shutdown time could be further reduced to prevent a given number of collisions. However, better knowledge about the effect of weather on the avoidance behavior of nocturnal migrants at offshore wind farms is needed to gauge the effect of turbine curtailment on the number of collision fatalities.

2 INTRODUCTION

During migration, many nocturnally migrating birds fly in predisposed directions with limited guidance by topographical features such as coastlines. This phenomenon is called broad-front migration (BERTHOLD et al. 2003). On their migration, these birds regularly cross stretches of open water. It has been estimated that a total of about 100 million and 300-500 million birds cross the North Sea (OREJAS et al. 2005; BSH 2019a) and the western Baltic Sea (BERTHOLD 2000; BELLEBAUM et al. 2010; BSH 2019b), respectively.

The number of migrants crossing the North and Baltic Sea varies substantially across the year with highest concentrations occurring in the main migration periods in spring and fall. However, also during peak migration, migration intensity is not uniform but usually shows high day-to-day variation. At least part of this variation is driven by the prevailing weather conditions. A number of studies have shown that meteorological variables such as wind direction and speed, air temperature, cloud cover, barometric pressure or precipitation have large effects on the number of birds migrating at night (ZEHNDER et al. 2001; ERNI et al. 2002; VAN BELLE et al. 2007; KEMP 2012; VAN DOREN & HORTON 2018).

The distinct weather-dependence of bird migration has led to several attempts to model and predict migration intensities based on atmospheric variables (ZEHNDER et al. 2001; ERNI et al. 2002; VAN BELLE et al. 2007; VAN DOREN & HORTON 2018). These models were often able to explain a substantial part of the variance in migration intensities and can be used to predict future migration intensities based on weather forecasts up to several days ahead (VAN DOREN & HORTON 2018). Multi-day migration forecasts can for example be used to inform flight schedules at airports (VAN BELLE et al. 2007). In the same way, predictions of migration activity at sea could potentially be used for wind turbine curtailment in order to prevent bird collisions during events of mass migration.

The collision risk of nocturnal migrants at offshore wind turbines is largely unknown. This is mainly due to the fact that in contrast to the situation at onshore wind farms it is impossible to conduct carcass searches at sea and, hence, it is impossible to estimate fatalities and collision risk based on direct evidence. Moreover, there are as yet no technical systems such as radar, camera-based or acoustic systems available that are capable of detecting collisions at offshore wind turbines, particularly at night. There is also ambiguous evidence with respect to the general collision risk of nocturnal migrants at wind energy facilities. On the one hand, nocturnally migrating passerines regularly collide with offshore structures such as platforms (MÜLLER 1981; AUMÜLLER et al. 2011; SCHULZ et al. 2013; HÜPPPOP et al. 2016), on the other hand several studies have reported a low risk of collision of this group of birds at onshore wind farms (KRIJGSVELD et al. 2009; KERLINGER et al. 2010; GRÜNKORN et al. 2016; WELCKER et al. 2017).

Besides the illumination of offshore facilities (EVANS OGDEN 1996), it is generally assumed that weather conditions may be an important factor affecting the collision risk of birds at night (AVERY et al. 1977; AUMÜLLER et al. 2011). Specifically in situations where high migration activity caused by favorable weather conditions at the departure sites meet inclement weather offshore, collision fatalities may be particularly high (AUMÜLLER et al. 2011). While migrating passerines faced with headwinds, low visibility or precipitation may find a stop-over site and discontinue migration onshore, they are forced to continue migration offshore and hence may be particularly prone to collision under such circumstances.

Given the lack of direct data on collisions, collision risk models (CRM) are to date the only possibility to estimate the number of fatalities at offshore wind farms. The so-called Band model (BAND 2000, 2012) is the most widely applied theoretical CRM. Based on physical characteristics of the birds and turbines, this mechanistic model estimates the probability of the shape of the bird overlapping with the swathe of the rotor blade (BAND 2000). In principle, the number of collisions is then estimated by multiplying the single transit collision risk by the number of potential bird transits and applying an avoidance rate that accounts for the fact that most birds will take evasive action to prevent collision. In addition to a number of simplifications inherent in the model, uncertainty about and variation of the various input parameters results in largely unknown accuracy of the model outcome. Especially the avoidance rate applied has a pivotal effect on the estimated collision risk (CHAMBERLAIN et al. 2006). Due to the lack of empirical data on collision fatalities offshore, model validation is not yet possible.

The potential impairment of bird migration has increasingly come into focus in connection with the ongoing development of offshore wind facilities in Germany. Uncertainty about the actual collision risk of nocturnal migrants has led to the inclusion of incidental provision 21 in the approval documents of German offshore wind farms which theoretically allows for mitigation measures such as turbine shutdown during events of mass migration. However, only few attempts have been made to estimate the number of collisions of nocturnal migrants at offshore wind farms (KRIJGSVELD et al. 2015) and virtually no information is available as to the cumulative collision risk of these birds crossing the North and Baltic Sea.

In this study, we used data from marine surveillance radars on nocturnal bird migration collected during environmental impact assessments as well as the construction an operational phase of offshore wind farms in the German Exclusive Economic Zone (EEZ) to determine the effect of weather parameters on migration intensity at offshore sites. We then evaluated the capability of the constructed models to predict migration. In addition, we determined how often high migration intensities at sea concurred with unfavorable weather conditions in order to estimate the frequency of occurrence of situations with an assumed particularly high collision risk.

To estimate the cumulative number of collision fatalities of nocturnal migrants at offshore wind farms we ran Band models based on the radar data on migration intensities and information on turbine and wind farm characteristics. Model outcomes were then used to evaluate the efficacy of potential turbine curtailment. To this end we estimated the number of collisions prevented if turbines were shut down at different levels of migration flux rates.

3 MATERIALS & METHODS

3.1 Data collection

Radar data were collected as described in WELCKER (2019). In short, data were collected at 10 different locations in the German EEZ of the North and Baltic Sea during the years 2008 – 2016 (Figure 3-1). The time period of data collection at each site is given in Table 3.1. The data used in this study were collected as part of pre-construction environmental impact assessments and effect studies during the construction and operational phases of offshore wind farms. Technical specifications and settings of radar devices as well as methods of data collection were standardized by guidelines issued by the Federal Maritime and Hydrographic Agency (BSH) (BSH 2013; WELCKER 2019). At sea, raw data was stored at regular intervals (3-5 min depending on project/year) as screenshots of the radar screen. The vertical, horizontal and absolute distance to the radar of all radar signals considered to represent a bird track was then calculated using purpose-built software. Screenshots with rain clutter masking bird signals were omitted from the analysis.

Table 3.1 Study sites and sample sizes of the data sets used in this study. In addition, seasons (spring or fall) with available data and the developmental phase of the wind farms during data collection (B – baseline, C – construction, O – operation) is given.

Location	N _{spring} , N _{fall}	N _{nights}	Years with data	Phase (years)
Albatros	2, 2	124	2008 - 2009	B (2)
Amrumbank West	2, 2	112	2011 - 2012, 2014	B (2); C (1)
Baltic 2	4, 5	244	2010, 2013 - 2016	B (1); C (3); O (2)
Butendiek	3, 2	276	2011, 2014 - 2015	B (1), C (2)
Cluster Helgoland	2, 2	424	2015 - 2016	O (2)
Global Tech I	5, 6	301	2009, 2012 - 2016	B (1), C (3), O (2)
Cluster 12	2, 2	118	2009 - 2010	B (2)
Meerwind	3, 5	181	2010 - 2014	B (2), C (3)
Nordsee Ost	3, 4	211	2010, 2012 - 2014	B (1), C (3)
Wikinger	2, 3	154	2014 - 2016	B (2), C (1)
TOTAL	41, 48	4705	2008 - 2016	B (16), C (19), O (16)

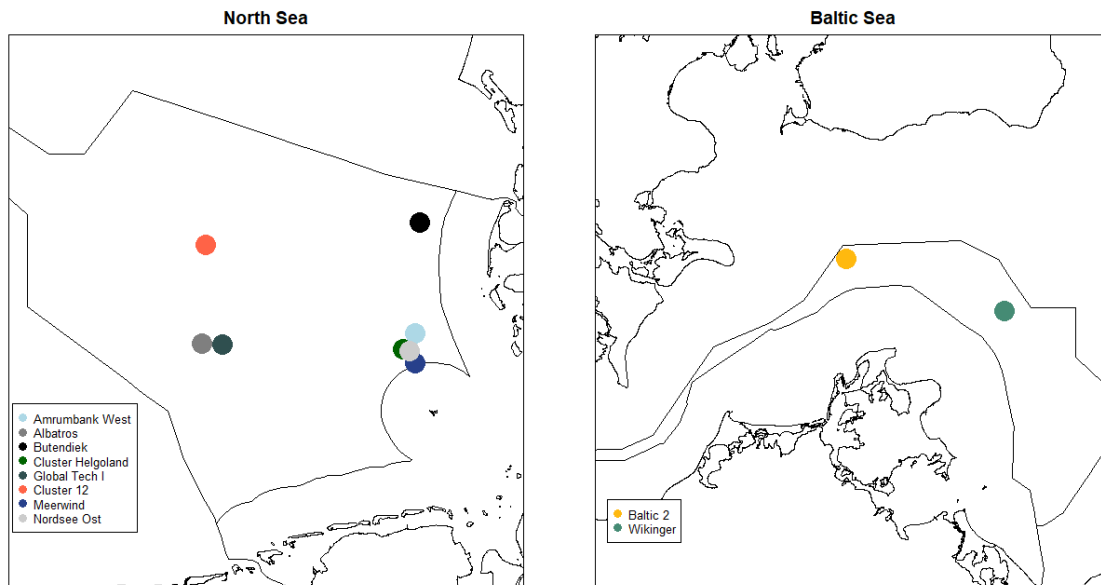


Figure 3-1 Location of the study sites in the EEZ of the German North and Baltic Sea.

3.2 Data analysis

3.2.1 Radar data

Radar data were analyzed and migration intensities (Migration Traffic Rates, MTR [signals*km⁻¹*h⁻¹]) were calculated as detailed in WELCKER (2019). In summary, the number of radar signals was corrected for distance-dependent detectability (HÜPPOP et al. 2006; WELCKER et al. 2017), and, based on the corrected number of signals, mean MTRs were calculated for each hour of data. MTRs were calculated for the altitude range from sea level to 1,000 m a.s.l. and from sea level to 200 m a.s.l.

3.2.2 Weather data and models

Data on atmospheric parameters were obtained from the National Oceanic and Atmospheric Administration (NOAA) database NCEP Reanalysis 2 (<https://www.esrl.noaa.gov/psd/data/gridded/data.ncep.reanalysis2.html>). The parameters used were barometric pressure at sea level [mbar], relative humidity at 1,000 mb [%], air temperature at 2 m height [°C], and wind speed [m/s] and direction [°] at 10 m height. Data were acquired at a 6 h temporal and a 2.5° x 2.5° spatial resolution. We used a 2-D interpolation routine (Akima spline interpolation; Akima package (AKIMA et al. 2016) in R (R CORE TEAM 2017) to estimate weather parameters for the specific radar sites and a Stineman monotone cubic interpolation (R package 'stinepack'; JOHANNESSON et al. (2018)) to derive values for each time stamp.

Based on information on wind direction and speed we calculated the tailwind component (TWC [m/s]) and crosswind component (CWC [m/s]) following ZEHNDER et al. (2001) and HÜPPOP & HILGERLOH (2012):

$$TWC = \cos(OWD - TWD) \cdot WS \quad (\text{eq. 1})$$

$$CWC = \sin(OWD - TWD) \cdot WS \quad (\text{eq. 2})$$

where OWD is the observed wind direction, TWD is the tailwind direction and WS is the wind speed. We assumed a mean migration direction of 225° in fall and 45° in spring. Positive TWC values correspond to supportive winds (tailwind), negative TWC values correspond to headwinds. The CWC describes the wind component perpendicular to the main migration direction. Positive CWC values correspond to a crosswind component from the left of the bird, negative values from the right. In relation to the assumed direction of migration positive CWC values translate to shoreward (north-westerly) winds in spring and seaward (southeasterly) winds in fall.

Furthermore, for TWC, air temperature, rel. humidity and barometric pressure we calculated the change within the previous 24 hours (δ TWC, δ temperature etc.). Positive values indicate increasing, negative values decreasing trends in these parameters. Furthermore, we calculated an accumulation variable representing the potential aggregation of migrants at the departure sites due to unfavorable wind conditions. This variable was computed according to ERNI et al. (2002) and VAN BELLE et al. (2007). It approaches the value 0 when no unfavorable winds occurred in a series of nights and 1 when unfavorable winds were prevalent in a number of consecutive nights.

In addition to atmospheric parameters, two variables accounting for temporal patterns in migration were included in the analyses. To capture the phenological pattern within the spring and fall migration periods we included Julian day in the models. As migration intensities are known to vary systematically within the course of the night we also included the variable “proportion of the night”. Finally, the variables study year (“year”), project location (“project”), the company responsible for data collection (“lab”) and the developmental stage of the wind farm (“phase”) were included as factors to account for these potential sources of variation.

Models

We used random forest (RF) regression models (BREIMAN 2001) to determine the effect of the different weather parameters on migration intensities. RF models are robust with respect to the inclusion of correlated variables (ARCHER & KIMES 2008) and do not make any prior assumptions about the data. At the same time, they have been proven to attain higher predictive performance than other methods commonly used for ecological prediction (BREIMAN 2001; PRASAD et al. 2006; CUTLER et al. 2007; CRISCI et al. 2012).

Models were fitted with square root transformed migration intensities (MTR) per hour for the whole altitude range and for altitudes up to 200 m as the response variable. For both response variables two models were fitted, one including all explanatory variables described above, and a second model including atmospheric and time-related variables (proportion of day, Julian day) only. The second set of models was run to determine the explanatory power of weather and time variables alone as those were the variables intended to use for predictions of migration intensities.

Similarly, RF models were used to determine the effect of weather on the mean flight height of nocturnal migrants. In these models, only data of hours were included in which at least 10 radar raw signals were recorded. This was done to ensure mean flight height to be based on an appropriate sample size and to minimize stochastic variation.

We used a similar RF model based on the mean migration intensity per night for predictions. This was done because the aim was to predict migration activity for whole nights rather than single hours. In this model all atmospheric explanatory variables described above as well as Julian day were included. In addition, latitude and longitude were included as predictors to account for the spatial variability of the data. The response variable was square root transformed, predictors were scaled and centered for modelling.

Model validation was performed using the K-fold cross validation method. Thus, the dataset was divided randomly into 10 folds, which empirically yields test error rate estimates that suffer neither from excessively high bias nor from very high variance (JAMES et al. 2013). Then each fold was used as a testing dataset for the model trained on the other 9 folds. We repeated this process three times, the final model error being the average of the k-fold error scores.

In all cases, separate models were run for spring and fall. All analyses were performed in R 3.5.2. (R CORE TEAM 2018) using the “rfUtilities” package (EVANS & MURPHY 2018), the “randomForest” package (LIAW & WIENER 2002) and the “caret” package (KUHN et al. 2019).

Furthermore, we evaluated the ability of the model to correctly predict events of high migration intensities, i.e. nights with flux rates >250 MTR. To do so, we constructed a confusion matrix for each season, using observed and predicted MRT above the selected threshold (i.e. 250 MTR) as the observed and predicted positive class, respectively. As predictions of our model for nights with very high migration intensities were systematically low, we additionally calculated an empirical threshold for the predicted positive class. The empirical threshold was computed as the value which maximized the predictive accuracy of the matrix according to Cohen’s Kappa score (COHEN 1960). This metric compares the observed accuracy with the expected accuracy (random chance), and ranges from -1 to 1. Values between 0.41–0.60 can be interpreted as moderate, 0.61–0.80 as substantial and 0.81–1 as in almost perfect agreement (LANDIS & KOCH 1977). The Kappa score is particularly suitable for very unbalanced classes (i.e. rare events) as in these cases it is more reliable than other accuracy metrics. The optimal empirical threshold for the predicted MTR was calculated in R using the cutpointr package (THIELE 2019).

3.2.3 Coincidence of high migration intensities and unfavorable weather

As the collision risk of nocturnal migrants is supposed to be particularly high in situations where high migration activity coincides with unfavorable weather conditions, we determined their frequency of co-occurrence based on the nocturnal migration intensities during the 16,907 hours of our data.

Strong headwinds, rain and low visibility are usually thought to be the prime atmospheric factors leading to high collision risk. As no data on precipitation or a direct measure of visibility were available to us, we used relative humidity as a surrogate. HÜPPOP & HILGERLOH (2012) could show that relative humidity $\geq 95\%$ was related with a high probability to fog, drizzle or rain at an offshore location in the North Sea.

Based on wind conditions (TWC) and relative humidity we defined three different levels of ‘unfavorable weather’:

- i.) poor sight (i.e. rel. humidity $\geq 95\%$) or strong headwinds (TWC ≤ -7 m/s)
- ii.) poor sight and moderate headwinds (humidity $\geq 95\%$ and TWC ≤ -5 m/s)
- iii.) moderate sight and no tailwind (humidity $\geq 90\%$ and TWC ≤ 0 m/s).

Likewise, three different levels of ‘high migration intensities’ (>250 MTR, >500 MTR and >750 MTR, for the altitude range up to 1,000 m) were considered. For each combination of levels, we calculated the proportion of hours which met the conditions of unfavorable weather and high migration activity relative to hours with high migration intensities and in relation to all hours.

As the majority of our data stem from ship-based surveys which are preferably conducted during benign weather conditions and thus may result in an underestimation of the occurrence of unfavorable weather, we repeated the analysis for data from platform-based surveys only. These data were collected independently of weather conditions.

3.2.4 Collision risk models (CRM)

We estimated collision fatalities of nocturnal migrants for each operational OWF and OWFs currently under construction in the German EEZ of the North and Baltic Sea using the extended (deterministic) Band model (BAND 2012; MCGREGOR et al. 2018). We used data on migration intensities (MTRs) derived from radar observations described above to estimate the number of birds flying through the wind farms each month during spring and fall migration periods. In contrast to the basic Band model, the extended model allows for the inclusion of the flight height distribution of birds. We calculated the mean flight height distribution up to 250 m altitude for each month based on the radar data from all available sites. To do this, we fitted cubic smoothing splines to the monthly height data (Figure 3-2) and calculated the proportion of birds per meter of height as required by the model.

CRMs were run separately for each wind farm, for each month and separately for two groups of species, passerines and non-passerines. We assumed that migration flux rates contained 90% passerines and 10% non-passerines. This assumption was based on results of a fixed-beam radar study at the research platform FINO2 in the Baltic Sea (SCHULZ et al. 2013). In this study the proportion of passerines was estimated based on wing-beat frequencies measured by the fixed-beam radar.

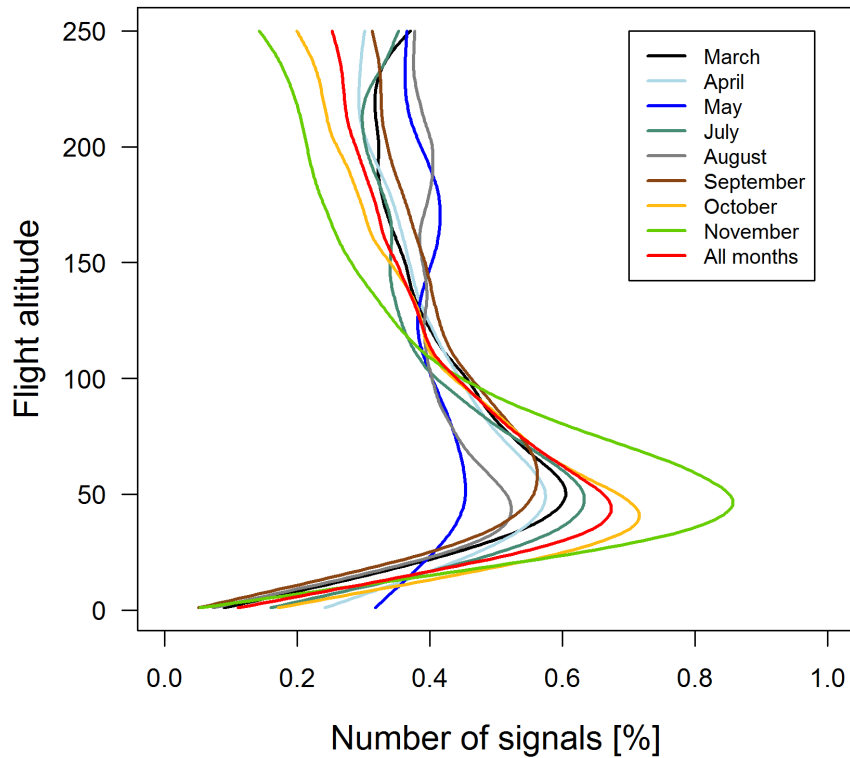


Figure 3-2 Monthly flight height distribution based on radar data from all available sites in the German EEZ. Lines represent cubic smoothing splines fitted to the raw data.

Morphometrical data and data on flight speed of the birds required by the model was taken from ALERSTAM et al.(2007), BRUDERER & BOLDT (2001) and the British Trust for Ornithology (BTO) Bird Facts (<https://www.bto.org/understanding-birds/birdfacts>). To estimate values of bird length, wing span and flight speed for a ‘representative’ passerine we took the mean values of thrush-sized passerines and warbler-sized passerines (Table 3.2). For non-passerines we used data on waterbirds and different sized waders.

Table 3.2 Bird related parameters used in Collision Risk Models

Species group	Bird length [m]	Wing span [m]	Flight speed [m/s]
Non-passerines	0.375	0.700	17.9
Passerines	0.175	0.290	11.8

With respect to turbine-related parameters, we used both wind farm-specific and generic values in the models. Data on the number of turbines in the different wind farms as well as relevant turbine dimensions like hub height, rotor radius and maximum blade width were provided by BSH and wind farm operators (Table 3.3). However, no wind farm specific data were available with respect to mean rotation speed, mean blade pitch angle and the mean operational time of turbines per month. These data are largely confidential and could not be disclosed by most wind farm operators. For these parameters we therefore used the same values for all wind farms based on information from two German and one British wind farm for which (partial) data were available to us. Due to a lack of information on between-month variation of these parameters we used the overall mean for all months.

Table 3.3 Turbine related parameters used in Collision Risk Models. For hub height, rotor radius and maximum blade width the range of the used values is given; the wind farm specific values were used in the models. Values of mean rotation speed, mean blade pitch angle and mean monthly operational time were based on information from a limited number of offshore wind farms (see text for details). The same values were used in all models.

Hub height [range, m]	Rotor radius [range, m]	Max. blade width [range, m]	Mean rotation speed [rpm]	Mean pitch angle [°]	Mean monthly operational time
78 - 110	58 - 82	4.2 - 6	10.3	7	92.5%

Collision fatalities were estimated for night hours only. Night was defined as the time between evening civil twilight and morning civil twilight for each month and each site.

We assumed a proportion of upwind flights of 30% in all models. This differs from the default value of 50% of the Band model that is generally used for resident birds. However, the flight of migrating birds is to a high degree directional. In addition, nocturnal migrants prefer to fly during tailwind conditions (ZEHNDER et al. 2001; ERNI et al. 2002, 2005; ÅKESSON et al. 2002; VAN BELLE et al. 2007). Therefore, the proportion of upwind flights is presumably lower than the 50% assumed in the default model.

Based on the limited information available with respect to avoidance behavior of nocturnal migrants at offshore wind farms (SCHULZ et al. 2014; KRIJGSVELD et al. 2015), we applied three different avoidance rates in the models: 95.6%, 98.0% and 99.0%.

To estimate the proportion of collision fatalities that occur in time periods when migration intensities exceed a number of different thresholds, we additionally ran models for all hours during which bird flux rates were higher than 100, 250, 500 and 750 MTR. Threshold values were chosen to cover a range of migration intensities from moderate to very high.

Finally, to assess the potential effect of the various assumptions made with regard to input parameters, we re-ran a subset of models varying a single input parameter at a time and calculating the proportional deviance of estimated collisions. Parameters evaluated included rotation speed, blade pitch angle, bird flight speed, bird length, wing span, flight height distribution, proportion of upwind flights and avoidance rates.

4 RESULTS

4.1 Weather models

Generally, RF models explained a high percentage of the variance in migration intensities as measured by radar (Table 4.1). Models containing only atmospheric and time related variables accounted for 73% and 74% of the variance in spring and fall, respectively. Adding the factorial variables “year”, “project”, “phase” and “lab” increased the explanatory power to about 80% in both seasons. Variation in MTRs up to 200 m altitude was slightly less well explained by RF models (Table 4.1).

The same was true for models on flight height. Here, the models explained between 47% and 62% of the variance (Table 4.1).

Table 4.1 Summary of results of random forest models (full model and weather only model) by season. Models were based on migration intensities for the whole altitude range (up to 1,000 m), on altitude range up to 200 m, and on flight height. N hours is the number of hours observed, % Var. explained is the percentage of variance explained by the model.

Response variable	Parameter	Spring		Fall	
		Full model	Weather only	Full model	Weather only
MTR, whole altitude range	N hours	5,990		10,644	
	% Var explained	0.793	0.730	0.805	0.744
MTR, 200 m altitude range	N hours	5,990		10,644	
	% Var explained	0.732	0.662	0.789	0.715
Flight height	N hours	2,263		3,721	
	% Var explained	0.617	0.595	0.512	0.472

Of the meteorological variables, the wind components were generally most important. Particularly during fall, TWC was by far the most important explanatory variable for both MTR and MTR up to 200 m (Figure 4-1 and Figure A 1). CWC played a prominent role during spring migration and – to a lesser extent – also in fall.

The Standardized Error Variable Importance of the other atmospheric variables was overall lower and more variable between seasons and MTR altitude ranges. Likewise, there was no clear pattern with regard to the importance of 24h-change variables of meteorological parameters.

With respect to time variables, Julian day was an important predictor of MTR in both spring and fall and for both altitude ranges. Time within the night (proportion of night) was also important, yet mainly in spring.

The importance of the factorial variables “year”, “project”, “phase” and “lab” included in the full models was highly variable. While “year” and “project” generally played an important role, “phase” and “lab” were consistently ranked as the least important predictors (Figure A 2).

With respect to models on flight height, migration intensity was the most important predictor variable (Figure 4-1). Of the meteorological parameters, wind components played also an important role.

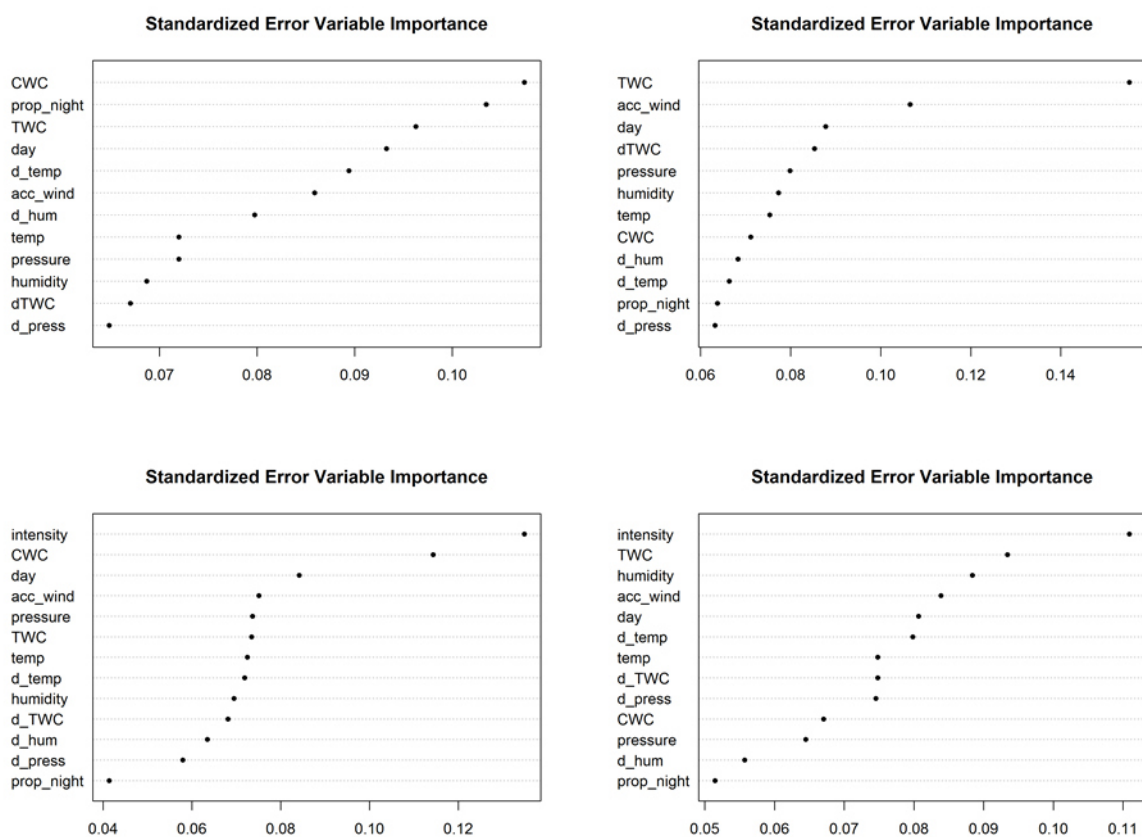


Figure 4-1 Standardized Error Variable Importance of Random Forest models on migration intensities (up to 1,000 m altitude, upper panels) and flight height (lower panels). Results for spring and fall migration are shown in left and right panels, respectively.

TWC

Migration intensities increased steeply with increasing tailwinds. This was the case in both spring and fall and for both altitude ranges (Figure 4-2 and Figure A 3). However, seasonal differences were evident with respect to the onset of the increase in flux rates. While in spring migration intensities mainly increased at positive TWC values, the increase already occurred at moderate headwinds in fall.

In contrast, the relationship between TWC and flight height was negative. Flight height consistently increased with decreasing TWC (Figure 4-2, lower panel).

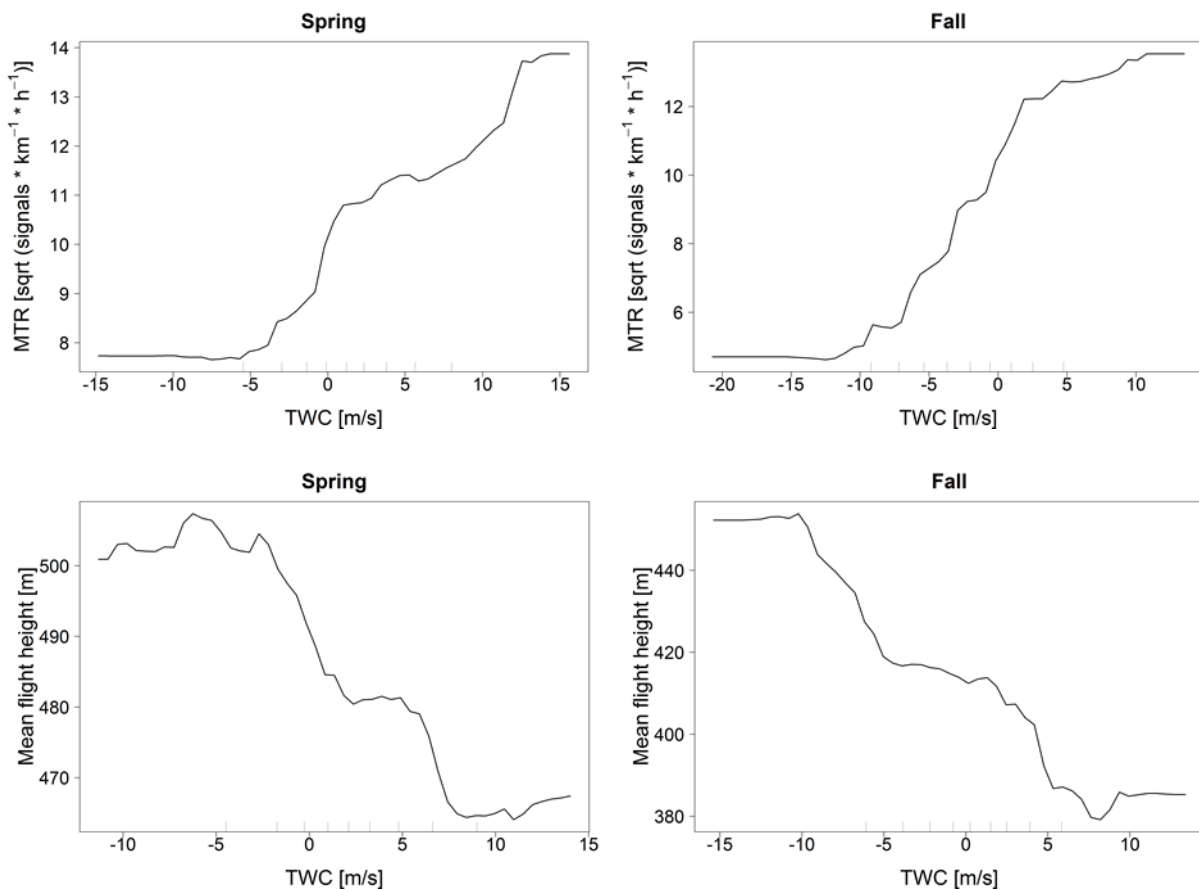


Figure 4-2 Partial dependence plots of TWC for RF models on migration intensities (MTR up to 1,000 m, upper panels) and flight height (lower panels). Results for spring and fall migration are shown in left and right panels, respectively.

CWC

There was a distinct seasonal difference with respect to the effect of CWC on MTR and flight height. During spring, there was a negative relationship between CWC and MTR. Similarly, flight height increased strongly with decreasing CWC values (Figure 4-3). In spring, negative CWC values reflect south-easterly (seaward) winds.

During fall migration, the effect of CWC on flux rates was less prominent (Figure 4-1) and no clear pattern was evident (Figure 4-3). MTRs were highest when CWC was positive (reflecting seaward winds in fall) but also increased when CWC was highly negative. Similarly, flight height increased at high and low CWC values.

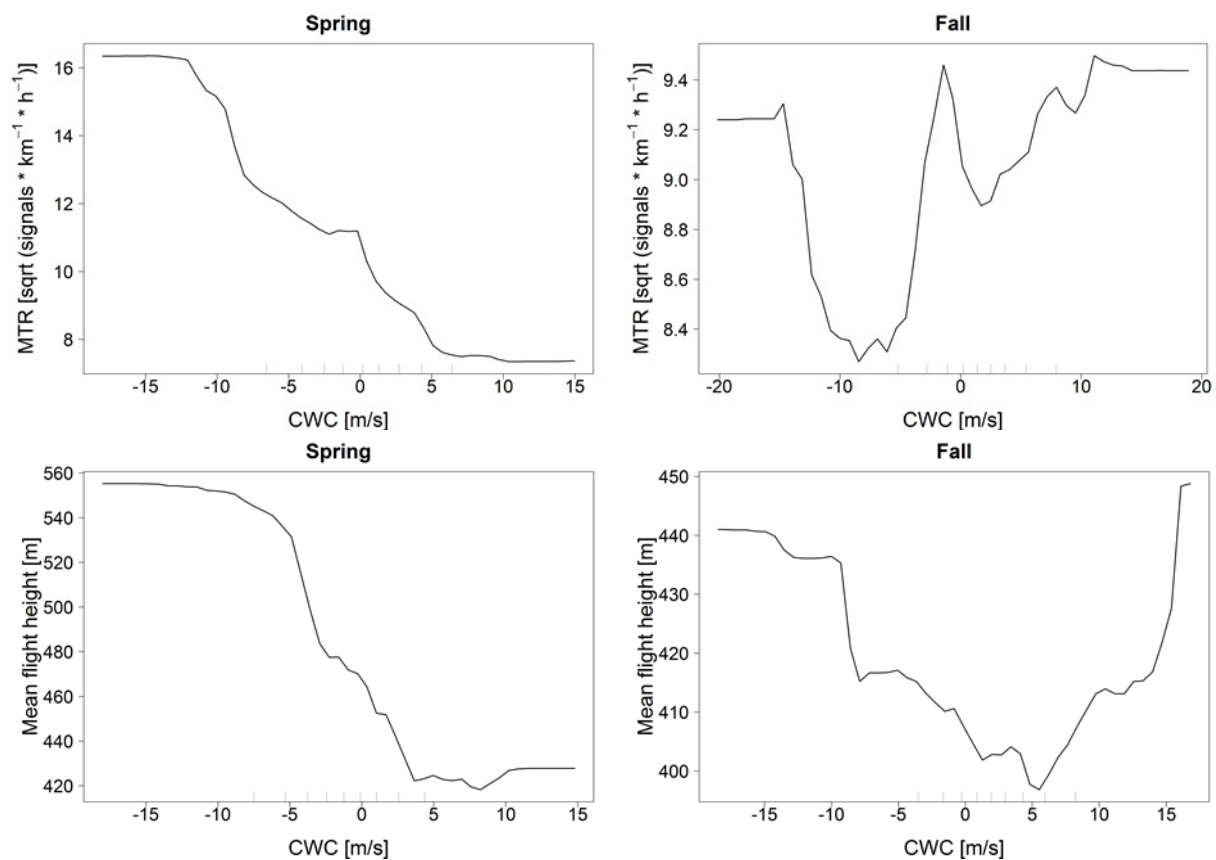


Figure 4-3 Partial dependence plots of CWC for RF models on migration intensities (MTR up to 1,000 m, upper panels) and flight height (lower panels). Results for spring and fall migration are shown in left and right panels, respectively.

Pressure

Barometric pressure was a more important predictor in fall compared to spring (Figure 4-1). In fall, there was a positive relationship between pressure and migration intensities with MTRs increasing notably when barometric pressure exceeded approx. 1020 mbar (Figure 4-4). Conversely, the relationship was more U-shaped in spring. MTRs increased at barometric pressure <1020 mbar but to a lesser degree also increased at values >1020 mbar.

The effect of barometric pressure on flight heights was comparable to that on MTRs. During fall migration, flight height increased with increasing pressure, while in spring flight height was highest when barometric pressure reached very high or low values (Figure 4-4).

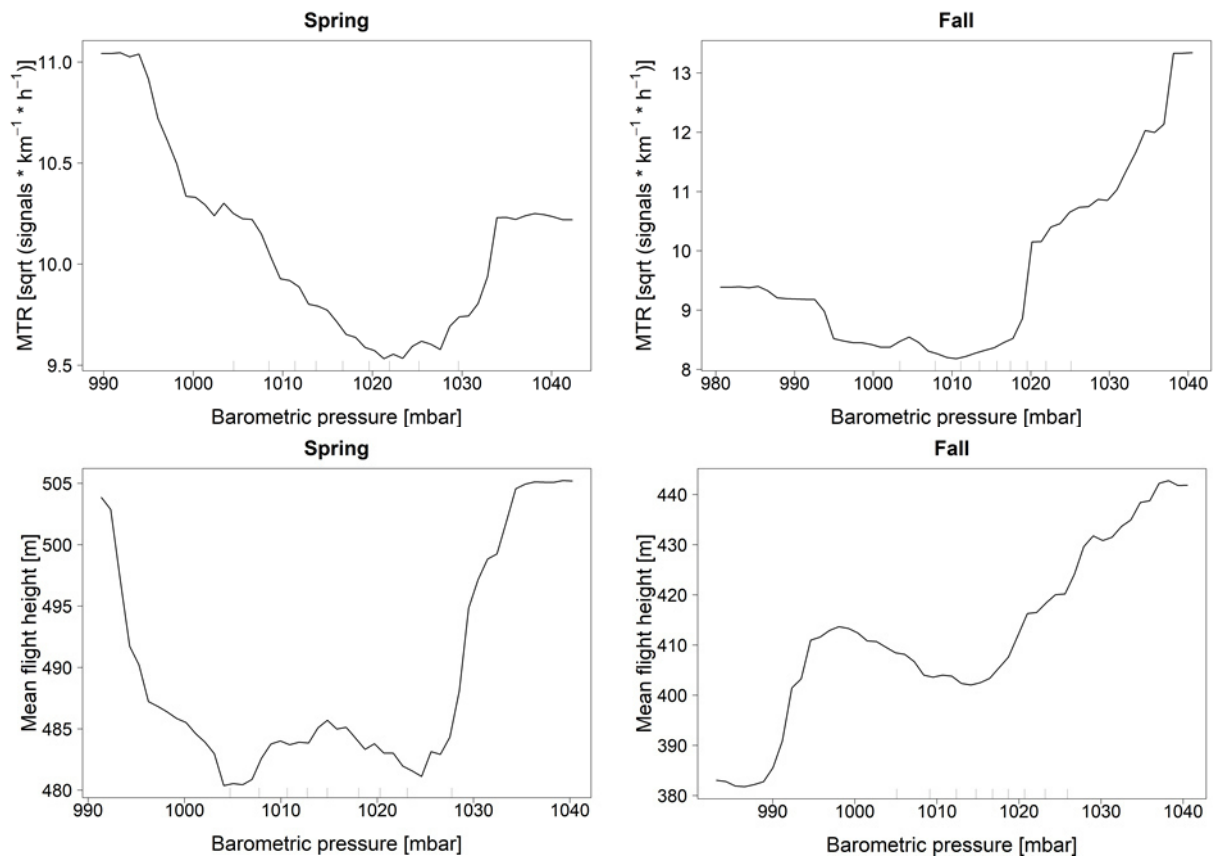


Figure 4-4 Partial dependence plots of barometric pressure for RF models on migration intensities (MTR up to 1,000 m, upper panels) and flight height (lower panels). Results for spring and fall migration are shown in left and right panels, respectively.

Relative humidity

The effect of relative humidity on migration intensities and flight height was to some extent also season specific. During spring migration, the relationship was negative with increasing MTRs with decreasing relative humidity (Figure 4-5). MTRs increased mainly when humidity fell below 70%. The relationship between humidity and flight height was similar, yet flight heights already increased when humidity fell below 95%.

In fall, MTRs increased when relative humidity was below 90% but there was also a positive effect on flux rates when humidity exceeded 90% (Figure 4-5). Flight height remained largely unaffected by humidity in fall and only increased at values below approx. 70%.

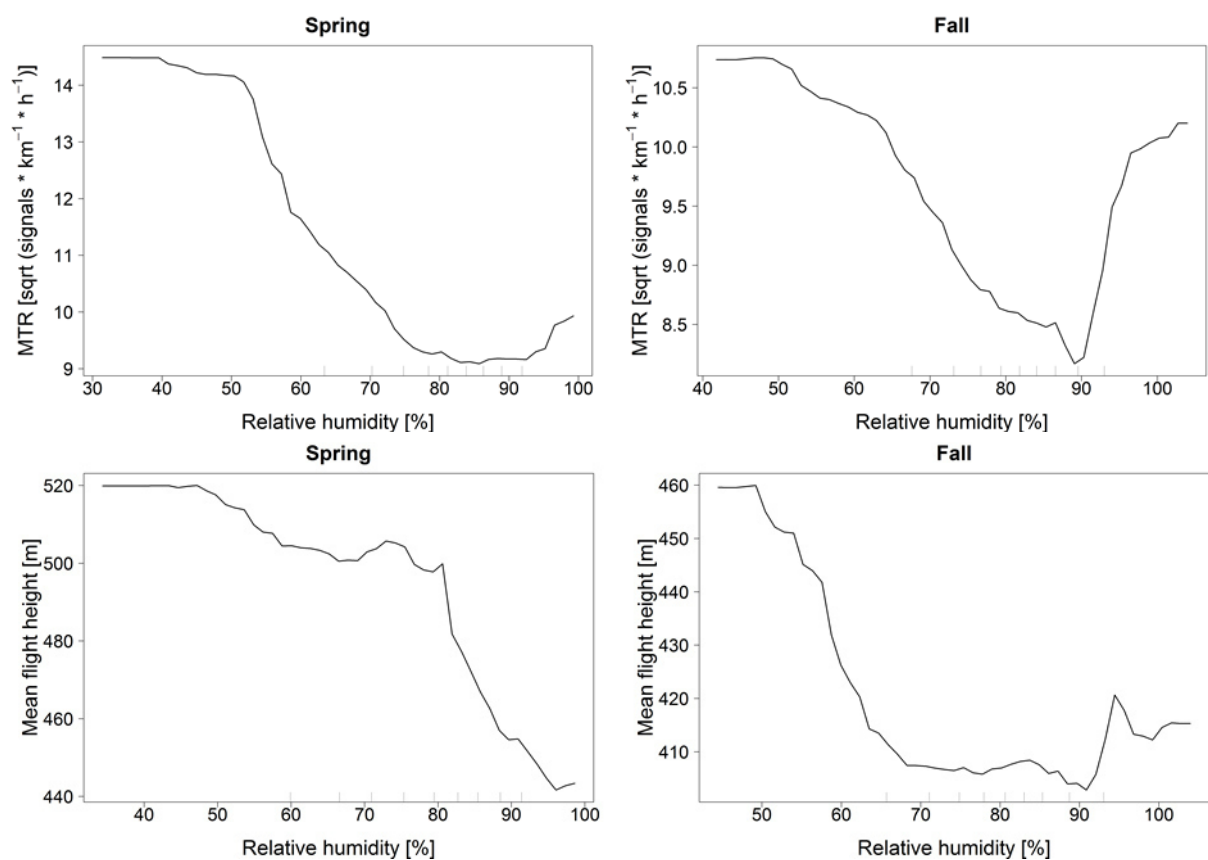


Figure 4-5 Partial dependence plots of relative humidity for RF models on migration intensities (MTR up to 1,000 m, upper panels) and flight height (lower panels). Results for spring and fall migration are shown in left and right panels, respectively.

Ambient temperature

The relationship of this parameter with migration intensity was highly contrasting between seasons. In spring the relationship was positive with strongly increasing MTRs above approx. 6°C (Figure 4-6 and Figure A 7). Conversely, in fall MTRs increased with decreasing temperatures.

The effect of ambient temperature on flight height in spring was similar. Flight height increased in a stepwise manner at about 5-6°C. In fall, flight height was largely independent of temperature and only increased in the rare occasions when temperature approached 0°C (Figure 4-6).

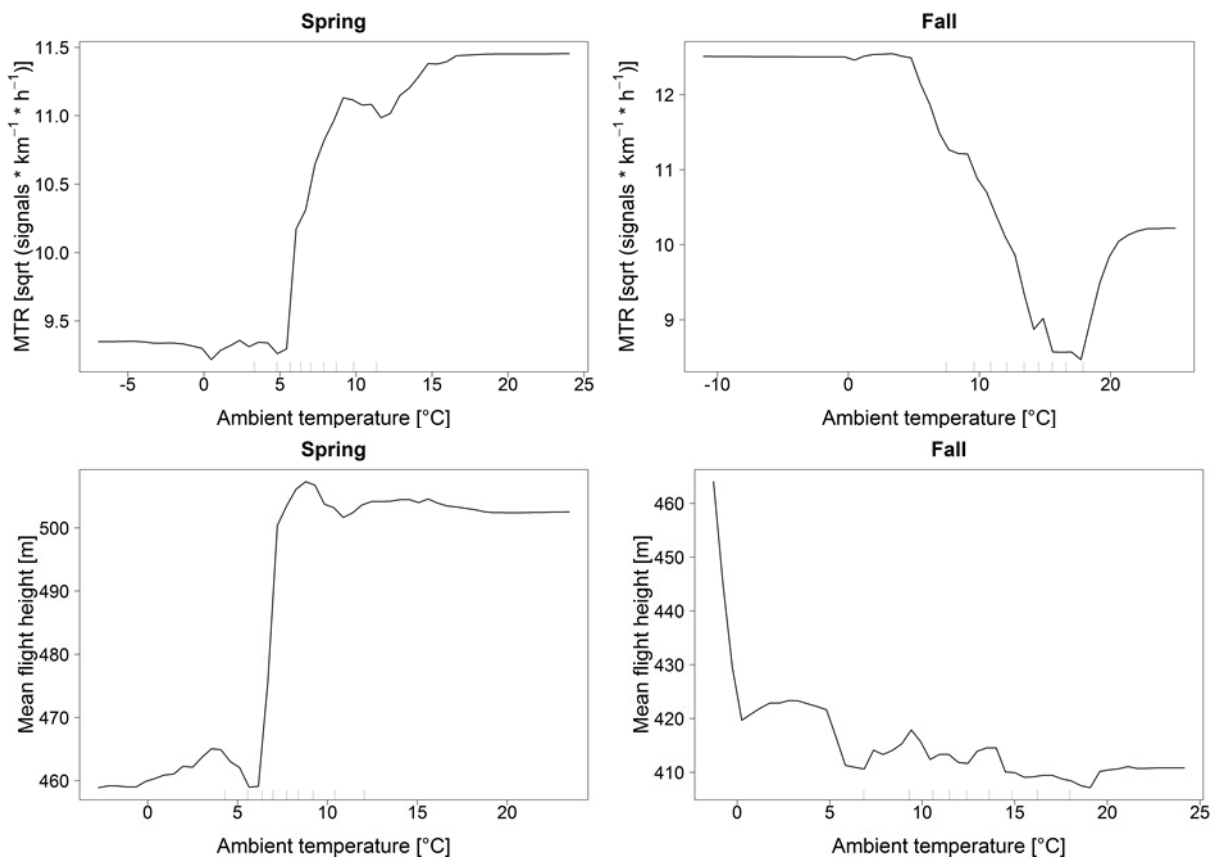


Figure 4-6 Partial dependence plots of ambient temperature for RF models on migration intensities (MTR up to 1,000 m, upper panels) and flight height (lower panels). Results for spring and fall migration are shown in left and right panels, respectively.

Accumulation due to unfavorable wind

Accumulation of migrants due to unfavorable wind was a more important predictor in fall compared to spring (Figure 4-1). The relationship with migration intensity also differed markedly between seasons. In fall, the accumulation parameter seemed to have no effect on MTR until it approached 1 at which point flux rates increased abruptly (Figure 4-7 and Figure A 8). An accumulation factor of 1 is approached after several days with unfavorable wind conditions.

In spring, results were less clear as they differed depending on the altitude range considered. MTR for the whole altitude range increased steeply when the accumulation parameter exceeded 0 but remained stable at higher values (Figure 4-7). With regard to MTRs up to 200 m, the accumulation factor had no effect on flux rates up to approx. 0.7 above which MTRs started to increase (Figure A 8).

The effect of the accumulation parameter on flight height resembled its relationship with MTRs up to 1,000 m (Figure 4-7).

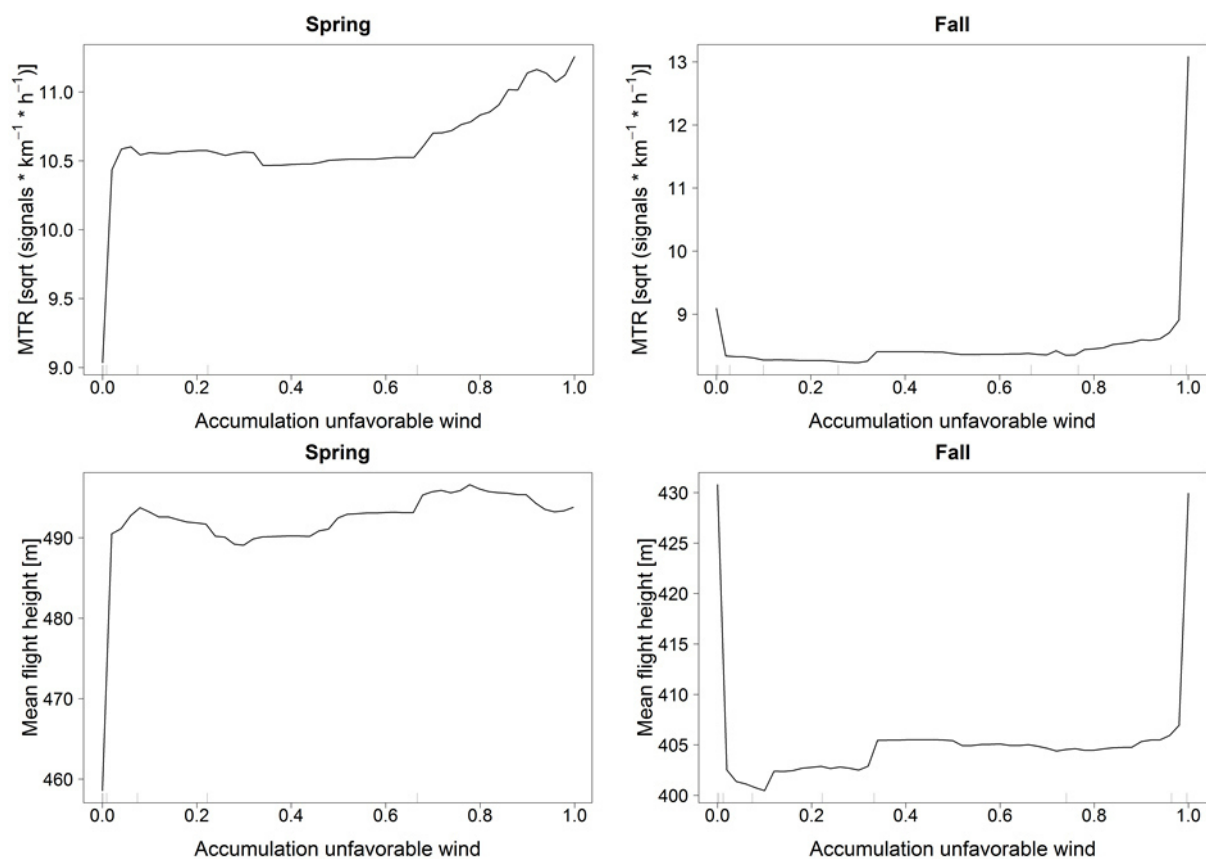


Figure 4-7 Partial dependence plots of the variable “accumulation unfavorable wind” for RF models on migration intensities (MTR up to 1,000 m, upper panels) and flight height (lower panels). Results for spring and fall migration are shown in left and right panels, respectively.

24h-change variables

Parameters capturing the 24h-change of atmospheric variables generally had a moderate to low importance in our models (Figure 4-1).

Particularly δ TWC and δ humidity showed a U-shaped relationship with migration intensities (Figure 4-8, Figure A 9 and Figure A 10). MTRs were highest when TWC or humidity changed strongly in either direction.

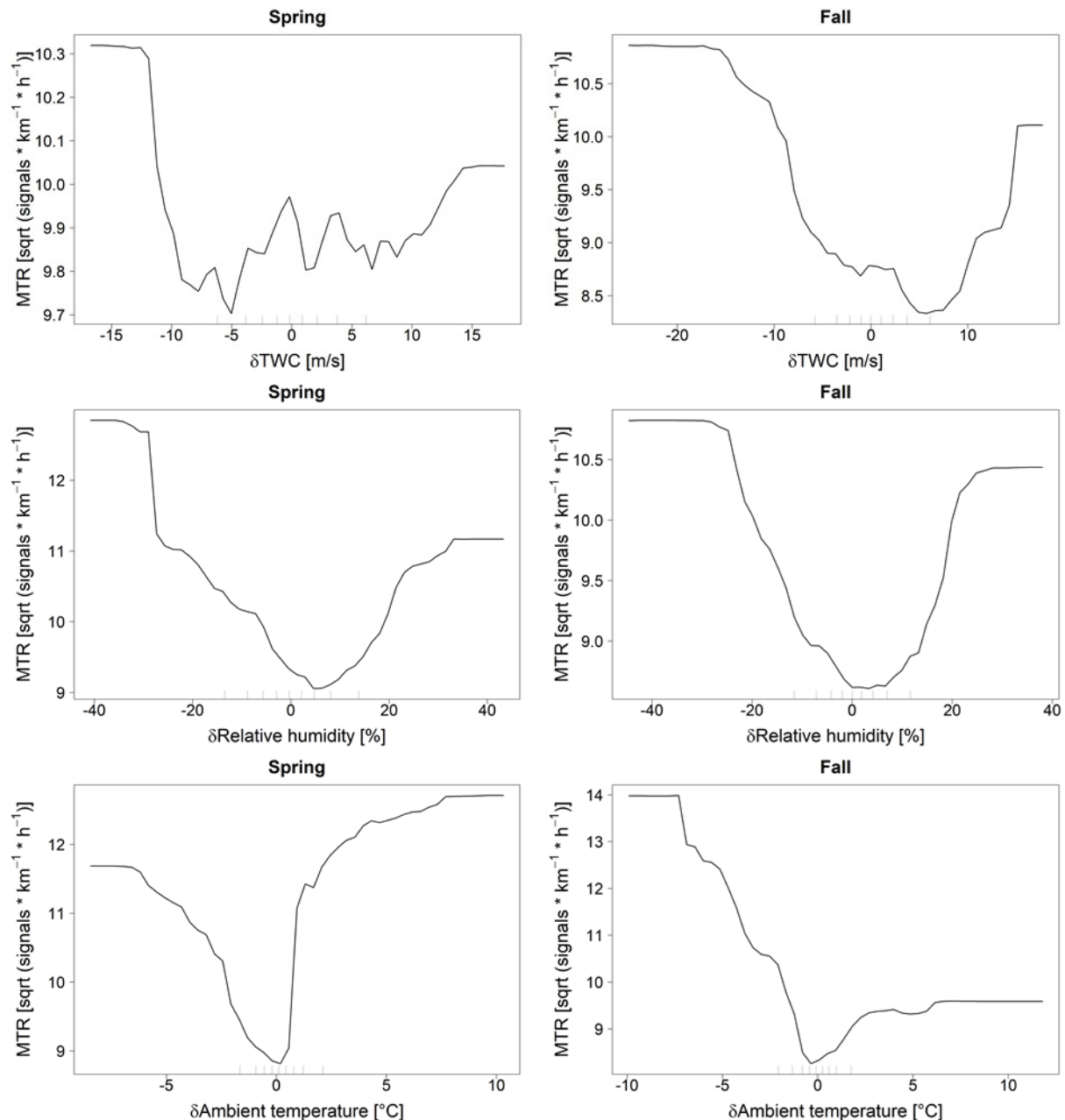


Figure 4-8 Partial dependence plots of the 24h-change variables δ TWC, δ relative humidity and δ ambient temperature for RF models on migration intensities (MTR up to 1,000 m). Results for spring and fall migration are shown in left and right panels, respectively.

The same was true for changes in ambient temperature in spring (Figure 4-8). MTRs increased considerably with positive temperature changes but also when temperatures decreased by more than

2°C within 24 h. In contrast, in fall a marked increase of flux rates only occurred when temperatures decreased.

We also found contrasting relationships of MTR with δ barometric pressure between seasons (Figure 4-9). While in spring flux rates increased when barometric pressure decreased within the previous 24 h, in fall the opposite was true. Here, MTR continuously increased with increasing positive change in barometric pressure. On the other hand, a negative change in pressure had no effect on flux rate.

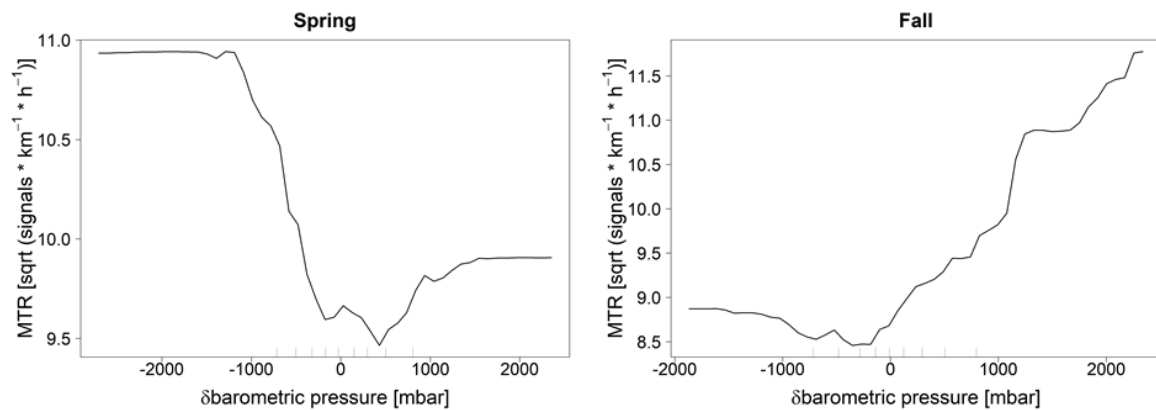


Figure 4-9 Partial dependence plots of 24h-change in barometric pressure for RF models on migration intensities (MTR up to 1,000 m). Results for spring and fall migration are shown in left and right panels, respectively.

The effect of δ TWC (Figure 4-10) and δ barometric pressure (Figure 4-11) on flight height was also roughly U-shaped. In contrast, δ relative humidity and δ ambient temperature were negatively related to flight height in both seasons (Figure 4-10).

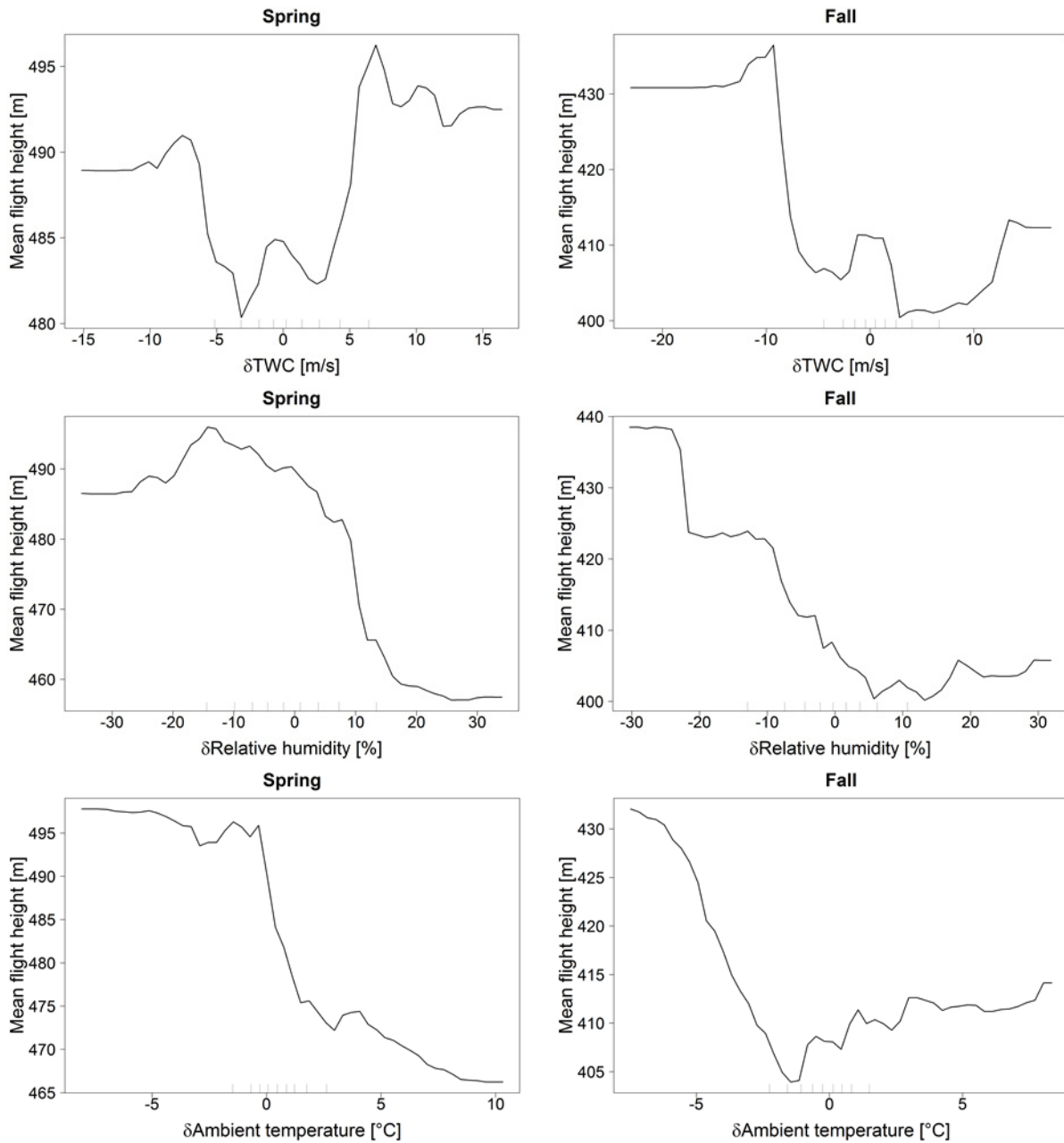


Figure 4-10 Partial dependence plots of the 24h-change variables δTWC , δ relative humidity and δ ambient temperature for RF models on flight height. Results for spring and fall migration are shown in left and right panels, respectively.

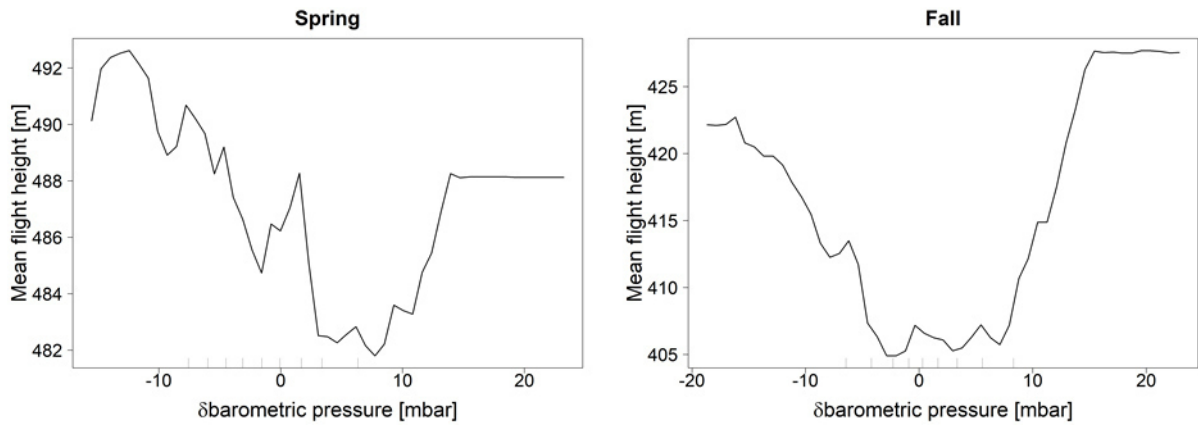


Figure 4-11 Partial dependence plots of 24h-change in barometric pressure for RF models on flight height. Results for spring and fall migration are shown in left and right panels, respectively.

Migration intensity

Migration intensity was by far the most important explanatory variable in models on flight height (Figure 4-1). In both spring and fall there was a strong positive relationship between the two variables (Figure 4-12). Flight height was higher in time periods with high migration activity.

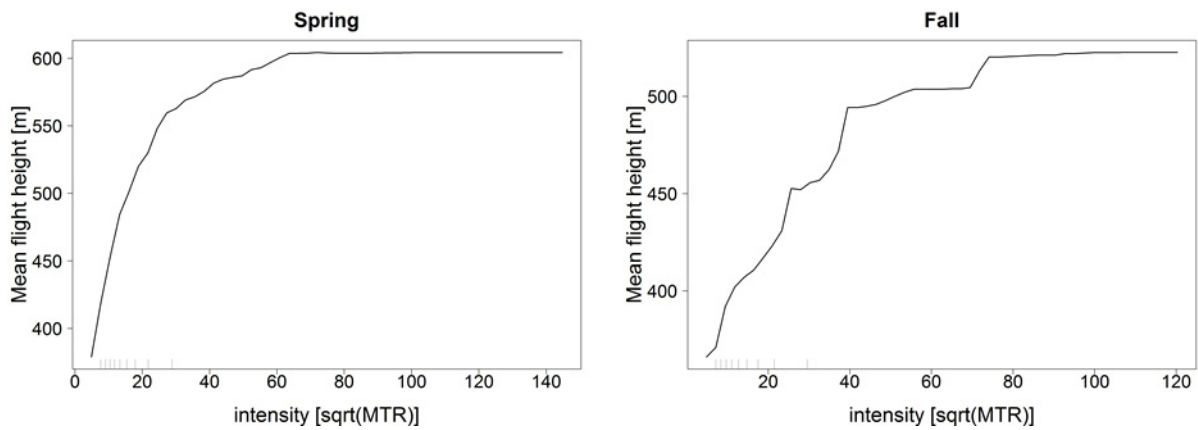


Figure 4-12 Partial dependence plots migration intensity for RF models on flight height. Results for spring and fall migration are shown in left and right panels, respectively.

Time variables

Julian day, which reflects the temporal pattern of migration within the season, was an important predictor in both spring and fall (Figure 4-1). In spring, flux rates were highest between mid-March and late April. In fall, the time period with highest migration activity lay between late September and early November (Figure 4-13).

Julian day also had a strong effect on flight height, particularly in spring (Figure 4-13). Here, flight height continuously increased in the course of the season. In fall, flight height slightly decreased for large part of the season and seemed highly variable towards the end of fall migration in November (Figure 4-13).

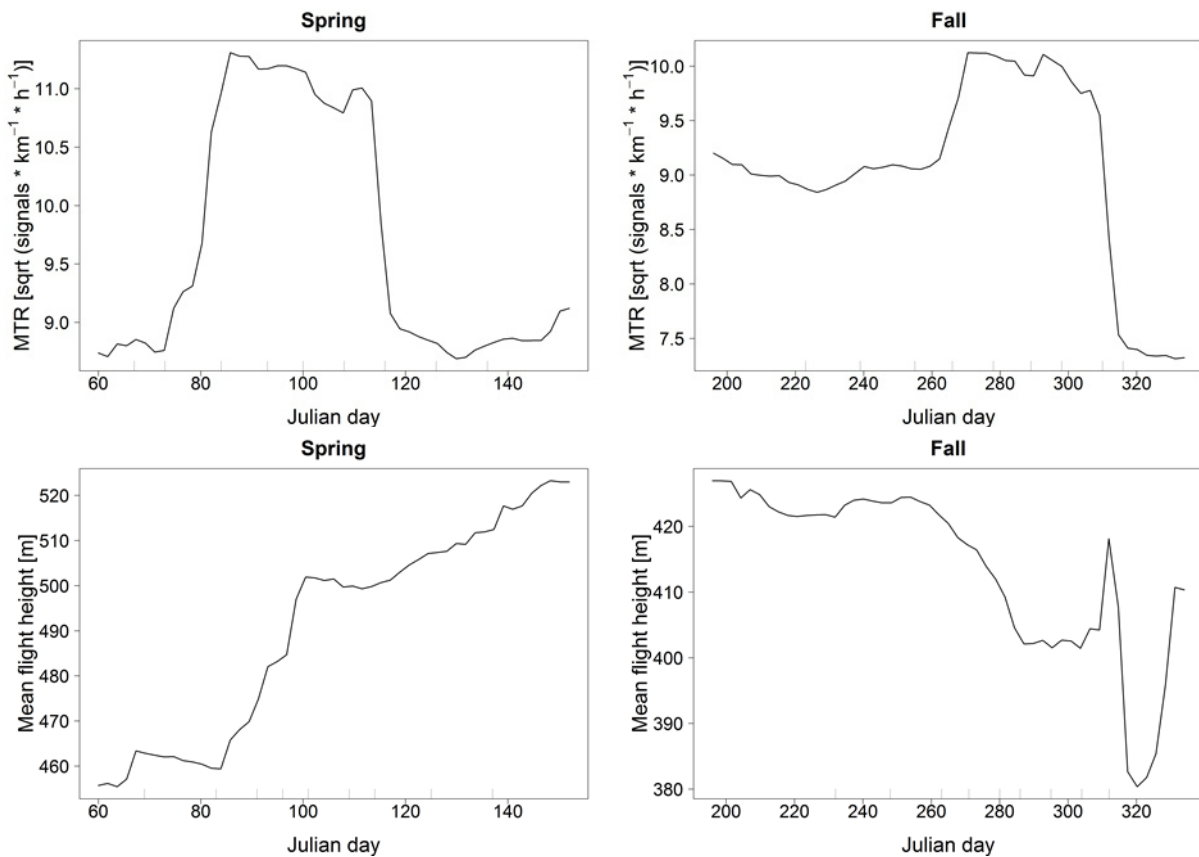


Figure 4-13 Partial dependence plots of Julian day for RF models on migration intensities (MTR up to 1,000 m, upper panels) and flight height (lower panels). Results for spring and fall migration are shown in left and right panels, respectively.

There were also strong patterns of both migration intensities and flight height within the night (Figure 4-14). Migration intensities increased considerably within the first quarter of the night in spring and fall. During spring migration, flux rates stayed high for the remaining night while in fall MTRs decreased to some extent in the inner part of the night and increased again before sunrise.

On the other hand, flight height decreased notably in the first half of the night with a slight increase shortly before sunrise in both seasons (Figure 4-14).

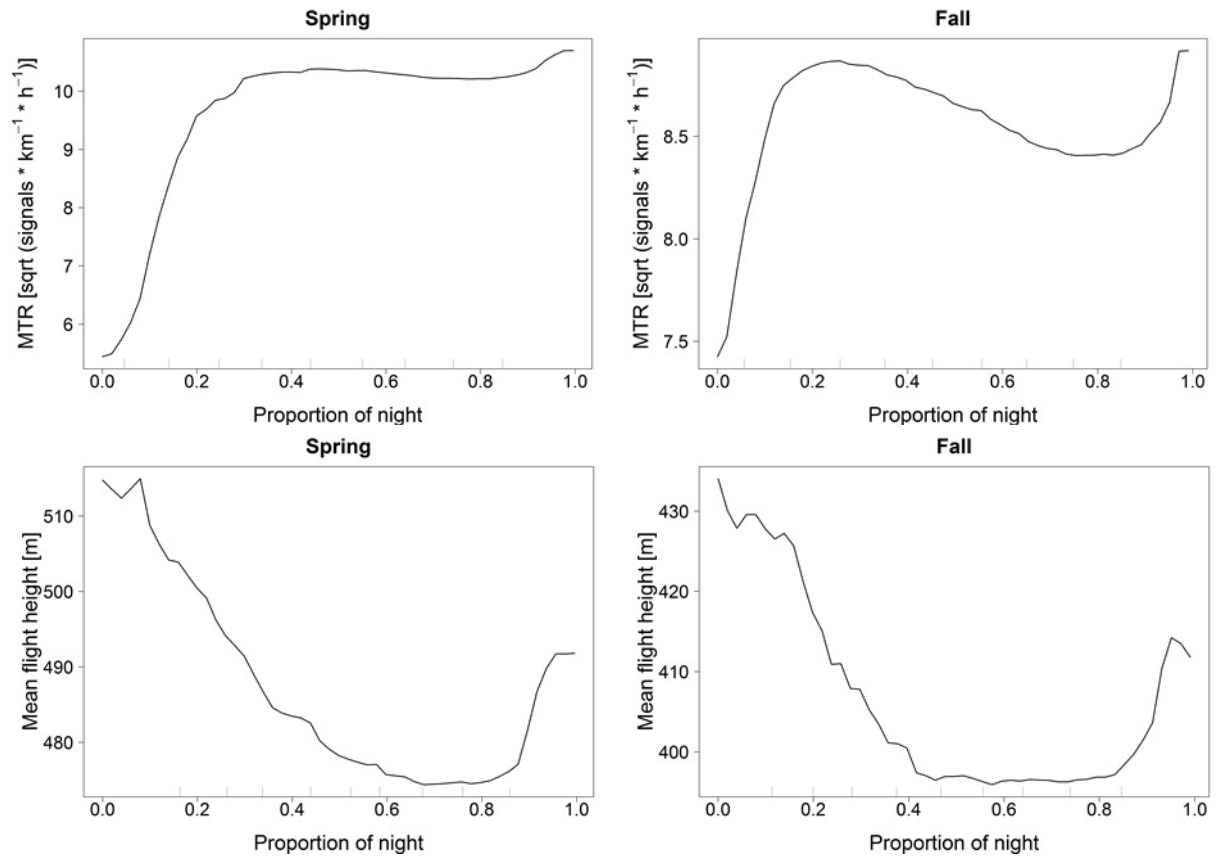


Figure 4-14 Partial dependence plots of the proportion of night for RF models on migration intensities (MTR up to 1,000 m, upper panels) and flight height (lower panels). Results for spring and fall migration are shown in left and right panels, respectively.

Interactions

Interaction plots of TWC with Julian day show how the effect of TWC changes in the course of the season. In both spring and fall the effect of TWC on migration intensities and flight height remained relatively constant throughout the migration seasons (Figure 4-15). Solely at the end of fall migration the effect of TWC seemed negligible.

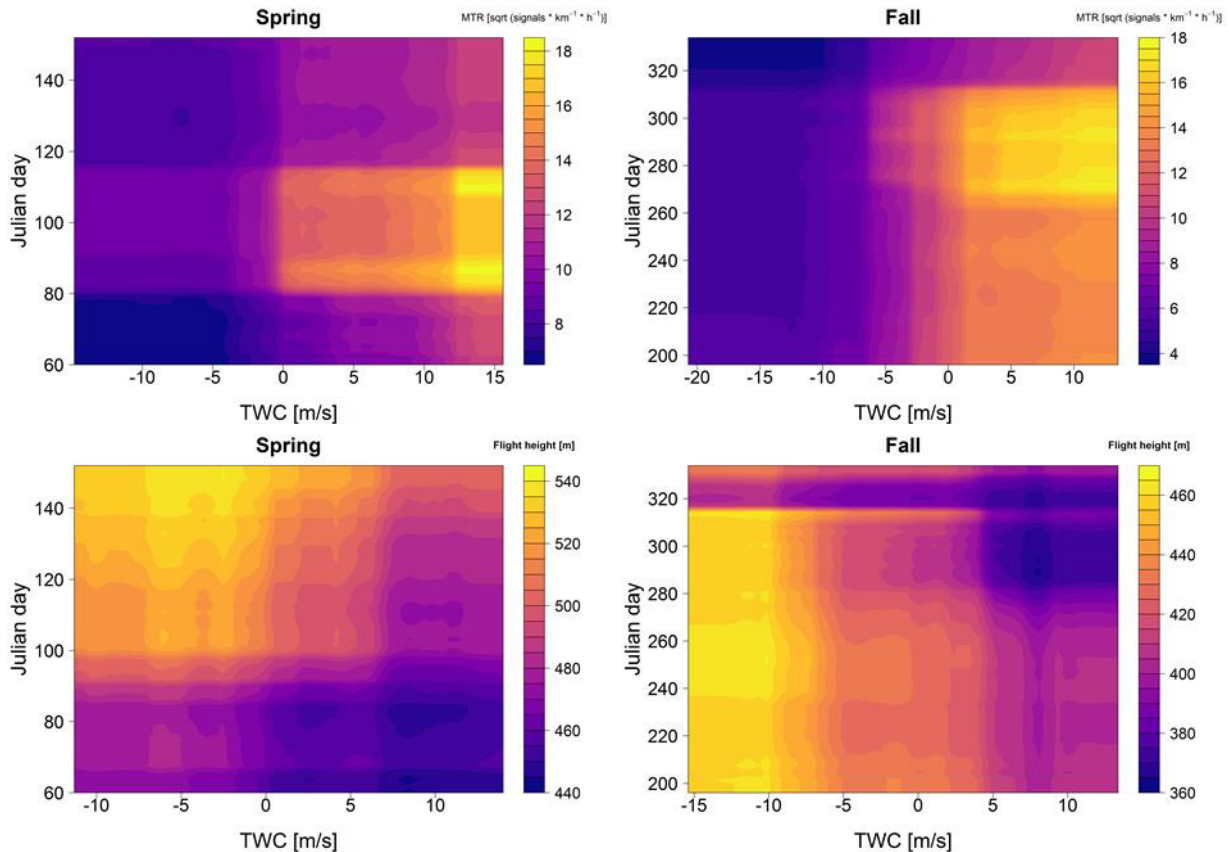


Figure 4-15 Interaction plots of TWC with Julian day for RF models on migration intensities (MTR up to 1,000 m, upper panels) and flight height (lower panels). Results for spring and fall migration are shown in left and right panels, respectively.

Interaction plots between TWC and CWC indicated a strong interaction between the two wind components in spring but not in fall (Figure 4-16). In spring, positive TWC resulted in high migration intensities primarily when they coincided with highly negative CWC. Likewise, negative TWC led to low flux rates when CWC was positive. Given the assumed migration direction of 45° in spring, high migration intensities were chiefly related to strong southerly, low migration intensities to strong northerly winds.

In contrast, in fall high TWC values resulted in high migration intensities independently of CWC.

With respect to flight heights, the interaction of wind components showed a different pattern (Figure 4-16, lower panel). In spring, flight height was highest when negative TWC concurred with negative CWC. This combination corresponds to easterly winds. Positive TWC with simultaneous negative CWC (westerly winds) resulted in low flight heights.

Similarly, in fall low flight heights also occurred when both TWC and CWC were highly positive. However, as positive CWC in fall corresponds to south-easterly winds, low flight heights were related to easterly winds.

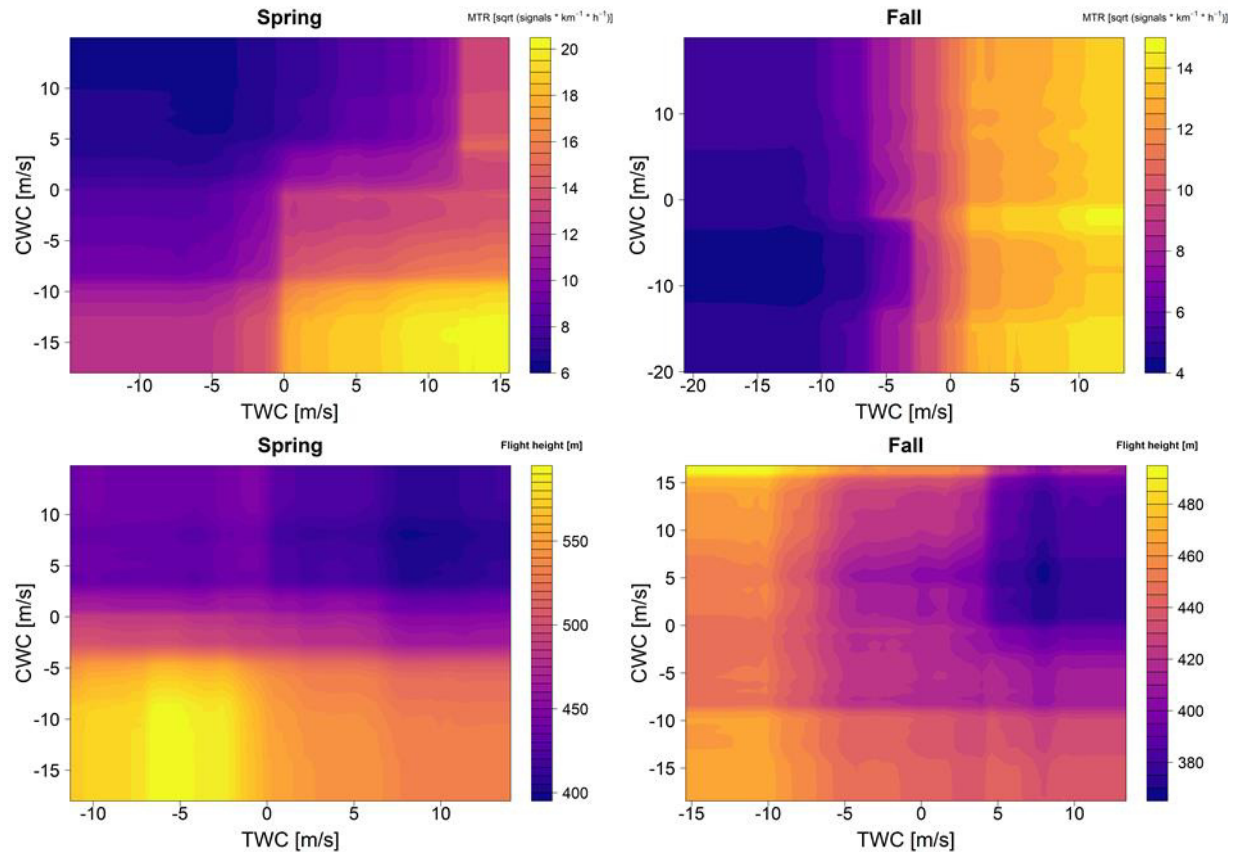


Figure 4-16 Interaction plots of TWC with CWC for RF models on migration intensities (MTR up to 1,000 m, upper panels) and flight height (lower panels). Results for spring and fall migration are shown in left and right panels, respectively.

Interaction plots of temperature vs. Julian day suggested that the effect of temperature on MTRs was most prominent during the first part of the migration season in both spring and fall (Figure 4-17). In spring, the effect of temperature seemed highest until mid-March (approx. day 80) with a strong increase of MTR above about 6°C. In contrast, toward the end of the spring season in May the effect of temperature on MTR was negligible. Similarly, in fall the effect of temperature was limited to the first half of the season, while during peak migration in October and the end of the season in November migration intensity was largely independent of ambient temperature. The effect of temperature on mean flight height was relatively constant throughout the spring season. In fall, temperature had only minor influence on flight height which was restricted to the first half of the season.

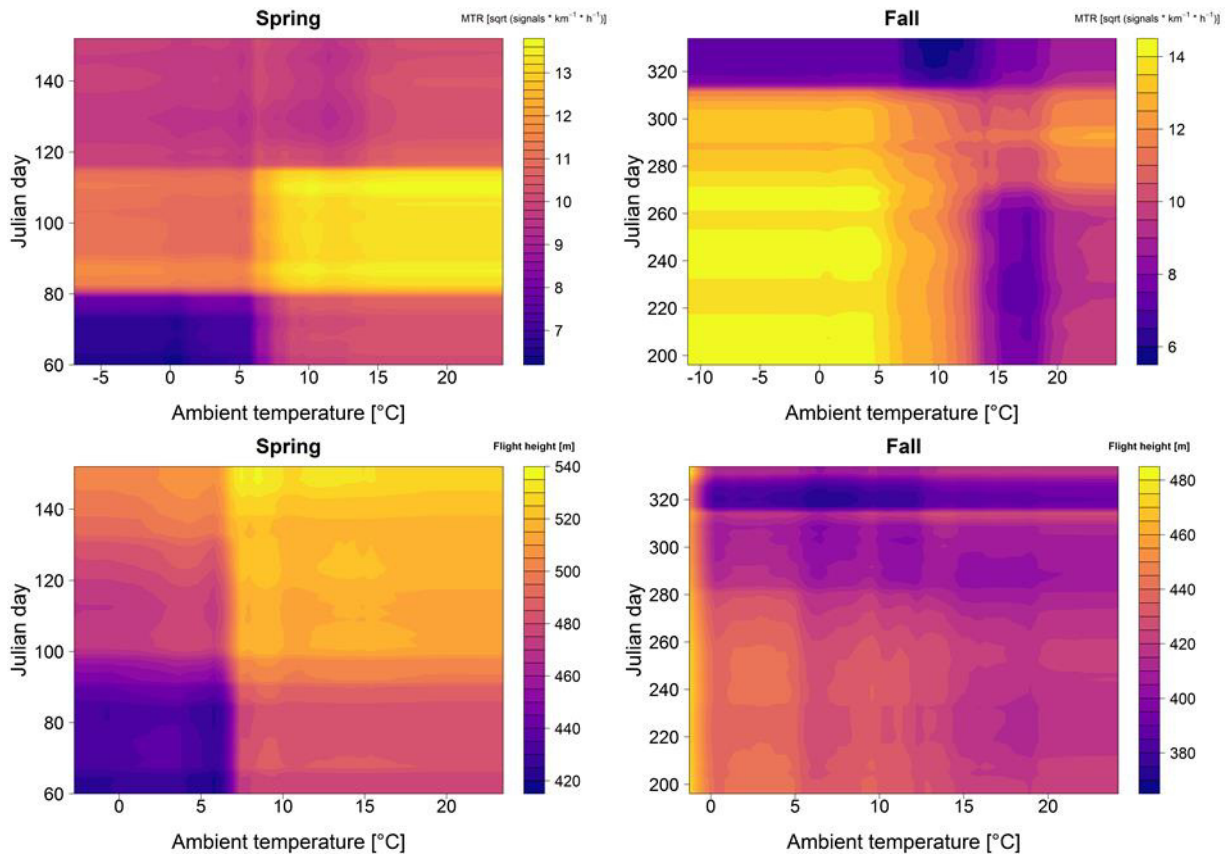


Figure 4-17 Interaction plots of ambient temperature with Julian day for RF models on migration intensities (MTR up to 1,000 m, upper panels) and flight height (lower panels). Results for spring and fall migration are shown in left and right panels, respectively.

Factorial variables year, project, phase and lab

Of the additional factorial variables (year, project, phase and lab) included in the full models, year and project were important predictors of MTR indicating high variability of migration intensities across years and locations (Figure 4-18, Figure 4-19 and Figure A 2). In contrast, the role of developmental phase of wind farms and the lab responsible for data collection was minor (Figure 4-20, Figure 4-21 and Figure A 2) with little variation in MTRs between factor levels. The same pattern applied to models on flight height (Figure 4-18 to Figure 4-21, Figure A 2).

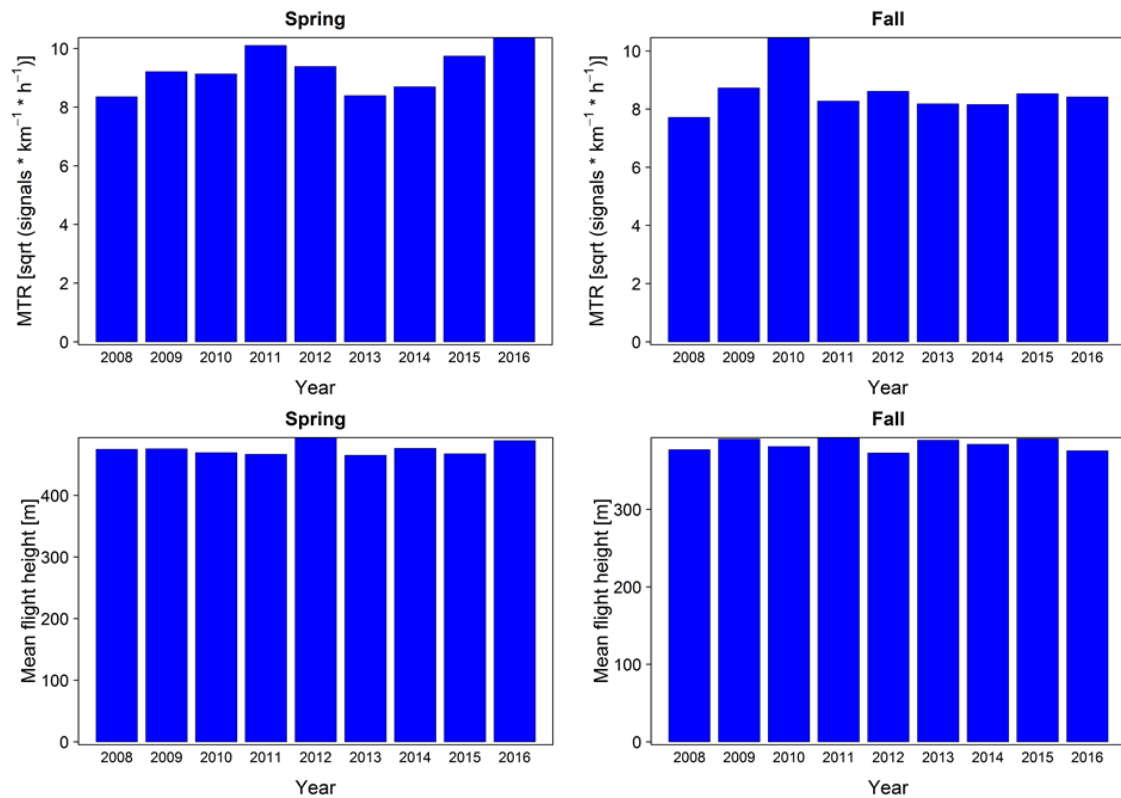


Figure 4-18 Partial dependence plots of the factor “year” for RF models on migration intensities (MTR up to 1,000 m, upper panels) and flight height (lower panels). Results for spring and fall migration are shown in left and right panels, respectively.

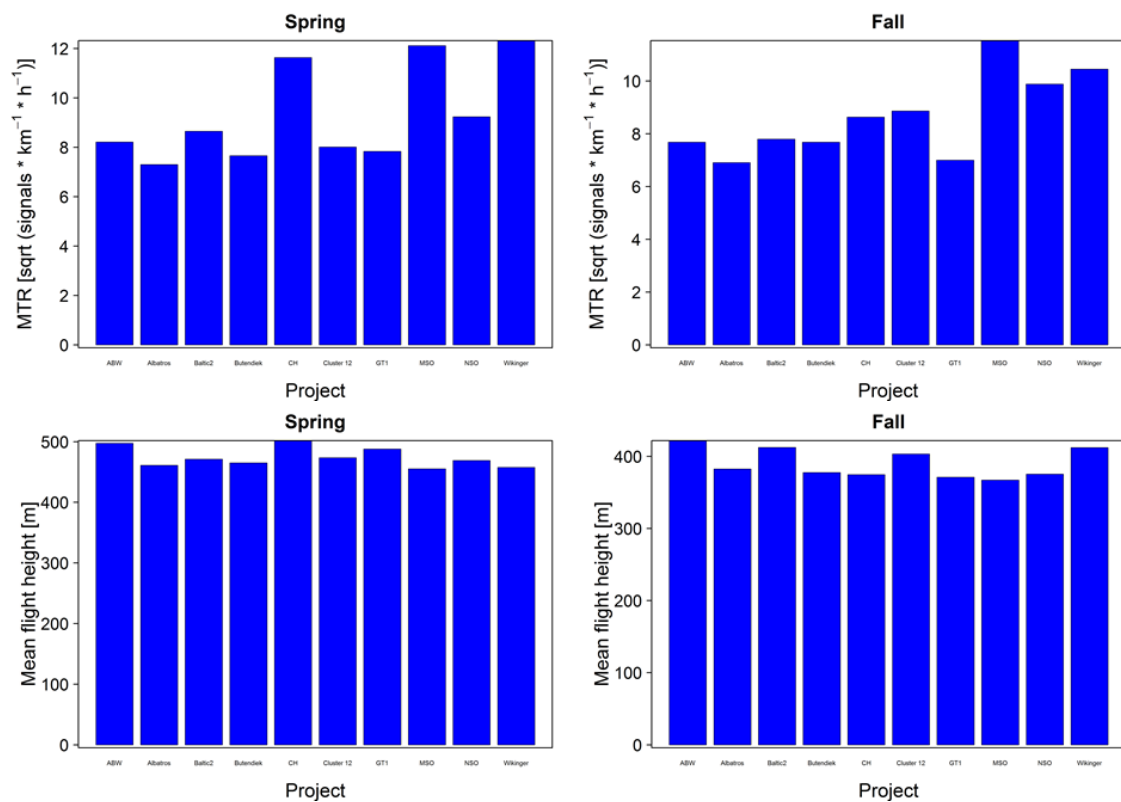


Figure 4-19 Partial dependence plots of the factor “project” for RF models on migration intensities (MTR up to 1,000 m, upper panels) and flight height (lower panels). Results for spring and fall migration are shown in left and right panels, respectively.

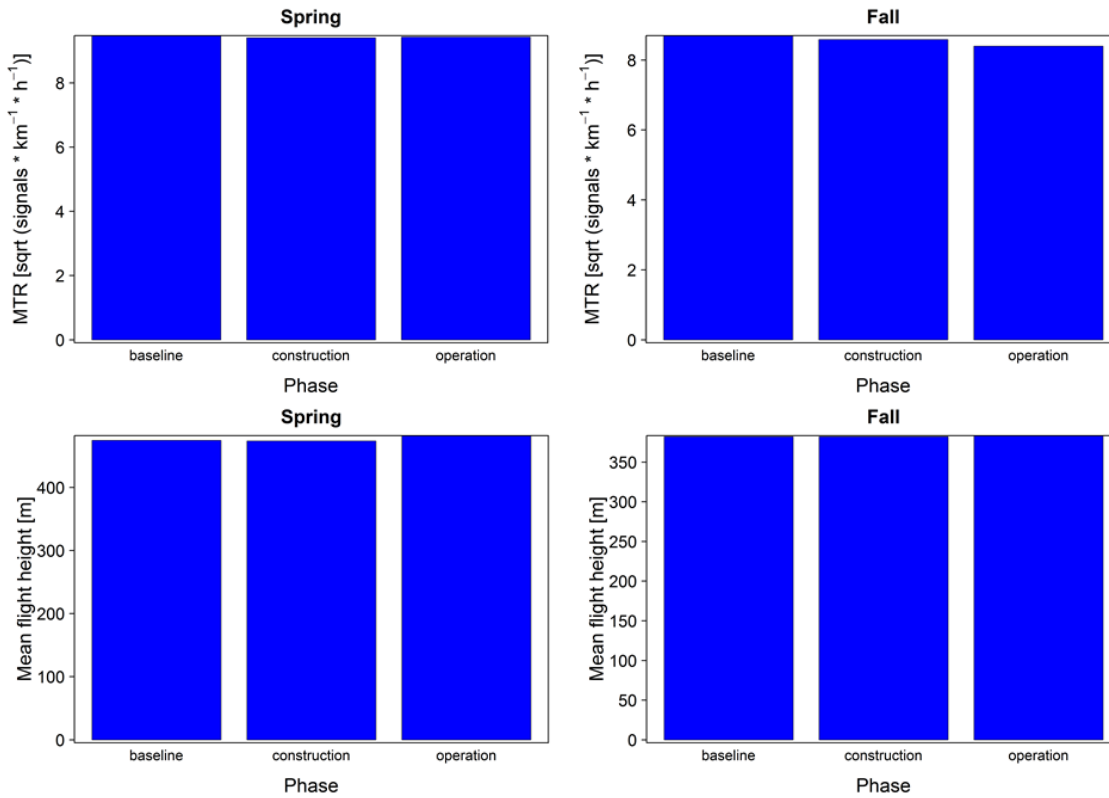


Figure 4-20 Partial dependence plots of the factor “phase” for RF models on migration intensities (MTR up to 1,000 m, upper panels) and flight height (lower panels). Results for spring and fall migration are shown in left and right panels, respectively.

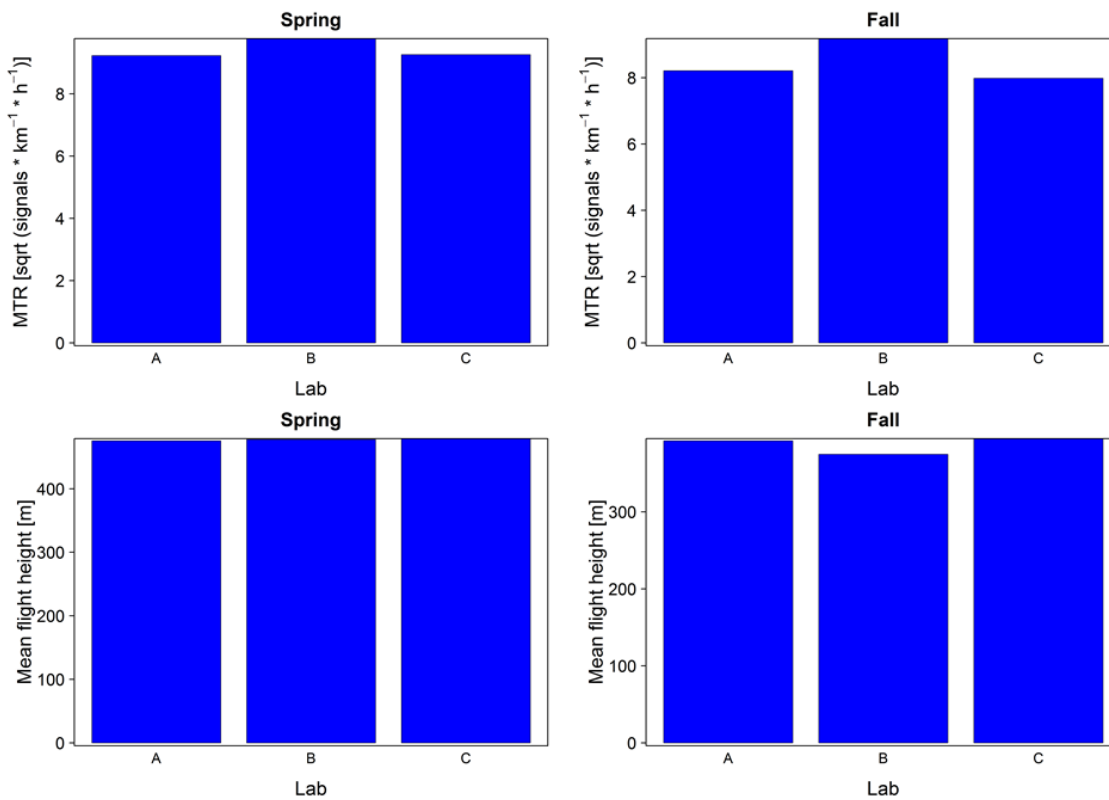


Figure 4-21 Partial dependence plots of the factor “lab” for RF models on migration intensities (MTR up to 1,000 m, upper panels) and flight height (lower panels). Results for spring and fall migration are shown in left and right panels, respectively.

4.2 Prediction of migration intensities

Cross-validations showed good performance of the predictive models. The unbiased R^2 of the models was 0.38 and 0.40 for spring and fall, respectively, i.e. the models constructed on the training datasets explained about 40% of the variance in the validation datasets.

There was also a high correlation between predicted and observed MTRs in both seasons (Figure 4-22). This was consistent across all years and seasons (Figure 4-23 and Figure 4-24).

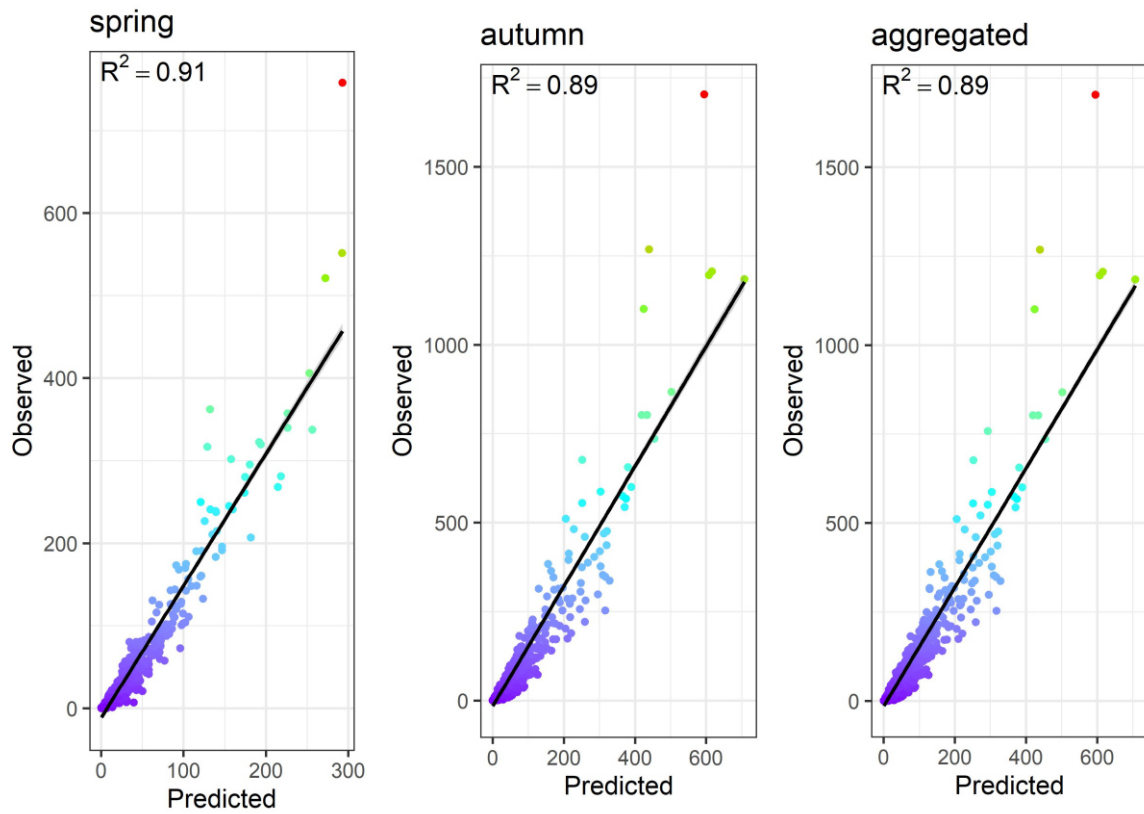


Figure 4-22 Observed and predicted migration intensities (MTR) for spring, fall and both seasons combined. Data from all study years are included.

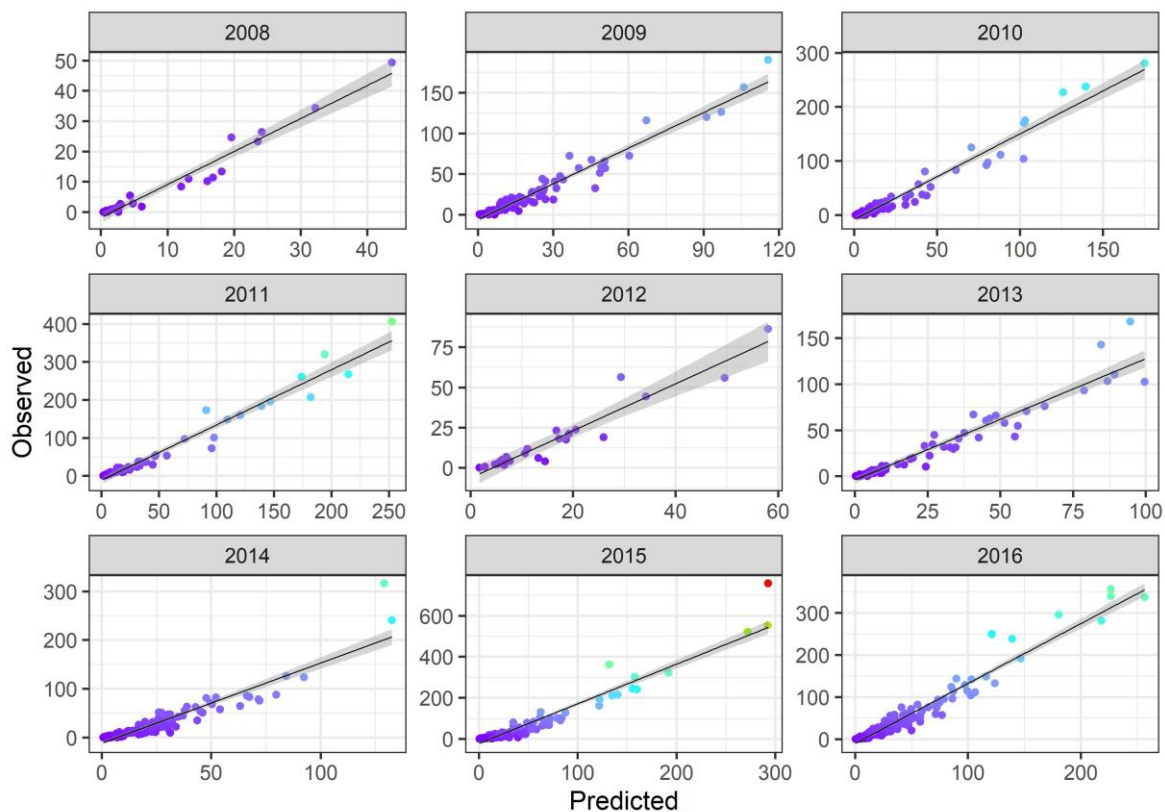


Figure 4-23 Scatterplots of observed and predicted migration intensities (MTR) in spring for all study years separately.

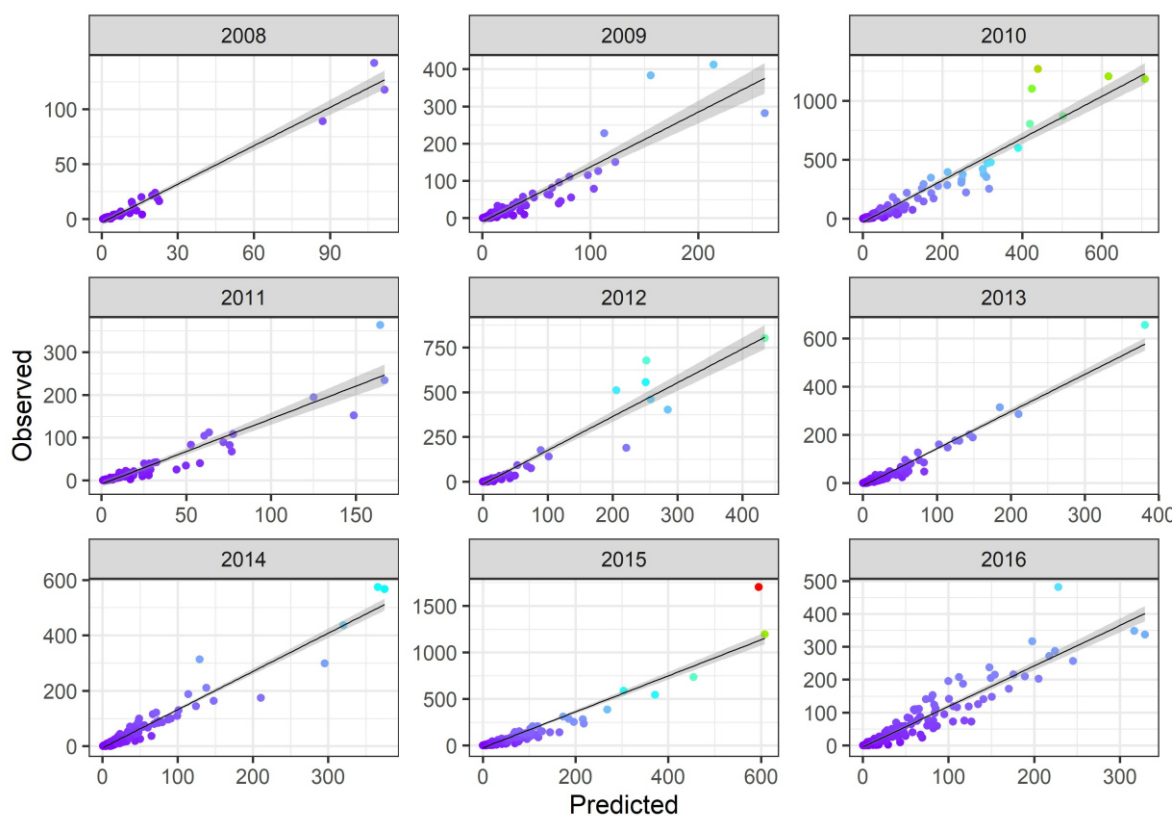


Figure 4-24 Scatterplots of observed and predicted migration intensities (MTR) in fall for all study years separately.

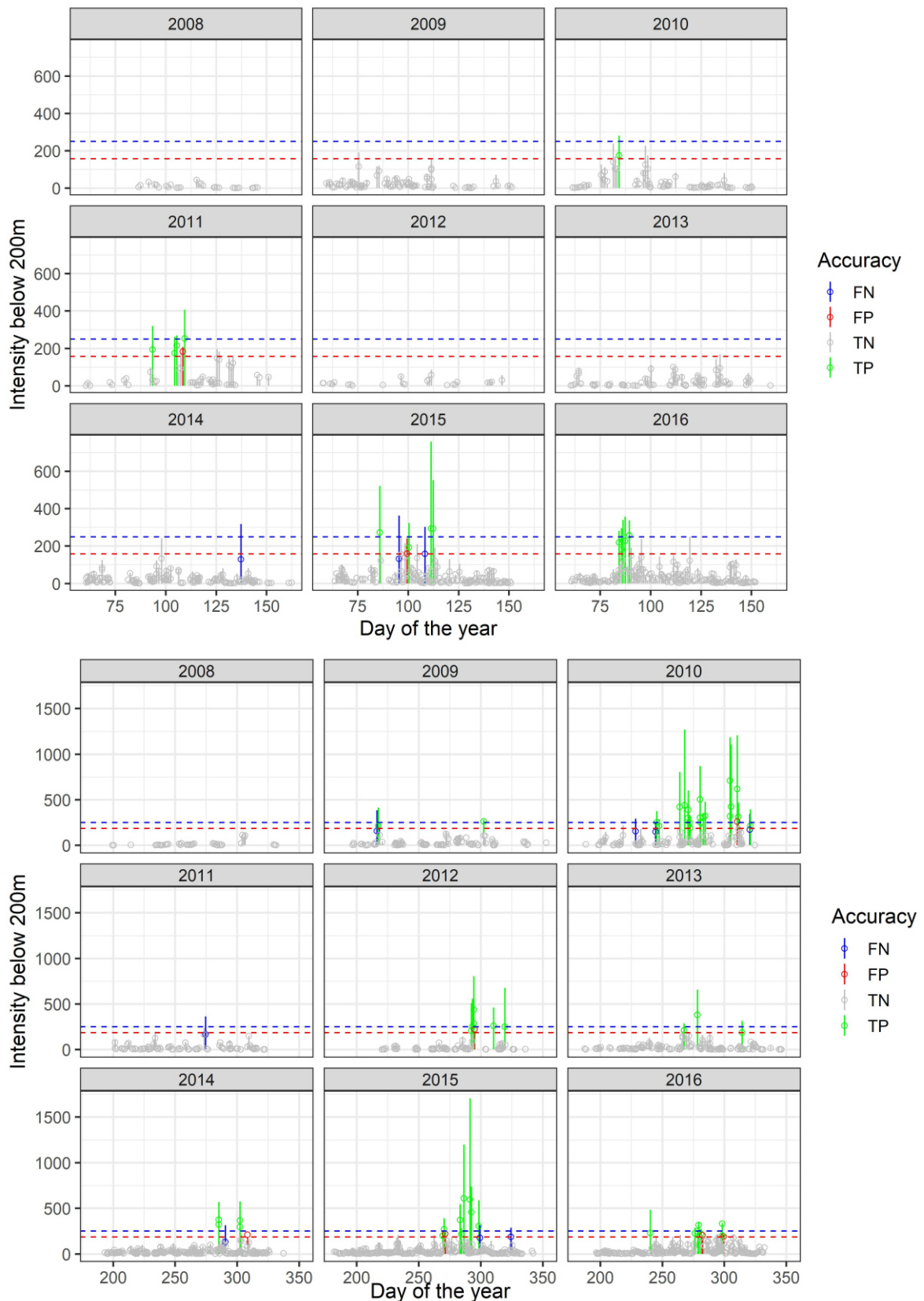


Figure 4-25 Observed and predicted migration intensities (MTR) in spring (upper panels) and fall (lower panels) for all study years with bars indicating the observed and open symbols the predicted values. In addition, the performance of the model in predicting nights with high migration intensities (>250 MTR) is indicated (FN = false negatives, FP = false positives, TN = true negatives, TP = true positives). The dashed blue line represents the threshold for observed values (250 MTR), the dashed red line is the optimized threshold for predicted values (157.7 MTR (spring) and 185.4 MTR (fall), see chap. 3.2.2).

However, our models seemed to systematically underpredict migration intensities particularly in nights with high flux rates (Figure 4-22 to Figure 4-24). Consequently, the accuracy of the model to predict events of high migration intensities (>250 MTR) was relatively low (Figure A 22 and Figure A 23). Only 29% and 58% of high migration events were predicted correctly (Table 4.2). This was mainly due to a high rate of false negatives. Optimizing the threshold value for predictions according to Cohen’s Kappa resulted in a substantially higher rate of correctly classified events of high migration intensity (spring: 82%, fall: 86%) while the rate of false positives was still low (Table 4.3, Figure 4-25).

Table 4.2 Confusion matrices of the observed and predicted classification of migration intensity exceeding the threshold of 250 MTR for spring (left) and fall (right). The cells represent true negatives (upper left), false positives (upper right), true positives (lower right) and false negatives (lower left).

Spring			Fall		
Predicted \ Observed	0	1	Predicted \ Observed	0	1
0	759	0	0	1179	1
1	12	5	1	24	33

Table 4.3 Confusion matrices of the observed and predicted classification of migration intensity exceeding the threshold of 250 MTR for spring (left) and fall (right). The threshold for predictions was optimized by maximizing Cohen’s Kappa (see chap. 3.2.2). The cells represent true negatives (upper left), false positives (upper right), true positives (lower right) and false negatives (lower left).

Spring			Fall		
Predicted \ Observed	0	1	Predicted \ Observed	0	1
0	757	2	0	1174	6
1	3	14	1	8	49

4.3 Coincidence of high migration intensities and unfavorable weather

Overall, high migration intensities coincided only very rarely with weather conditions considered unfavorable for nocturnal bird migration (Table 4.4). During weather conditions of moderate headwinds ($TWC \leq -5$ m/s) and concurrent poor sight (humidity $\geq 95\%$) only 4 hours with migration intensities above 250 MTR were recorded. This corresponds to 0.02% of all available hours or less than 0.5 h per year in the study area.

Table 4.4 Coincidence of high migration intensities and unfavorable weather. Given is the number and percentage of hours in which migration intensity was above three different thresholds for “high migration intensities” and in which three different levels of unfavorable weather conditions prevailed. Results are based on data from all available radar sites.

	MTR >250	MTR >500	MTR >750
All weather conditions			
Hours below threshold	16,163	16,639	16,767
Hours above threshold	744	268	140
% above threshold	4.40	1.59	0.83
weather: $TWC \leq -7$ m/s OR humidity $\geq 95\%$			
Hours above threshold	58	28	17
% above threshold	0.34	0.17	0.10
weather: $TWC \leq 0$ m/s AND humidity $\geq 90\%$			
Hours above threshold	56	24	15
% above threshold	0.33	0.14	0.09
weather: $TWC \leq -5$ m/s AND humidity $\geq 95\%$			
Hours above threshold	4	1	0
% above threshold	0.02	0.01	0.0

Furthermore, the percentage of hours >250 MTR did not exceed 0.4% even when “unfavorable” weather conditions were defined less strict (Table 4.4). Also, considering higher thresholds for high migration intensities (>500 MTR and <750 MTR) resulted in markedly lower percentages of hours with concurrent unfavorable weather conditions.

Regarding only data from platform-based surveys did not considerably alter these results. In fact, the number of hours with unfavorable weather conditions during which the different thresholds for high migration intensities were exceeded was consistently lower than when the whole dataset was considered (Tab. A 1).

4.4 Collision risk models

The cumulative number of collision fatalities of nocturnal migrants at German offshore wind farms during the migration periods was estimated between approx. 8,000 and 35,000 birds depending on the avoidance rate assumed (Table 4.5). This corresponds to between 5.6 and 24.4 casualties per turbine and year for the whole German EEZ. About 11.2% of estimated collisions were related to non-passerines. As we assumed a proportion of 90% passerines in our models (see chap. 3.2.4) this suggests a slightly higher collision risk of non-passerine birds.

Table 4.5 Total estimated number of collisions of nocturnal migrants for all OWFs currently in operation or under construction in the German EEZ. Numbers reflect estimated collisions during the migration periods (spring and fall) per year (see text for details). In addition, mean collisions per turbine [\pm SE, range] is given.

Avoidance rate	Total number of collisions			Collisions per turbine		
	passerines	non-passerines	total	passerines	non-passerines	total
0.956	30,964	3,931	34,895	21.66 \pm 1.9 [8.5 - 45.1]	2.75 \pm 0.3 [1.1 - 5.7]	24.41 \pm 2.14 [2.1 - 50.8]
0.980	14,075	1,787	15,862	9.85 \pm 0.9 [3.9 - 20.5]	1.25 \pm 0.1 [0.5 - 2.6]	11.10 \pm 1.0 [1.0 - 23.1]
0.990	7,037	893	7,930	4.92 \pm 0.4 [1.9 - 10.3]	0.62 \pm 0.1 [0.3 - 1.3]	5.55 \pm 0.5 [2.2 - 11.5]

Due to the higher number of turbines in the North Sea, about 80% of all collisions were estimated to occur in that region (Table 4.6). However, the number of collisions per turbine was about 50% higher in the Baltic compared to the North Sea.

Within spring migration, the highest number of collisions was calculated to occur in March and April (

Table 4.7). In May, the number of estimated fatalities was considerably lower with only 25% of collisions compared to March.

During fall, estimated collisions peaked in October (

Table 4.7). In this month more collisions (52%) were modelled to occur than during all other months of fall migration combined. With respect to both migration seasons, 36% of fatalities can be expected in October alone.

Table 4.6 Total estimated number of collisions of nocturnal migrants and mean collisions per turbine for OWFs in the German EEZ of the North Sea and Baltic Sea. Numbers reflect estimated collisions during the migration periods (spring and fall) per year (see text for details). The wind farms included in each region are given in Tab. A 3.

Avoidance rate	Total number of collisions			Collisions per turbine		
	North Sea	passerines	non-passerines	total	passerines	non-passerines
0.956	24,873	3,158	28,032	20.34	2.58	22.92
0.980	11,306	1,436	12,742	9.25	1.17	10.42
0.990	5,653	718	6,371	4.62	0.59	5.21
Baltic Sea						
0.956	6,091	773	6,863	30.46	3.86	34.32
0.980	2,768	351	3,120	13.85	1.76	15.60
0.990	1,384	176	1,560	6.92	0.88	7.80

Table 4.7 Monthly estimated number of collisions of nocturnal migrants and mean collisions per turbine per month combined for all OWFs currently in operation or under construction in the German EEZ.

Month	Total number of collisions			Collisions per turbine		
	0.956	0.980	0.990	0.956	0.980	0.990
March	5,001	2,273	1,137	3.45	1.57	0.79
April	4,460	2,027	1,014	3.11	1.42	0.71
May	1,230	559	280	0.85	0.39	0.19
July	513	233	117	0.36	0.16	0.08
August	1,591	723	362	1.16	0.50	0.25

Month	Total number of collisions			Collisions per turbine		
	0.956	0.980	0.990	0.956	0.980	0.990
September	4,194	1,906	953	2.88	1.31	0.65
October	12,649	5,749	2,875	8.84	4.02	2.01
November	5,258	2,390	1,195	3.81	1.73	0.87

As the estimated number of collisions is linearly related to the number of birds passing the wind farms, collision fatalities were concentrated on nights/hours with high migration intensity (Table 4.8). Thus, during the hours with the highest migration intensities (>750 MTR) 17.8% of all collisions were estimated to occur even though such high flux rates were reached in only 0.7% of the time corresponding to about 15 h per year. That means that shutting down turbines during these hours would theoretically result in the prevention of between 1,400 and 6,200 collisions per year depending on the avoidance rate applied (Table 4.8) or between 1.0 and 4.4 collisions per turbine. Likewise, according to the models almost half of all collisions (47.5%) happen in hours during which migration intensity exceeds 250 MTR equalling a total of 90.5 h per year.

Table 4.8 Total number of collisions and collisions per turbine for different thresholds of migration traffic rates (MTR). In addition, the proportion of collisions that occur when MTR was above different thresholds, the proportion of time and the absolute number of hours that MTRs were above thresholds is given. Except for the total number of collisions the mean ±SE [range] of all single wind farms is given.

MTR threshold	Avoidance rate	Total number of collisions	Collisions per turbine	% collisions	% time above threshold	Hours per year above threshold
>100	0.956	25,137	17.5 ±1.9 [3.4 - 38.8]	72.0 ±2.1 [35.6 - 81.5]	11.2 ±0.9 [2.9 - 21.3]	251.6 ±21.1 [65.9 - 477.7]
	0.980	11,426	8.0 ±0.9 [1.6 - 17.6]			
	0.990	5,713	4.0 ±0.4 [0.8 - 8.8]			
>250	0.956	16,571	11.6 ±1.4 [1.1 - 23.6]	47.5 ±2.6 [11.9 - 62.3]	4.0 ±0.4 [0.5 - 7.5]	90.5 ±9.0 [10.8 - 167.8]
	0.980	7,532	5.3 ±0.6 [0.5 - 10.7]			
	0.990	3,766	2.6 ±0.3 [0.3 - 5.4]			

MTR threshold	Avoidance rate	Total number of collisions	Collisions per turbine	% collisions	% time above threshold	Hours per year above threshold
>500	0.956	9,457	6.6 ±1.0 [0.0 – 14.8]	27.1 ±2.6 [0.0 – 43.9]	1.4 ±0.2 [0.0 – 3.2]	30.9 ±3.9 [0.0 – 72.5]
	0.980	4,299	3.0 ±0.4 [0.0 – 6.7]			
	0.990	2,149	1.5 ±0.2 [0.0 – 3.4]			
>750	0.956	6,199	4.4 ±0.7 [0.0 – 11.1]	17.8 ±2.3 [0.0 – 32.9]	0.7 ±0.1 [0.0 – 1.8]	14.7 ±2.3 [0.0 – 40.9]
	0.980	2,818	2.0 ±0.3 [0.0 – 5.0]			
	0.990	1,409	1.0 ±0.2 [0.0 – 2.5]			

Of all the input parameters of the Band model avoidance rates (AR) had by far the largest impact on estimated collision fatalities (Table 4.9).

Assuming an avoidance rate of 0.98 (the upper range estimated by SCHULZ et al. (2014) for nocturnal migrants at offshore turbines) led to a decrease of estimated casualties by 54.5% compared to an AR of 0.956 (the lower range estimated by SCHULZ et al. (2014)). Adopting an AR of 0.99 (KRIJGSVELD et al. 2015) resulted in a reduction of collision numbers by 77% and 50% in comparison to an AR of 0.956 and 0.98, respectively. Collision estimates derived with an AR of 0.999 as has been reported for some diurnally active seabird species (SKOV et al. 2018) amount to only 2.3% of estimates calculated with an AR of 0.956.

Assumptions made regarding turbine-related and other bird-related parameters had less impact on collision estimates (Table 4.9). With respect to the mean rotation speed of turbines, models applying the rotation speed at nominal power (13 rpm, mean for all turbine types) instead of the actual mean rotation speed (10.3 rpm, based on the limited information available to us) led to only 1.4% higher collision estimates. Models with a mean blade pitch angle of 20° (the default value of the Band model) resulted in 8.7% lower collision estimates compared to an angle of 7° as applied in our models.

Of the bird-related input parameters, the proportion of upwind flights had the highest potential influence on estimated collision numbers (Table 4.9). Assuming an upwind proportion of 7.9% as estimated by SCHULZ et al. (2014) caused the number of fatalities to decline by 14% in comparison to an upwind proportion of 30% adopted in our approach (see chap. 3.2.4). On the other hand, applying a proportion of 50% upwind flights as is the default value of the Band model resulted in a 10% increase of estimated collisions.

Uncertainty about the bird-related parameters flight speed, bird length and wing span overall had only a minor effect on estimated casualties (Table 4.9). Assuming a 15% slower flight speed for passerines (10.0 m/s instead of 11.8 m/s) and non-passerines (15.2 m/s instead of 17.9 m/s) increased collision risk on average by only 1.0%. Similarly, if mean wing span and body length were

taken to be 15% larger for passerines and non-passerines the collision risk would increase on average by only 0.5% and 2.4%, respectively.

Overall, results from models implementing month-specific flight height distributions varied only marginally from results derived with the mean flight height distribution over all months. Monthly flight height distributions resulted in on average 0.7% higher collision numbers than the combined flight height. The difference varied between months and wind farms (depending on turbine dimensions) with a maximum deviation of up to $\pm 8\%$. Whereas applying the monthly height distribution resulted in higher collision risk estimates in March, September and November, it led to lower estimated collision numbers in May, July, August and October.

Table 4.9 Effect of variation of the different input parameters of the Band model on estimated collisions. The values of input parameters used in the models for this report are given as well as alternative values and the deviation of estimated collision numbers [%] for the whole year. In addition, the range of deviation with respect to estimates for single months and wind farms is given.

Parameter	Value in original models	Alternative value(s)	Deviation overall	Deviation range
Turbine related				
Rotation speed [rpm]	10.3	13	+1.4%	+1.2% - 2.9%
Pitch angle [°]	7	20	-8.7%	- 8% - -11%
Bird related				
Flight speed [m/s]	11.8 / 17.9	10.0 / 15.2	+1.0%	+0.8% - 2.0%
Bird length [m]	0.175 / 0.375	0.201 / 0.431	+2.4%	+2.2 - 2.5%
Wing span [m]	0.290 / 0.700	0.334 / 0.805	+0.5%	+0.4 - 0.6%
Flight height distribution	monthly	overall mean	-0.7%	$\pm 8\%$
Proportion upwind flights [%]	30	7.9 / 50	-14% - +10%	-15% - +11%
Avoidance rate	0.956	0.98/0.99/0.999	-54.5% - -97.7%	-54.5% - -97.7%

5 DISCUSSION

This study is based on data on nocturnal bird migration obtained by marine surveillance radars that have been operated at 10 different sites in the German EEZ in the North and Baltic Sea over a period of nine years. This multi-site, multi-year dataset constituted a suitable basis for assessing the effects of weather on offshore nocturnal bird migration and allowed for the first time the estimation of the cumulative collision risk at German offshore wind farms.

However, several limitations of the data have to be considered when interpreting the results of this study. First and foremost, the use of marine surveillance radar as a means to record bird movements has never been thoroughly validated or calibrated with other dedicated bird radars (WENDELN et al. 2007; URMY & WARREN 2017; LIECHTI et al. 2018; NILSSON et al. 2018). As has been discussed in detail elsewhere (WELCKER 2019), migration intensities reported here have therefore to be treated with caution and have to be regarded as a relative measure of flux rates until further validation.

Furthermore, several factors presumably inflated the variability of the data. Radars used for data collection were of different type, different labs and personnel were involved in data collection and processing, and data were obtained at different stages of wind farm development. The effects of these factors have also been discussed in more detail in an earlier report from this project (WELCKER 2019) and they also likely hampered the predictive performance of the weather models reported here (see below).

In this study, bird migration was recorded up to a height of 1,000 m. This height range was devised by StUK (BSH 2013) and reflects the limitations of the radars deployed. However, data from radars with larger detection ranges show that bird migration at or close to the study sites also takes place well above 1,000 m height. Flight height distributions from the Baltic Sea (Fehmarn, Rügen and FINO2), the North Sea (FINO1) and the Netherlands suggest that on average about 30% of nocturnal migrants fly above 1,000 m (FEBI 2013; KEMP et al. 2013; SCHULZ et al. 2013, 2014; BRUDERER et al. 2018). Consequently, the migration intensities reported in this study consistently underestimated actual migration intensities of the whole altitude range. Due to high day-to-day variation in flight heights (KEMP et al. 2013; BRUDERER et al. 2018) the degree of the underestimation is not constant in time. Thus, the incomplete recording of bird migration by the marine surveillance radars added additional noise to the data with corresponding negative effects on the explanatory and predictive performance of the models in this study.

5.1 Weather models

We used NCEP Reanalysis 2 weather data available from NOAA Earth System Research Laboratory's Physical Sciences Division at a 2.5° spatial and a 6 h temporal resolution (see also KANAMITSU et al. 2002). Data were interpolated in both space and time to derive values for each specific site and each hour of observations. The reanalysis data fully covered all study periods and, hence, no data had to be dismissed due to missing weather observations. In contrast, in-situ weather observations were not conducted during all time periods and were, in particular, missing for all platform-based observations of bird migration. In addition, reanalysis data comprised potentially important variables such as barometric pressure and relative humidity, not available from in-situ observations, and also allowed the calculation of 24h-change of weather parameters.

However, there were also several drawbacks related to the reanalysis data in comparison to in-situ observations. First, due to the interpolation of the data local variation of weather parameters was likely underestimated. Second, reanalysis data did not contain information on cloud cover, an important variable explaining variation in bird call rates of nocturnal migrants (WELCKER & VILELA 2018), and on precipitation which earlier studies have shown to affect nocturnal migration intensities (ERNI et al. 2002; VAN BELLE et al. 2007). In addition, our data did not include a direct measurement of visibility, another potentially important factor affecting bird migration. To some extent, relative humidity may serve as a proxy for visibility, as humidity $\geq 95\%$ is highly associated with fog, drizzle and rain (HÜPPOP & HILGERLOH 2012). Yet, the inclusion of a direct measure of visibility may have enhanced the performance of our models.

Nonetheless, weather and time variables alone explained more than 70% of the variance in our data on nocturnal migration intensities. This was comparable to other single and multi-site studies (ZEHNDER et al. 2001; ERNI et al. 2002; VAN BELLE et al. 2007; VAN DOREN & HORTON 2018). Additionally included factorial explanatory variables such as study site, study year, phase and lab increased the proportion of explained variance by 6% to close to 80%. This suggests that the importance of these variables was limited and most of the variance was explained by weather and time alone. Models on migration intensities up to 200 m height had slightly less explanatory power compared to models up to 1,000 m height. This might be related to the fact that atmospheric (and time) variables not only affect flux rates but also flight height (KEMP et al. 2013). Our weather data reflected conditions at 10 m altitude, no information was available as to variation in conditions with increasing height. However, wind conditions in particular are likely to vary within the flight range of the birds which may select flight height accordingly (KEMP et al. 2013). Thus, flux rates at a small altitude range close to the surface not only depend on weather conditions close to the surface but also on conditions higher up for which we could not account for in our models.

This could also be an explanation for why models on flight height performed less well. Here, weather and time variables explained only about 50% of the variance. Information on changes in atmospheric conditions with altitude would presumably improve flight height models.

Wind condition was the primary factor affecting migration intensities in both spring and fall (ALERSTAM 1979; RICHARDSON 1990; LIECHTI & BRUDERER 1998; ERNI et al. 2002; VAN BELLE et al. 2007). Specifically, migration intensities increased steeply with increasing tailwind. Yet, our results suggest that in fall birds tolerated moderate headwinds to a larger degree than in spring. Given the predominance of westerly and south-westerly winds in the study area supporting winds occur substantially less often in fall compared to spring. Thus, in fall the costs of delaying migration might exceed more often the energetic costs of migrating with moderate headwinds than in spring resulting in the observed pattern (KARLSSON et al. 2011; HÜPPOP & HILGERLOH 2012).

The relationship of flux rates with CWC indicated that during spring migration intensities were highest with strong seaward (i.e. south-easterly) crosswinds. High offshore migration intensities coinciding with a strong seaward wind component are probably a consequence of wind drift which is assumed to happen more often in nocturnal than diurnal migrants (LIECHTI 2006). Furthermore, our results show a strong interaction between TWC and CWC in spring suggesting that the interplay of wind components is a main driver of nocturnal migration intensities offshore. The highest migration activities at the offshore sites were the result of the co-occurrence of a strong TWC and a strong seaward CWC corresponding to southerly winds. Conversely, when high TWC coincided with a strong landward CWC (i.e. westerly winds) offshore migration intensities remained low. During fall however, the effect of CWC on flux rates was minor with only a weak indication of increasing

migration intensities with seaward crosswinds (see also BRUST et al. 2019). Accordingly, interaction plots indicated that TWC was the dominating wind-related factor determining migration intensities in fall independently of CWC.

Overall, nocturnal migrants tended to prefer high barometric pressure and low relative humidity, conditions which at the study sites are usually associated with clear skies, moderate winds and no precipitation. Thus our results corroborate earlier studies which have reported similar relationships (ZEHNDER et al. 2001; ERNI et al. 2002; VAN BELLE et al. 2007; VAN DOREN & HORTON 2018). However, in spring there was also a tendency for migration intensities to increase when barometric pressure was low. This may be related to the wind regime in low pressure systems in the area where decreasing air pressure between a warm and cold front is often associated with south or south-western winds (RICHARDSON 1990).

Temperature was a predictor variable of only moderate importance in our models. Yet, there were distinct patterns between migration intensities and temperature which contrasted between spring and fall. Spring migration intensities increased with increasing temperatures, particularly at temperatures of 6°C and above, and increased with decreasing temperature in fall. It has been suggested that temperature is an important driver of the general disposition of birds to migrate but has less influence on the decision to migrate in a specific night (BERTHOLD 2000). The shape of the relationship with temperature in our study is in line with this notion and may also explain why temperature apparently had only limited impact on the decision of birds to migrate during a particular night. Also other local studies found little evidence of temperature affecting nocturnal flux rates to a large degree (ZEHNDER et al. 2001; VAN BELLE et al. 2007). Yet, a recent continental-scale study identified temperature as the most important predictor of migration intensities (VAN DOREN & HORTON 2018). Even though there is usually agreement between studies with respect to the general effects of atmospheric variables on bird migration (RICHARDSON 1990; BERTHOLD 2000), local conditions are bound to cause differences between single sites. Accordingly, VAN BELLE et al. (2007) showed that local models cannot be easily transferred to other sites. Hence, the spatial scale considered may also affect the importance of different predictors.

The intrinsic temporal pattern of migration activity which varies between migratory species, determines the seasonal migration phenology which, in turn, determines the general number of birds disposed to migrate. This has been accounted for by the inclusion of Julian day in the models. However, the actual number of birds ready to depart at any one night may depend on the weather conditions during the previous night(s). Migrants may accumulate at the departure sites if unfavorable weather conditions prevented their departure during one or more consecutive nights. Likewise, the number of birds departing may be low even during favorable conditions if such conditions had already prevailed for several days.

We calculated an accumulation factor following ERNI et al. (2002) based on unfavorable local wind conditions. This factor appeared to have relatively high importance in our models in fall but not in spring. The shape of the relationship differed between spring and fall which may reflect seasonal differences in the prevalence of opposing winds. In spring, migration intensities dropped after several days with favorable conditions, while in fall intensities increased sharply after several days with unfavorable winds.

Precipitation and accumulation of migrants due to rain have been shown to be important predictors of bird migration in the past (RICHARDSON 1990; ERNI et al. 2002). Unfortunately, data on rain at the study sites was not available and hence we could not consider this factor. However, as rain impairs

the detectability of birds by the marine surveillance radars, these data as such are not suitable to fully evaluating the effect of rain on nocturnal migration.

With respect to flight height, migration intensity was the most important predictor variable in our models. Flight height was strongly positively correlated with flux rates (see also WELCKER 2019). As high migration intensities are associated with favorable weather conditions this suggests that under favorable conditions nocturnal migrants tend to fly higher.

Variation in flight height was less well explained by atmospheric conditions than migration intensity itself. Several factors may account for this. Firstly, we used mean flight height as the response variable. To ensure reliable means and to avoid introducing additional noise we included only hours with at least 10 radar raw signals. By doing so we indirectly excluded hours with very low migration intensities and hence introduced a bias with potential consequences on model performance. Secondly, as discussed above, our data were truncated at 1,000 m height which may exclude as much as one third of the migration activity (BRUDERER et al. 2018). Finally, we had no information as to the species composition of nocturnal migration at the study sites. The composition of migratory species is likely to vary considerably within a season and different species may have different flight height preferences. Thus, seasonality of species composition may be an important factor affecting patterns of flight height independent of weather conditions (LA SORTE et al. 2015).

The relationships between meteorological variables and flight height were mostly comparable to their effect on migration intensity which might be expected given the correlation between flight height and flux rates. However, there were also noticeable differences, particularly related to TWC. In both seasons, mean flight height increased with decreasing TWC, i.e. flight height was higher during headwinds. This is at odds with the general notion that birds fly lower when facing opposing winds (RICHARDSON 1990; KEMP et al. 2013). The cause of this pattern is unclear. One potential explanation may be related to the fact that we calculated TWC based on wind speed and direction close to sea level (10 m a.s.l.). Wind conditions at other altitudes may differ and nocturnal migrants are known to select flight altitudes accordingly (BRUDERER et al. 1995; LIECHTI et al. 2000; SCHMALJOHANN et al. 2009). Thus, our results may suggest that when wind conditions are unfavorable at sea level birds may choose to fly at higher altitudes where conditions may be superior. The pattern might be further enhanced by the fact that our data on flight height excluded hours with low migration intensities. I.e. moderate or high migration intensities during strong headwinds at sea level may only occur in situations in which wind conditions at higher altitudes are less unfavorable.

Our results also showed temporal trends in flight heights. Mean flight height decreased in the course of the night until shortly before sunrise. A similar pattern has been reported earlier (BRUDERER & LIECHTI 1998; FORTIN et al. 1999; HÜPPOP et al. 2004; WELCKER 2019), yet its cause is not fully understood. The decrease of flight heights during the night is accompanied by a similar decrease in migration intensities (FORTIN et al. 1999; ZEHNDER et al. 2001; HÜPPOP et al. 2004, 2009). As most nocturnal migrants initiate migration around sunset this suggests that birds often do not migrate throughout the whole night (BRUDERER & LIECHTI 1998). Hence, the decrease of flight altitudes in the course of the night might reflect an increasing proportion of birds preparing to land.

In addition, our data indicate opposing seasonal trends of flight heights in spring and fall. Mean flight height increased in the course of spring season but decreased with time in fall. It has been hypothesized that systematic seasonal changes in wind regime at mid-latitudes, specifically an increase in speed of westerly winds at higher altitudes in fall may prompt migrants to progressively

migrate at lower altitudes in the course of the season (LA SORTE et al. 2015). A similar but oppositional trend in wind conditions may then cause increasing flight heights in spring. Alternatively, and as discussed above, seasonal changes in flight height may be related to seasonality of the species composition of nocturnal migrants and variation in their migration behavior and preferred flight heights. With respect to nocturnally migrating passerines, presumably the by far most numerous species group at our study sites, the species composition early in spring and late in fall is dominated by short-distance migrants while in late spring and early fall long-distance migrants are predominant. Hence, the observed pattern might be caused by differences in preferred flight height between these groups of species.

5.2 Prediction of migrating intensities

Explaining about 40% of the variance in validation datasets, the performance of the predictive models was good. This resulted in very high correlations between predicted and observed migration intensities. This was despite the fact that our data likely contained substantial noise caused by several factors such as the use of different radar devices and the involvement of different labs in data acquisition and processing. A higher degree of standardization at these levels would presumably result in less residual error and better predictive power of the models. Furthermore, we attempted to predict migration intensities below 200 m altitude as this constitutes the altitude range of interest with respect to effects of offshore wind farms. As variance in flux rates at this small altitude range was less well explained by atmospheric variables, the predictive performance of models for the whole altitude range would likely be higher.

In accordance with earlier attempts to predict nocturnal migration intensities, our models tended to underpredict high flux rates (VAN BELLE et al. 2007; VAN DOREN & HORTON 2018). It appears that a crucial factor causing particularly high migration intensities has not yet been accounted for in these models. The nature of this factor remains speculative.

The underestimation of high migration intensities caused a relatively low accuracy of models predicting nights in which a given threshold of migration intensity was exceeded (in our case 250 MTR). However, optimizing the threshold value for predictions (optimization of Cohen's Kappa) increased the accuracy of predictions (true positives) from 30-60% to about 85% while keeping the rate of false positives low (11-13%, see chap. 4.2). Thus, the application of the models may provide ample indication of whether an event of mass migration is likely to occur during the following night(s). Yet, predictions seem not accurate enough for models regulating potential turbine curtailment directly. It has also to be kept in mind that any forecast of future migration activity would not only contain the error of modelling migration but also the potential error of the weather forecasts the migration model would have to be based on. This additional error will deflate the accuracy of predictions reported here.

We used the threshold value of 250 MTR (for the altitude range up to 200 m) for our predictions of nights with high migration intensities. An empirical definition of "mass migration" or "events of high migration intensity" utilizing the distribution of the data proved to be impossible (WELCKER 2019) and, hence, any definition of threshold values has to be based on other considerations. We chose 250 MTR as the threshold because it was exceeded in only 3.7% of the nights. We regarded this as a suitable proportion to represent nights with high migration intensities. Also, the threshold value was exceeded in a sufficient number of nights for the models to perform well. Threshold values which are exceeded in only very few instances resulted in poor model performance.

5.3 Collision risk

We attempted for the first time to estimate the cumulative number of collision fatalities of nocturnal migrants at offshore wind farms in the German EEZ. Despite the fact that collision risk and the potential impairment of bird migration is regarded by German authorities as one of the main potential environmental impacts of OWFs, little is known with respect to the number of collisions of these birds let alone potential impacts on population level. This knowledge gap is mainly due to the lack of direct information on collisions at sea and the unfeasibility of carcass searches offshore. Up to now, collision risk models are therefore the only possibility to obtain estimates of collision fatalities.

We applied the SOSS Band model (BAND 2000, 2012) to estimate collision mortality, the most widespread mechanistic model (MASDEN & COOK 2016) which is also regularly used to estimate collisions of seabirds at OWFs. Although the Band model constitutes a convenient tool, an essential drawback is the difficulty to validate the model. Model validation is, as of now, virtually impossible for offshore wind farms, and attempts to validate the model onshore have yielded ambiguous results (DE LUCAS et al. 2008; FERRER et al. 2012; EVERAERT 2014; GRÜNKORN et al. 2016; KLEYHEEG-HARTMAN et al. 2018).

Model outcome is highly sensitive to input parameters. Sensitivity analyses have identified bird speed, rotor diameter and rotation speed as key parameters determining collision risk in the absence of avoidance behavior (CHAMBERLAIN et al. 2006; MASDEN 2015). However, variation of $\pm 10\%$ in these and other turbine-related parameters usually resulted in changes of estimated collisions of substantially less than 10% (MASDEN 2015). These findings are corroborated by our results. Conversely, our data suggest that variation in the proportion of upwind flights, a parameter with a high degree of uncertainty, may cause changes in estimated mortality of $>10\%$. The default value usually applied for resident birds is 50%. However, it seems reasonable to assume that the directional movements of migratory birds that prefer tailwind conditions lead to a higher proportion of downwind flights. With 30% upwind flights we chose a conservative approach, the only published estimate for nocturnal migrants being as low as 7.9% (SCHULZ et al. 2014). A proportion of upwind flights as low as this would result in about 15% lower estimated collision fatalities.

Virtually all input parameters of our models except the number and dimensions of wind turbines were subject to uncertainty. Uncertainty about bird-related input parameters arose mainly due to a lack of information about the species composition of nocturnal migrants. Our estimates of bird morphology and flight speed were based on mean values of the main species known to migrate through the study area. We could not consider the fact that species composition varies in the course of the seasons and consequently the mean size and speed of the birds. However, the resulting error is presumably low as our sensitivity analysis showed only marginal differences in estimated fatalities when bird parameters varied as much as 15%.

There was also uncertainty about turbine-related input parameters such as mean rotation speed and blade pitch angle as well as the monthly proportion of operational time. The effect of the latter parameter is strictly proportional, i.e. a 10% decrease in operational time will result in a 10% decrease of estimated collisions. The relatively high value of 92.5% operational time applied in our models was based on information from a limited number of OWFs and did not take into consideration potential temporal variation of operational time. Operation time will vary annually and seasonally and also depends on maintenance plans that are likely to differ between wind farms. The mean operational time is presumably lower in months with lower average wind speed such as May,

July and August and higher in months with high wind speed (e.g. March, October, November), but it seems unlikely that the overall effect on estimated collisions exceeds 10%. Effects of uncertainty in rotation speed and pitch angle are likely to be negligible (MASDEN 2015). According to our sensitivity analysis, assuming a mean rotation speed as high as the maximum rotation speed would result in only 1-2% higher collision estimates. Similarly, even an unrealistically high mean pitch angle of 20° reduced modelled collisions by only about 9%.

The input parameter having by far the largest effect on model outcome was the assumed avoidance rate. This has been shown in multiple previous studies and was also corroborated by our results (CHAMBERLAIN et al. 2006; MASDEN 2015; COOK et al. 2018; KLEYHEEG-HARTMAN et al. 2018). Information on avoidance behavior of nocturnal migrants is very scarce. To our knowledge, the only estimate for nocturnal migrants based on empirical data has been published by SCHULZ et al. (2014). Their estimate was based on a combination of radar and camera data and contained a considerable margin of uncertainty (0.956 - 0.980). It also reflected within wind farm behavior only. However, as the authors found indication for an attraction effect on nocturnal migrants in their study, the inclusion of macro-avoidance would have resulted in even lower overall avoidance rates in their case.

In comparison, more recent estimates of avoidance by diurnally active seabirds range between 0.989 and 0.999 (COOK et al. 2018; SKOV et al. 2018). Also, KRIJGSVELD et al. (2011) using radar data of diurnal and nocturnal bird movements at a Dutch offshore wind farm estimated a within wind farm avoidance rate of at least 0.976, which, including their macro-avoidance rate of 0.28, would result in a total avoidance rate of >0.98. In a later study estimating nocturnal collisions at this wind farm, KRIJGSVELD et al. (2015) adopted an avoidance rate of 0.99.

Given this high uncertainty of avoidance behavior, we presented estimated collision fatalities for three different avoidance rates ranging between 0.956 - 0.990. The application of an avoidance rate of 0.980 instead of 0.956 reduces estimated collisions by >55%. Using an avoidance rate of 0.990 again halves collision numbers compared to an avoidance rate of 0.980. This exemplifies the need for a better understanding of the avoidance behavior of nocturnal migrants to better gauge the potential magnitude of bird collisions offshore. It also illustrates that the collision numbers reported in this study can only be regarded as a rough indication of actual fatalities.

The uncertainty is further increased by the fact that little is known about the avoidance behavior of birds during unfavorable weather conditions. It has been argued that nocturnal migrants encountering conditions like fog, drizzle or strong headwinds at sea may be less capable to perceive turbines and may be attracted by the illumination of the structures (AVERY et al. 1977; EVANS OGDEN 1996; HÜPPOP et al. 2006; AUMÜLLER et al. 2011). Hence, under such circumstances avoidance behavior might substantially deviate. In contrast to the situation onshore, nocturnal migrants facing inclement weather at sea are forced to continue migration. Events where high migration activity coincides with unfavorable weather offshore may therefore have a large effect on overall collision risk.

To get a better idea of the potential impact of such events we estimated the frequency of co-occurrence of high migration intensities and poor weather conditions. Our results suggest that this happens only rarely. Moderate thresholds for high migration intensities and unfavorable weather were exceeded in only about 0.3% of the time which corresponds to less than 8 hours per year in the study area. Setting higher thresholds reduced the time of co-occurrence to less than half an hour per year.

The potential impact on fatalities depends on the magnitude of the collision risk (i.e. the attraction effect or lack of avoidance behavior) during these short time periods. However, unless collision risk was extremely high, it seems unlikely that collisions during these time periods are the main driver of overall fatalities at offshore wind farms. Clearly, more research is needed to better understand potential attraction of nocturnal migrants to offshore turbines during different weather conditions and the resulting number of birds crossing the rotor-swept area.

The estimated cumulative number of collisions of nocturnal migrants in the German EEZ was approx. 35,000 birds assuming a low avoidance rate of 0.956. This would mean that in relation to the estimated total number of nocturnal migrants crossing the North and Baltic Sea, about 0.03% and 0.002% of these birds would collide each year, respectively. Naturally, it has to be kept in mind that these numbers are only crude estimations as both the total number of migrants as well as the number of collisions come with a high degree of uncertainty. Nonetheless, these numbers suggest that an impairment of nocturnal bird migration in the sense of significant negative effects on population size at this stage seems unlikely. Besides better estimates of the total number of migrants as well as the number of collisions, population models on the effect of the additional mortality through collisions at offshore turbines are needed to substantiate this conclusion.

As bird migration shows a high day-to-day variability, collisions are not equally distributed in time. We calculated the proportion of collisions that theoretically occur when migration intensity exceeds a variety of thresholds. These numbers may serve as a basis for cost-benefit considerations with respect to potential mitigation measures such as turbine curtailment. Threshold values have been chosen to represent migration intensities from moderate to very high and to illustrate the potential effect of turbine shutdown at different levels of flux rates. These values do not constitute recommendations for actual turbine curtailment.

Our models indicate that close to 50% of collisions happen when migration intensity exceeds 250 MTR (at altitudes up to 200 m) which on average is the case in 4% of the night hours. As a consequence, turbine shut-down during approx. 90 h per year would prevent about half of the modelled collisions of nocturnal migrants during the migration periods. Likewise, setting the threshold for turbine curtailment at 500 MTR would lead to turbine downtime of on average approx. 40 h per annum and would theoretically prevent about 27% of collision fatalities.

These calculations assume that collisions are strictly proportional to the number of birds migrating and do not consider possible effects of weather conditions on collision risk. If collisions are further aggregated by the simultaneous occurrence of high flux rates and inclement weather the necessary turbine downtime for the prevention of a given number of collisions could be further reduced. However, to fully assess the effect of conditioning turbine shutdown on weather conditions more information is needed on the effect of inclement weather and turbine illumination on the collision risk at offshore wind farms.

6 LITERATURE

- ÅKESSON, S., WALINDER, G., KARLSSON, L. & EHNBOOM, S. (2002): Nocturnal migratory flight initiation in reed warblers *Acrocephalus scirpaceus*: effect of wind on orientation and timing of migration. *Journal of Avian Biology* 33/4, S: 349–357.
- AKIMA, H., GEBHARDT, A., PETZOLD, T. & MAECHLER, M. (2016): Package „akima“.
- ALERSTAM, T. (1979): Wind as selective agent in bird migration. *Ornis Scandinavica*, S: 76–93.
- ALERSTAM, T., ROSÉN, M., BÄCKMAN, J., ERICSON, P. G. P. & HELLGREN, O. (2007): Flight Speeds among Bird Species: Allometric and Phylogenetic Effects. *PLoS Biology* 5/8, S: e197. DOI: 10.1371/journal.pbio.0050197, ISSN: 1545-7885.
- ARCHER, K. J. & KIMES, R. V. (2008): Empirical characterization of random forest variable importance measures. *Computational Statistics & Data Analysis* 52/4, S: 2249–2260.
- AUMÜLLER, R., BOOS, K., FREIENSTEIN, S., HILL, K. & HILL, R. (2011): Beschreibung eines Vogelschlagereignisses und seiner Ursachen an einer Forschungsplattform in der Deutschen Bucht. *Vogelwarte* 49, S: 9–16.
- AVERY, M., SPRINGER, P. F. & CASSEL, J. F. (1977): Weather influences on nocturnal bird mortality at a North Dakota tower. *The Wilson Bulletin* 89/2, S: 291–299.
- BAND, W. (2000): Windfarms and Birds: Calculating a theoretical collision risk assuming no avoiding action. *Guidance Notes Series. Scottish Natural Heritage*.
- BAND, B. (2012): Using a collision risk model to assess bird collision risks for offshore wind farms, Final Report. British Trust for Ornithology (BTO), Bureau Waardenburg bv, and University of St Andrews/The Nunnery, Thetford (GBR), S: 62.
- BELLEBAUM, J., GRIEGER, C., KLEIN, R., KÖPPEN, U., KUBE, J., NEUMANN, R., SCHULZ, A., SORDYL, H. & WENDELN, H. (2010): Ermittlung artbezogener Erheblichkeitsschwellen von Zugvögeln für das Seegebiet der südwestlichen Ostsee bezüglich der Gefährdung des Vogelzuges im Zusammenhang mit dem Kollisionsrisiko an Windenergieanlagen. Abschlussbericht, Forschungsvorhaben des Bundesministeriums für Umwelt, Naturschutz und Reaktorsicherheit (FKZ 0329948). IfAÖ, LUNG MV/Neu Broderstorf (DEU), S: 333.
- BERTHOLD, P. (2000): Vogelzug. Eine aktuelle Gesamtübersicht. (4., stark überarb. und erw. Aufl. Auflage). Wissenschaftliche Buchgesellschaft/Darmstadt, 280 Seiten. ISBN: 978-3-534-13656-8.
- BERTHOLD, P., GWINNER, E. & SONNENSCHNEIN, E. (Hrsg.) (2003): Avian migration. Springer/Berlin, Heidelberg & New York, 610 Seiten.
- BREIMAN, L. (2001): Random Forests. *Machine Learning* 45/1, S: 5–32.
- BRUDERER, B. & BOLDT, A. (2001): Flight characteristics of birds: I. Radar measurements of speeds. *ibis* 143, S: 178–204.
- BRUDERER, B. & LIECHTI, F. (1998): Flight behaviour of nocturnally migrating birds in coastal areas - crossing or coasting. *Journal of Avian Biology* 29/4, S: 499–507.
- BRUDERER, B., PETER, D. & KORNER-NIEVERGELT, F. (2018): Vertical distribution of bird migration between the Baltic Sea and the Sahara. *Journal of Ornithology* 159/2, S: 315–336.
- BRUDERER, B., UNDERHILL, L. & LIECHTI, F. (1995): Altitude choice by night migrants in a desert area predicted by meteorological factors. *Ibis* 137/1, S: 44–55.
- BRUST, V., MICHALIK, B. & HÜPPOP, O. (2019): To cross or not to cross – thrushes at the German North Sea coast adapt flight and routing to wind conditions in autumn. *Movement Ecology* 7/1, S: 32.
- BUNDESAMT FÜR SEESCHIFFFAHRT UND HYDROGRAPHIE (Hrsg.) - **BSH** (2013): Standard - Untersuchung der Auswirkungen von Offshore-Windenergieanlagen auf die Meeresumwelt (StUK 4), (Hrsg. BUNDESAMT FÜR SEESCHIFFFAHRT UND HYDROGRAPHIE). Hamburg & Rostock (DEU).
- BUNDESAMT FÜR SEESCHIFFFAHRT UND HYDROGRAPHIE (Hrsg.) - **BSH** (2019a): Umweltbericht zum Flächenentwicklungsplan 2019 für die deutsche Nordsee, (Hrsg. BUNDESAMT FÜR SEESCHIFFFAHRT UND HYDROGRAPHIE). Hamburg (DEU), S: 330.

- BUNDESAMT FÜR SEESCHIFFFAHRT UND HYDROGRAPHIE (Hrsg.) - **BSH** (2019b): Umweltbericht zum Flächenentwicklungsplan 2019 für die deutsche Ostsee, (Hrsg. BUNDESAMT FÜR SEESCHIFFFAHRT UND HYDROGRAPHIE). Hamburg und Rostock (DEU), S: 318.
- CHAMBERLAIN, D. E., REHFISCH, M. R., FOX, A. D., DESHOLM, M. & ANTHONY, S. J. (2006): The effect of avoidance rates on bird mortality predictions made by wind turbine collision risk models. *Ibis* 148/s1, S: 198–202.
- COHEN, J. (1960): A coefficient of agreement for nominal scales. *Educational and psychological measurement* 20/1, S: 37–46.
- COOK, A. S. C. P., HUMPHREYS, E. M., BENNET, F., MASDEN, E. A. & BURTON, N. H. K. (2018): Quantifying avian avoidance of offshore wind turbines: Current evidence and key knowledge gaps. *Marine Environmental Research*.
- CRISCI, C., GHATTAS, B. & PERERA, G. (2012): A review of supervised machine learning algorithms and their applications to ecological data. *Ecological Modelling* 240, S: 113–122.
- CUTLER, D. R., EDWARDS JR, T. C., BEARD, K. H., CUTLER, A., HESS, K. T., GIBSON, J. & LAWLER, J. J. (2007): Random forests for classification in ecology. *Ecology* 88/11, S: 2783–2792.
- DE LUCAS, M., JANSSE, G. F. E., WHITFIELD, D. P. & FERRER, M. (2008): Collision fatality of raptors in wind farms does not depend on raptor abundance. *Journal of Applied Ecology* 45/6, S: 1695–1703.
- ERNI, B., LIECHTI, F. & BRUDERER, B. (2005): The role of wind in passerine autumn migration between Europe and Africa. *Behavioral Ecology* 16/4, S: 732–740.
- ERNI, B., LIECHTI, F., UNDERHILL, L. G. & BRUDERER, B. (2002): Wind and rain govern the intensity of nocturnal bird migration in central Europe - a log-linear regression analysis. *Ardea* 90/1, S: 155–166.
- EVANS OGDEN, L. J. (1996): Collision course: the hazards of lighted structures and windows to migrating birds. World Wildlife Fund Canada & Fatal Light Awareness Programm/Ontario (CAN).
- EVERAERT, J. (2014): Collision risk and micro-avoidance rates of birds with wind turbines in Flanders. *Bird Study* 61/2, S: 220–230.
- FEBI (2013): Fehmarnbelt Fixed Link EIA. Bird Investigations in Fehmarnbelt – Baseline. Volume II. Waterbirds in Fehmarnbelt. Nr. E3TR0011.
- FERRER, M., DE LUCAS, M., JANSSE, G. F., CASADO, E., MUNOZ, A. R., BECHARD, M. J. & CALABUIG, C. P. (2012): Weak relationship between risk assessment studies and recorded mortality in wind farms. *Journal of Applied Ecology* 49/1, S: 38–46.
- FORTIN, D., LIECHTI, F. & BRUDERER, B. (1999): Variation in the nocturnal flight behaviour of migratory birds along the northwest coast of the Mediterranean Sea. *Ibis* 141/3, S: 480–488.
- GRÜNKORN, T., BLEW, J., COPPACK, T., KRÜGER, O., NEHLS, G., POTIEK, A., REICHENBACH, M., VON RÖNN, J., TIMMERMANN, H. & WEITEKAMP, S. (2016): Ermittlung der Kollisionsraten von (Greif-)Vögeln und Schaffung planungsbezogener Grundlagen für die Prognose und Bewertung des Kollisionsrisikos durch Windenergieanlagen (PROGRESS). Schlussbericht zum durch das Bundesministerium für Wirtschaft und Energie (BMWi) im Rahmen des 6. Energieforschungsprogrammes der Bundesregierung geförderten Verbundvorhaben PROGRESS, FKZ 0325300A-D. S: 332.
- HÜPPOP, O., DIERSCHKE, J., EXO, K. M., FREDRICH, E. & HILL, R. (2006): Bird migration studies and potential collision risk with offshore wind turbines. *Ibis* 148, S: 90–109.
- HÜPPOP, O., DIERSCHKE, J. & WENDELN, H. (2004): Zugvögel und Offshore-Windkraftanlagen: Konflikte und Lösungen. *Berichte zum Vogelschutz* 41, S: 127–217.
- HÜPPOP, O. & HILGERLOH, G. (2012): Flight call rates of migrating thrushes: effects of wind conditions, humidity and time of day at an illuminated offshore platform. *Journal of Avian Biology* 43/1, S: 85–90.
- HÜPPOP, O., HILL, R., HÜPPOP, K. & JACHMANN, F. (2009): Auswirkungen auf den Vogelzug - Begleitforschung im Offshore-Bereich auf Forschungsplattformen in der Nordsee (FINOBIRD), Abschlussbericht. Institut für Vogelforschung „Vogelwarte Helgoland“/Helgoland (DEU), S: 278.
- HÜPPOP, O., HÜPPOP, K., DIERSCHKE, J. & HILL, R. (2016): Bird collisions at an offshore platform in the North Sea. *Bird Study* 63/1, S: 1–10.

- JAMES, G., WITTEN, D., HASTIE, T. & TIBSHIRANI, R. (2013): An Introduction to Statistical Learning, Vol. 112. Springer/New York.
- JOHANNESSON, T., BJORNSSON, H. & GROTHENDIECK, G. (2018): stinepack: Stineman, a consistently well behaved method of interpolation (R package version 1.4).
- KANAMITSU, M., EBISUZAKI, W., WOOLLEN, J., YANG, S., HNILO, J., FIORINO, M. & POTTER, G. (2002): NCEP–DOE AMIP-II REANALYSIS (R-2). *Bulletin of the American Meteorological Society*.
- KARLSSON, H., NILSSON, C., BÄCKMAN, J. & ALERSTAM, T. (2011): Nocturnal passerine migration without tailwind assistance. *Ibis* 153/3, S: 485–493.
- KEMP, M. U. (2012): How birds weather the weather: avian migration in the mid-latitudes (*Dissertation*). Universiteit van Amsterdam / Amsterdam (NLD), 207 S.
- KEMP, M. U., SHAMOUN-BARANES, J., DOKTER, A. M., LOON, E. & BOUTEN, W. (2013): The influence of weather on the flight altitude of nocturnal migrants in mid-latitudes. *Ibis* 155/4, S: 734–749.
- KERLINGER, P., GEHRING, J. L., ERICKSON, W. P., CURRY, R., JAIN, A. & GUARNACCIA, J. (2010): Night migrant fatalities and obstruction lighting at wind turbines in North America. *The Wilson Journal of Ornithology* 122/4, S: 744–754.
- KLEYHEEG-HARTMAN, J. C., KRIJGSVELD, K. L., COLLIER, M. P., POOT, M. J. M., BOON, A. R., TROOST, T. A. & DIRKSEN, S. (2018): Predicting bird collisions with wind turbines: Comparison of the new empirical Flux Collision Model with the SOSS Band model. *Ecological Modelling* 387, S: 144–153.
- KRIJGSVELD, K. L., AKERSHOEK, K., SCHENK, F., DIJK, F. & DIRKSEN, S. (2009): Collision risk of birds with modern large wind turbines. *Ardea* 97/3, S: 357–366.
- KRIJGSVELD, K. L., FIJN, R. C., JAPINK, M., VAN HORSSSEN, P. W., HEUNKS, C., COLLIER, M. P., POOT, M. J. M., BEUKER, D. & DIRKSEN, S. (2011): Effect studies Offshore Wind Farm Egmond aan Zee - Final report on fluxes, flight altitudes and behaviour of flying birds, Final Report. Bureau Waardenburg bv/Culemborg (NDL), S: 328.
- KRIJGSVELD, K. L., FIJN, R. C. & LENSINK, R. (2015): Occurrence of peaks in songbird migration at rotor heights of offshore wind farms in the southern North Sea, Final Report. Bureau Waardenburg bv/Culemborg (NDL), S: 28.
- KUHN, M., WING, J., WESTON, S., WILLIAMS, A., KEEFER, C., ENGELHARDT, A., COOPER, T., MAYER, Z., KENKEL, B., R CORE TEAM & OTHERS (2019): caret: Classification and regression training. R package version 6.0–84.
- LA SORTE, F. A., HOCHACHKA, W. M., FARNSWORTH, A., SHELDON, D., VAN DOREN, B. M., FINK, D. & KELLING, S. (2015): Seasonal changes in the altitudinal distribution of nocturnally migrating birds during autumn migration. *Royal Society open science* 2/12, S: 150347.
- LANDIS, J. R. & KOCH, G. G. (1977): The measurement of observer agreement for categorical data. *biometrics*, S: 159–174.
- LIECHTI, F. (2006): Birds: blowin’ by the wind? *Journal of Ornithology* 147/2, S: 202–211.
- LIECHTI, F., ASCHWANDEN, J., BLEW, J., BOOS, M., BRABANT, R., DOKTER, A. M., KOSAREV, V., LUKACH, M., MARURI, M., REYNIERS, M. & OTHERS (2018): Cross-calibration of different radar systems for monitoring nocturnal bird migration across Europe and the Near East. *Ecography* 42, S: 1–12.
- LIECHTI, F. & BRUDERER, B. (1998): The relevance of wind for optimal migration theory. *Journal of Avian Biology* 29, S: 561–568.
- LIECHTI, F., KLAASSEN, M. & BRUDERER, B. (2000): Predicting migratory flight altitudes by physiological migration models. *The Auk* 117/1, S: 205–214.
- MASDEN, E. (2015): Developing an avian collision risk model to incorporate variability and uncertainty. Environmental Research Institute, North Highland College – UHI University of the Highlands and Islands/Thurso (GBR), S: 26.
- MASDEN, E. A. & COOK, A. S. C. P. (2016): Avian collision risk models for wind energy impact assessments. *Environmental Impact Assessment Review* 56, S: 43–49.
- MCGREGOR, R. M., KING, S., DONOVAN, C. R., CANECO, B. & WEBB, A. (2018): A stochastic collision risk model for seabirds in flight, (Hrsg. HiDEF AERIAL SURVEYING LIMITED & BIOCONSULT SH). Cleator Moor (GBR), prepared for Marine Scotland.

- MÜLLER, H. (1981): Vogelschlag in einer starken Zugsnacht auf der Offshore-Forschungsplattform „Nordsee“ im Oktober 1979. *Seevögel* 2, S: 33–37.
- NILSSON, C., DOKTER, A. M., SCHMID, B., SCACCO, M., VERLINDEN, L., BÄCKMAN, J., HAASE, G., DELL’OMO, G., CHAPMAN, J. W., LEIJNSE, H. & LIECHTI, F. (2018): Field validation of radar systems for monitoring bird migration. *Journal of Applied Ecology*.
- OREJAS, C., SCHROEDER, A., JOSCHKO, T., DIERSCHKE, J., EXO, K. M., FRIEDRICH, E., HILL, R., HÜPPOP, O., POLLEHNE, F., ZETTLER, M. L. & BOCHERT, R. (2005): Ökologische Begleitforschung zur Windenergienutzung im Offshore-Bereich auf Forschungsplattformen in der Nord- und Ostsee (BeoFINO), BMU 0327526-Abschlußbericht. Alfred Wegener Institut für Polar und Meeresforschung/Bremerhaven (DEU), S: 354.
- PRASAD, A. M., IVERSON, L. R. & LIAW, A. (2006): Newer classification and regression tree techniques: bagging and random forests for ecological prediction. *Ecosystems* 9/2, S: 181–199.
- R CORE TEAM (2017): R: A Language and Environment for Statistical Computing. R Foundation for Statistical Computing/Vienna (AUT).
- R CORE TEAM (2018): R: A Language and Environment for Statistical Computing. R Foundation for Statistical Computing.
- RICHARDSON, W. (1990): Timing of bird migration in relation to weather: updated review. In: *Bird migration* Springer, S. 78–101.
- SCHMALJOHANN, H., LIECHTI, F. & BRUDERER, B. (2009): Trans-Sahara migrants select flight altitudes to minimize energy costs rather than water loss. *Behavioral ecology and sociobiology* 63/11, S: 1609–1619.
- SCHULZ, A., DITTMAN, T. & COPPACK, T. (2014): Erfassung von Ausweichbewegungen von Zugvögeln mittels Pencil Beam Radar und Erfassung von Vogelkollisionen mit Hilfe des Systems VARS. StUKplus Schlussbericht. Rostock, Im Auftrag des Bundesamts für Seeschifffahrt und Hydrographie (BSH), S: 89.
- SCHULZ, A., DITTMANN, T., WEIDAUER, A., KILIAN, M., LÖFFLER, T., RÖHRBEIN, V. & SCHLEICHER, K. (2013): Weiterentwicklung der Technik für Langzeituntersuchungen der Vögel mittels Radar und automatischer Kamerabeobachtung am Standort FINO 2 und Durchführung von Langzeitmessungen am Standort für den Zeitraum 2010 bis 2012, Abschlussbericht. Institut für Angewandte Ökologie/Neu Brodersdorf (DEU), Teilprojekt Vogelzug. Bestandteil des Forschungsvorhabens „Betrieb für Forschungsplattform FINO 2“ (BMU; FKZ 0329905D), S: 103.
- SKOV, H., HEINÄNEN, S., NORMAN, T., WARD, R., MÉNDEZ-ROLDÁN, S. & ELLIS, I. (2018): ORJIP Bird Collision and Avoidance Study, Final Report. The Carbon Trust/London (GBR), S: 247.
- THIELE, C. (2019): cutpointr: Determine and Evaluate Optimal Cutpoints in Binary Classification Tasks. R package version 1.0.0.
- URMY, S. S. & WARREN, J. D. (2017): Quantitative ornithology with a commercial marine radar: standard-target calibration, target detection and tracking, and measurement of echoes from individuals and flocks. *Methods in Ecology and Evolution* 8/7, S: 860–869.
- VAN BELLE, J., SHAMOUN-BARANES, J., VAN LOON, E. & BOUTEN, W. (2007): An operational model predicting autumn bird migration intensities for flight safety. *Journal of Applied Ecology* 44/4, S: 864–874.
- VAN DOREN, B. M. & HORTON, K. G. (2018): A continental system for forecasting bird migration. *Science* 361/6407, S: 1115–1118.
- WELCKER, J. (2019): Patterns of nocturnal bird migration in the German North and Baltic Seas. ProBIRD report 2. BioConsult SH/Husum (DEU), S: 70.
- WELCKER, J., LIESENJOHANN, M., BLEW, J., NEHLS, G. & GRÜNKORN, T. (2017): Nocturnal migrants do not incur higher collision risk at wind turbines than diurnally active species. *Ibis* 159/2, S: 366–373.
- WELCKER, J. & VILELA, R. (2018): Analysis of bird flight calls from the German North and Baltic Seas. Report from the ProBIRD project, Final Report. BioConsult SH/Husum (DEU), S: 128.
- WENDELN, H., LIECHTI, F., HILL, R., HÜPPOP, O. & KUBE, J. (2007): Sind Schiffsradargeräte für quantitative Vogelzugmessungen geeignet? - Ein Vergleich mit dem Zielfolgeradar „Superfledermaus“. *Vogelwarte* 45, S: 336–337.

ZEHNDER, S., ÅKESSON, S., LIECHTI, F. & BRUDERER, B. (2001): Nocturnal autumn bird migration at Falsterbo, South Sweden. *Journal of Avian Biology* 32/3, S: 239–248.

A APPENDIX

A.1 Weather models

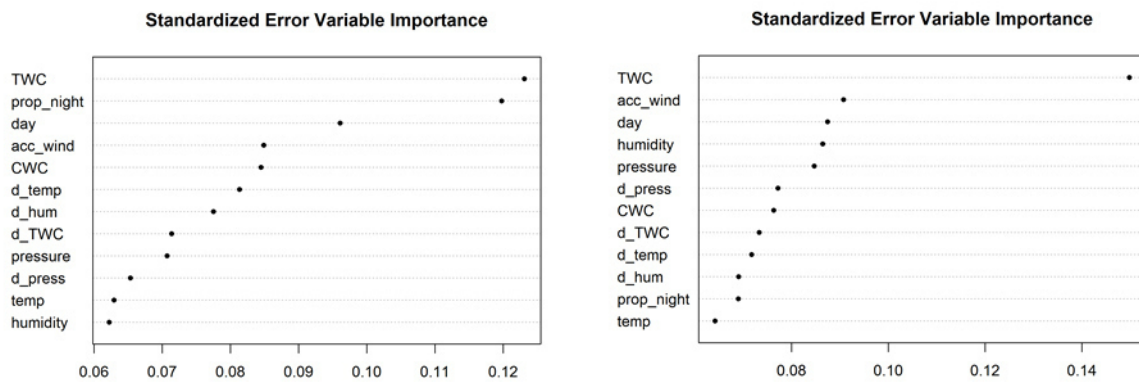


Figure A 1 Standardized Error Variable Importance of Random Forest models on migration intensities up to 200 m altitude). Results for spring and fall migration are shown in left and right panels, respectively.

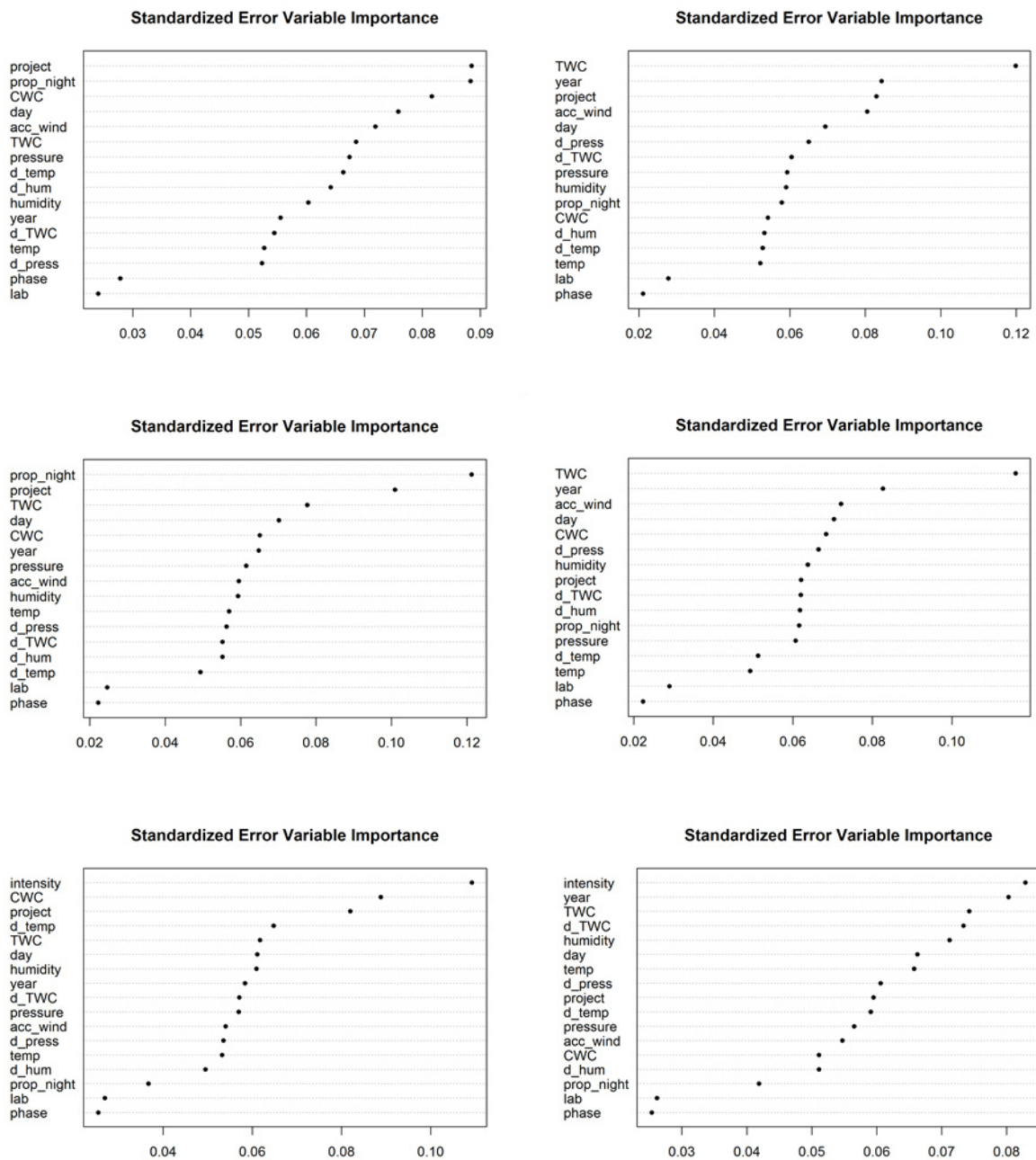


Figure A 2 Standardized Error Variable Importance of Random Forest models on migration intensities up to 1,000 m altitude (upper panels), up to 200 m (mid panels) and flight height (lower panels) including the explanatory variables “year”, “project”, “phase” and “lab”. Results for spring and fall migration are shown in left and right panels, respectively.

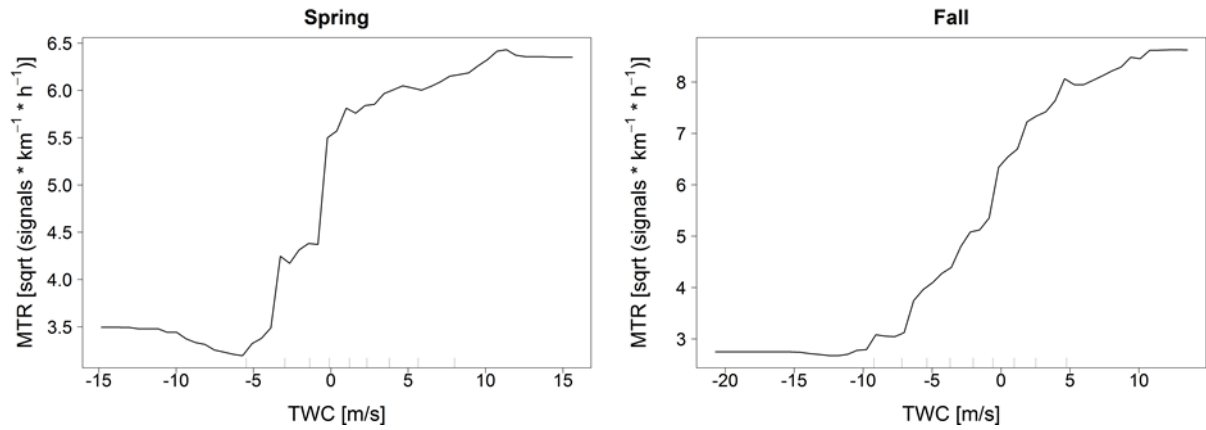


Figure A 3 Partial dependence plots of TWC for RF models on migration intensities (MTR up to 200 m). Results for spring and fall migration are shown in left and right panels, respectively.

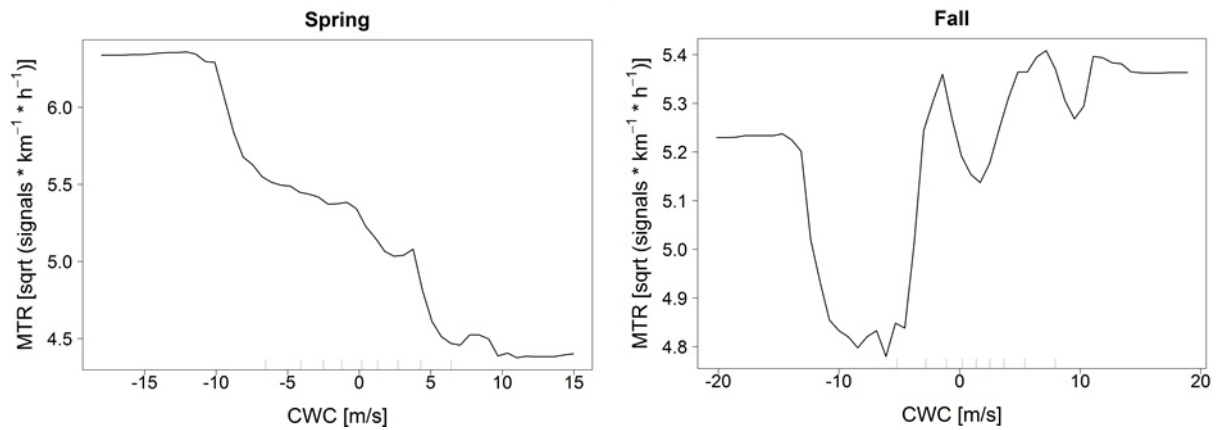


Figure A 4 Partial dependence plots of CWC for RF models on migration intensities (MTR up to 200 m). Results for spring and fall migration are shown in left and right panels, respectively.

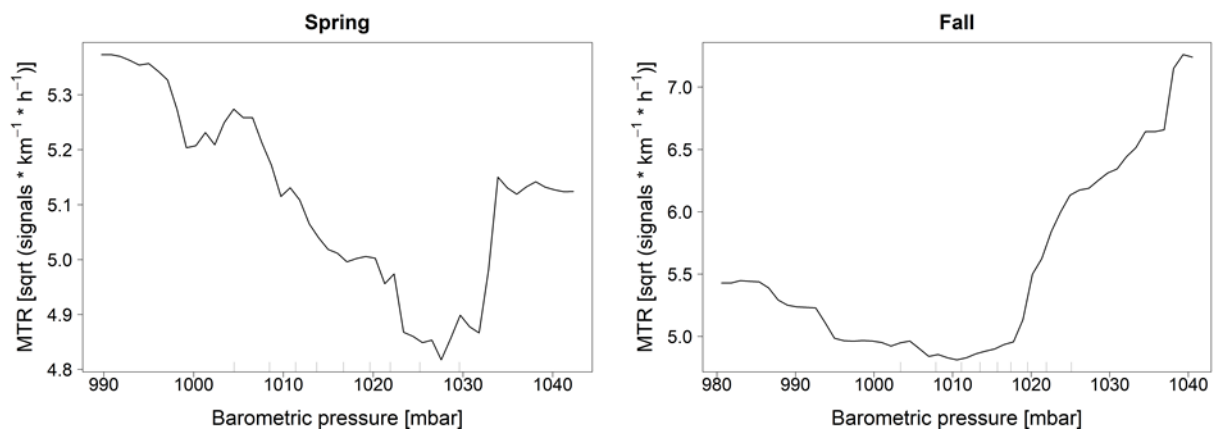


Figure A 5 Partial dependence plots of barometric pressure for RF models on migration intensities (MTR up to 200 m). Results for spring and fall migration are shown in left and right panels, respectively.

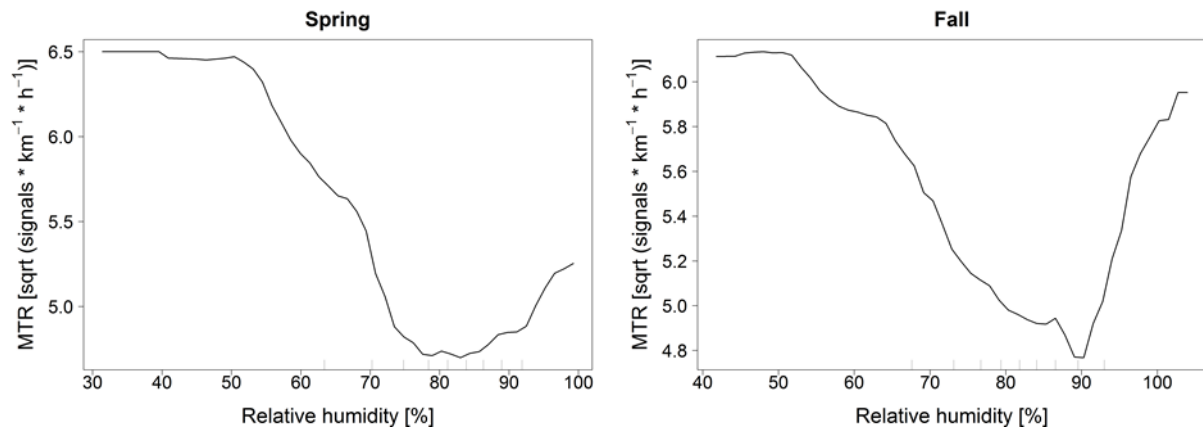


Figure A 6 Partial dependence plots of relative humidity for RF models on migration intensities (MTR up to 200 m). Results for spring and fall migration are shown in left and right panels, respectively.

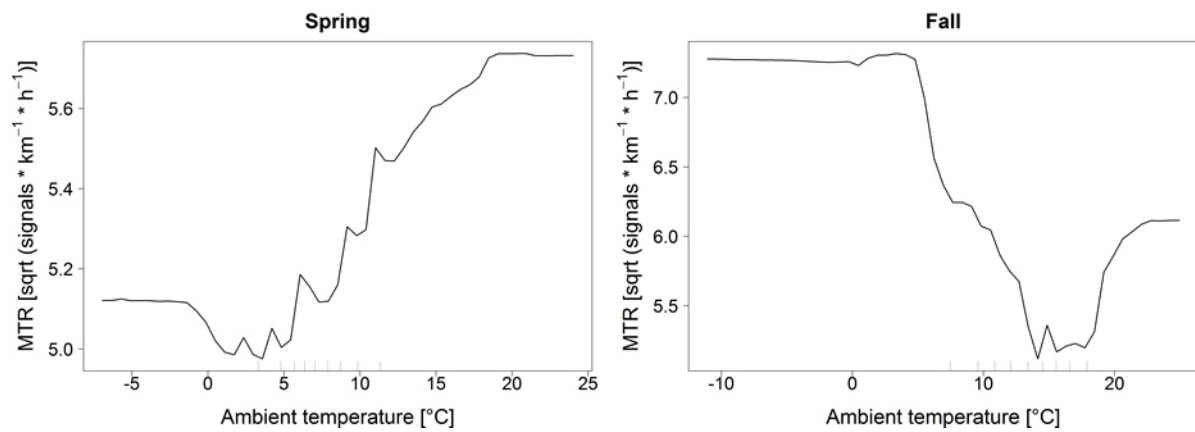


Figure A 7 Partial dependence plots of ambient temperature for RF models on migration intensities (MTR up to 200 m). Results for spring and fall migration are shown in left and right panels, respectively.

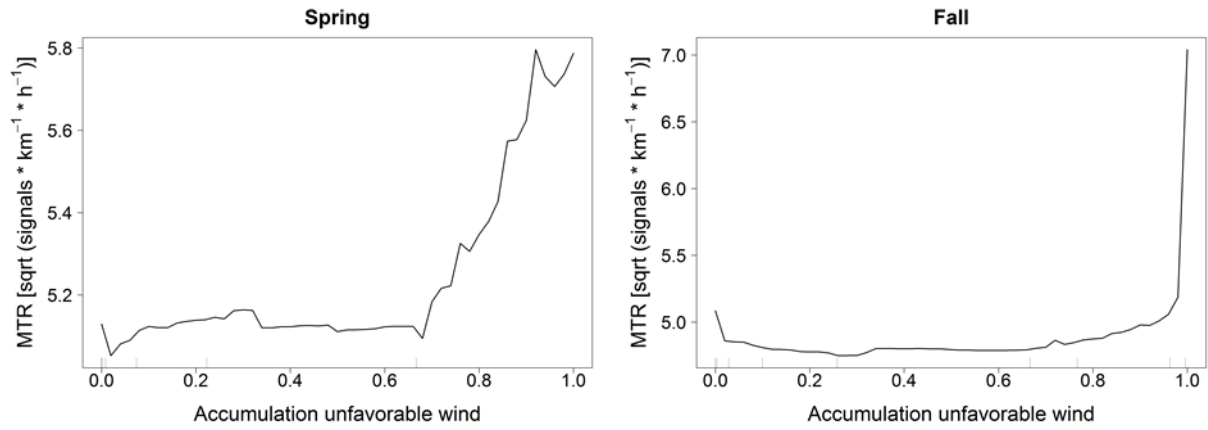


Figure A 8 Partial dependence plots of variable “accumulation unfavorable wind” for RF models on migration intensities (MTR up to 200 m). Results for spring and fall migration are shown in left and right panels, respectively.

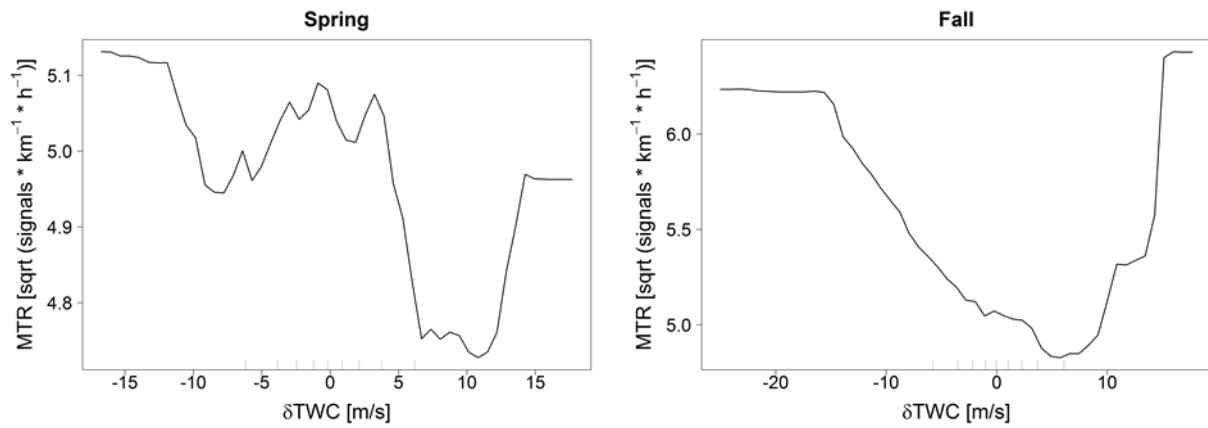


Figure A 9 Partial dependence plots of δ TWC for RF models on migration intensities (MTR up to 200 m). Results for spring and fall migration are shown in left and right panels, respectively.

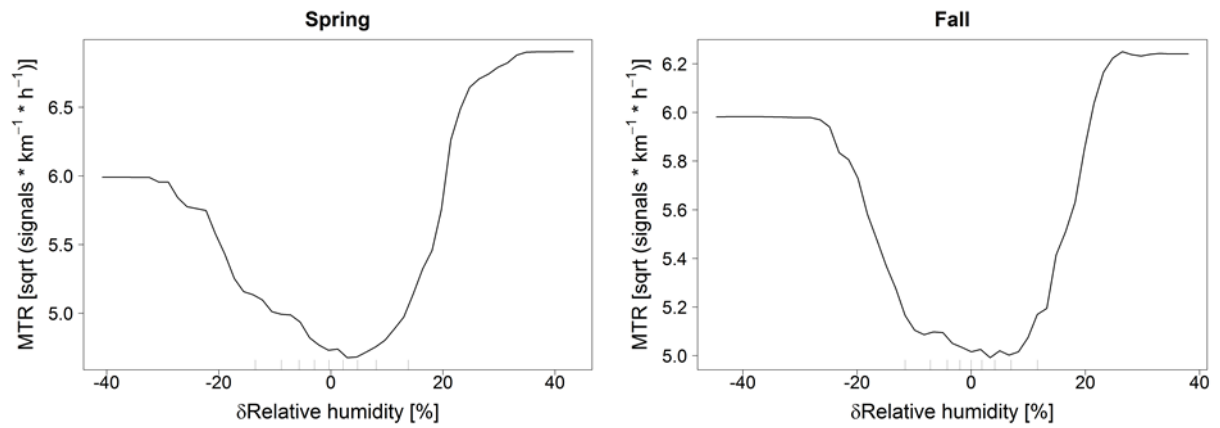


Figure A 10 Partial dependence plots of δ relative humidity for RF models on migration intensities (MTR up to 200 m). Results for spring and fall migration are shown in left and right panels, respectively.

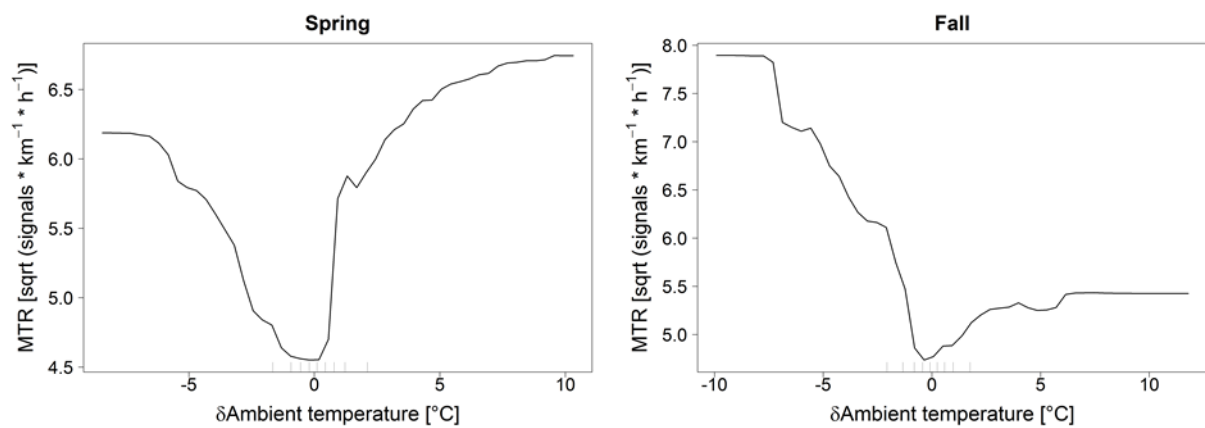


Figure A 11 Partial dependence plots of δ ambient temperature for RF models on migration intensities (MTR up to 200 m). Results for spring and fall migration are shown in left and right panels, respectively.

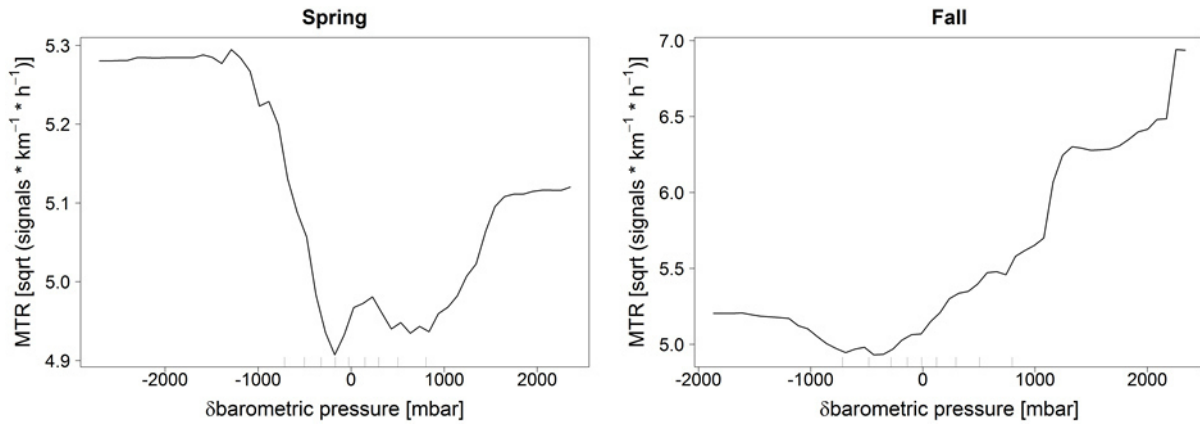


Figure A 12 Partial dependence plots of δ barometric pressure for RF models on migration intensities (MTR up to 200 m). Results for spring and fall migration are shown in left and right panels, respectively.

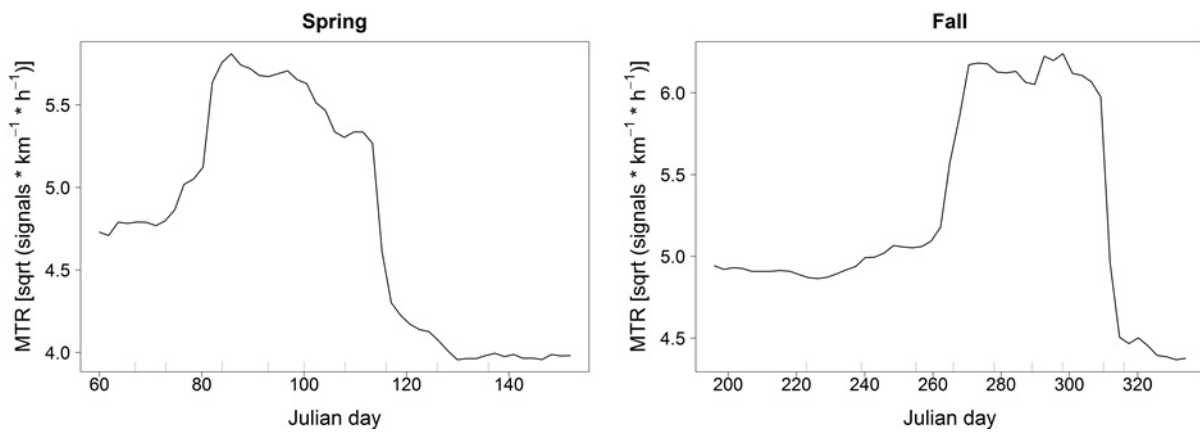


Figure A 13 Partial dependence plots of Julian day for RF models on migration intensities (MTR up to 200 m). Results for spring and fall migration are shown in left and right panels, respectively.

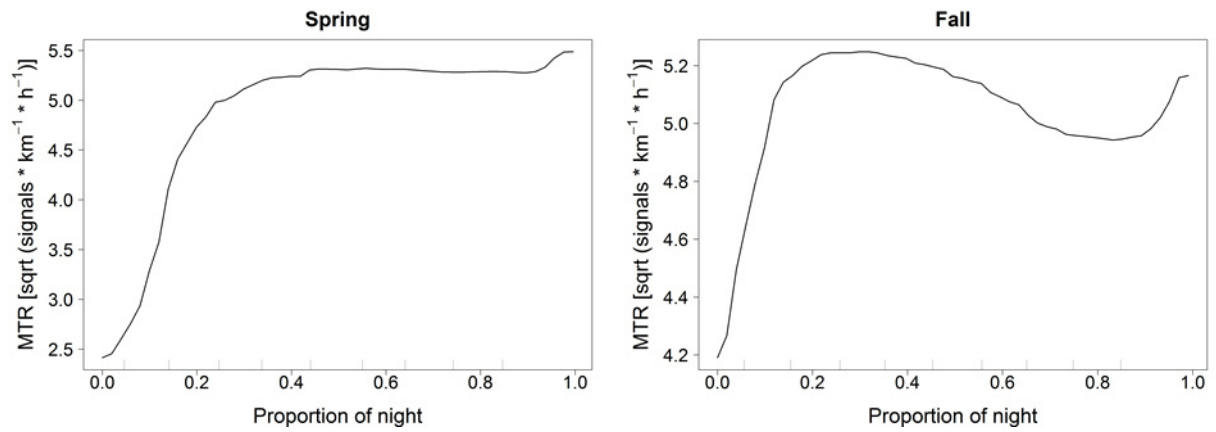


Figure A 14 Partial dependence plots of the proportion of night for RF models on migration intensities (MTR up to 200 m). Results for spring and fall migration are shown in left and right panels, respectively.

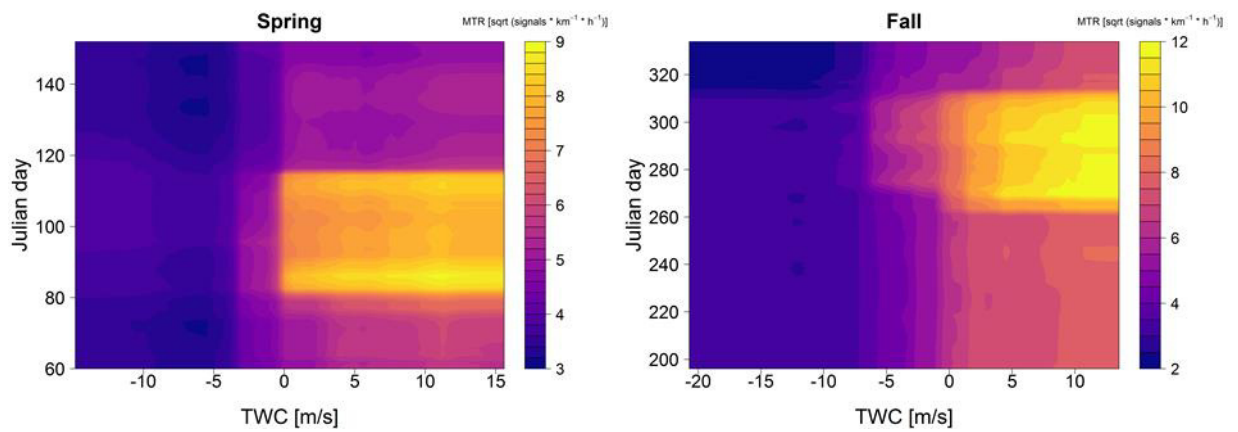


Figure A 15 Interaction plots of TWC with Julian day for RF models on migration intensities (MTR up to 200 m). Results for spring and fall migration are shown in left and right panels, respectively.

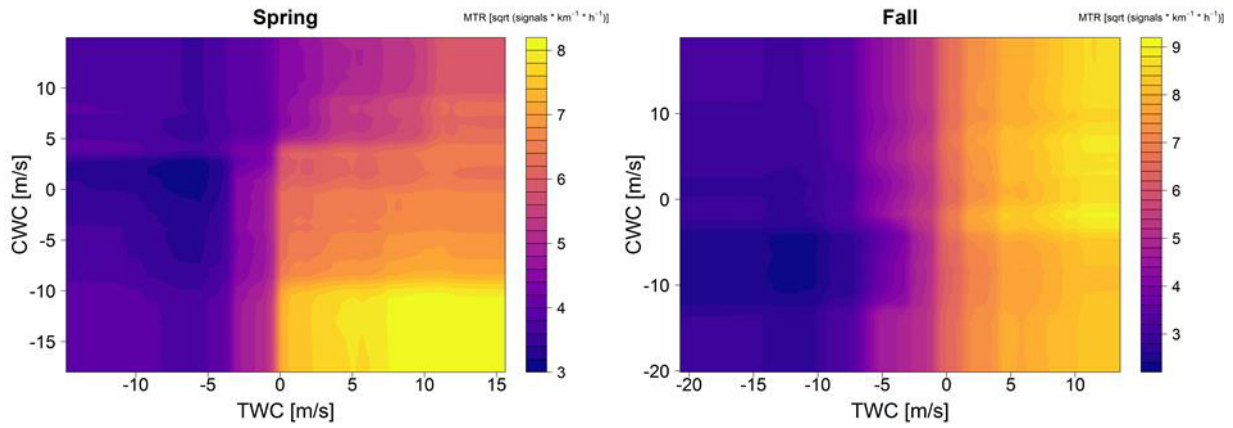


Figure A 16 Interaction plots of TWC with CWC for RF models on migration intensities (MTR up to 200 m). Results for spring and fall migration are shown in left and right panels, respectively.

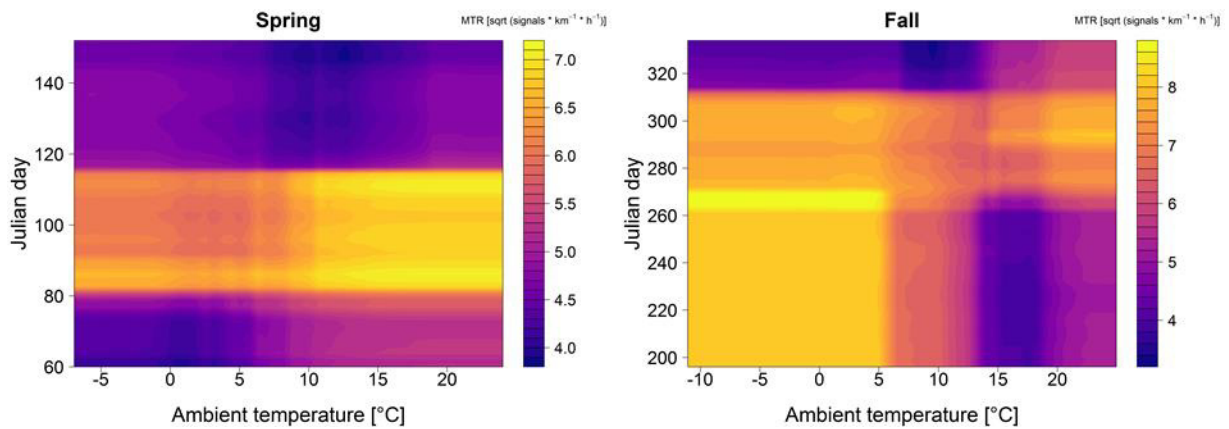


Figure A 17 Interaction plots of ambient temperature with Julian day for RF models on migration intensities (MTR up to 200 m). Results for spring and fall migration are shown in left and right panels, respectively.

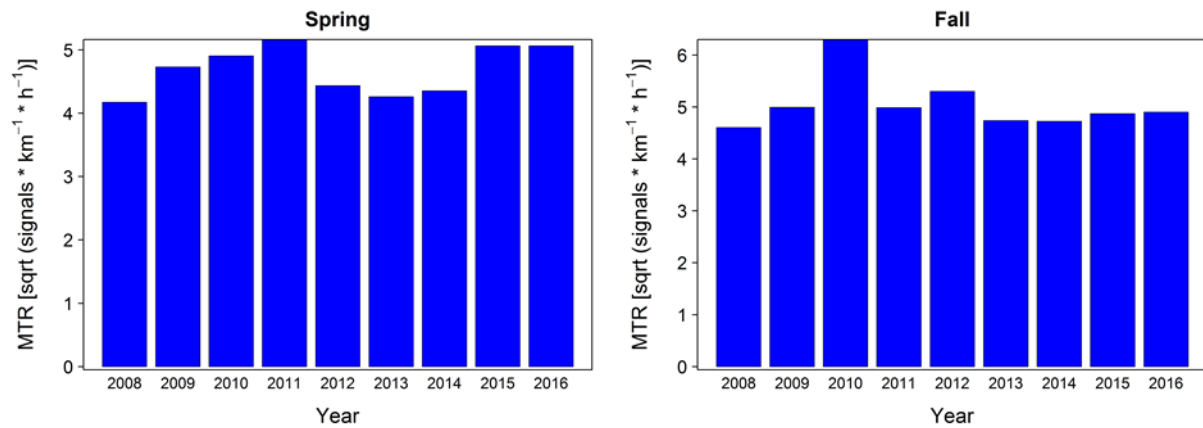


Figure A 18 Partial dependence plots of the factor “year” for RF models on migration intensities (MTR up to 200 m). Results for spring and fall migration are shown in left and right panels, respectively.

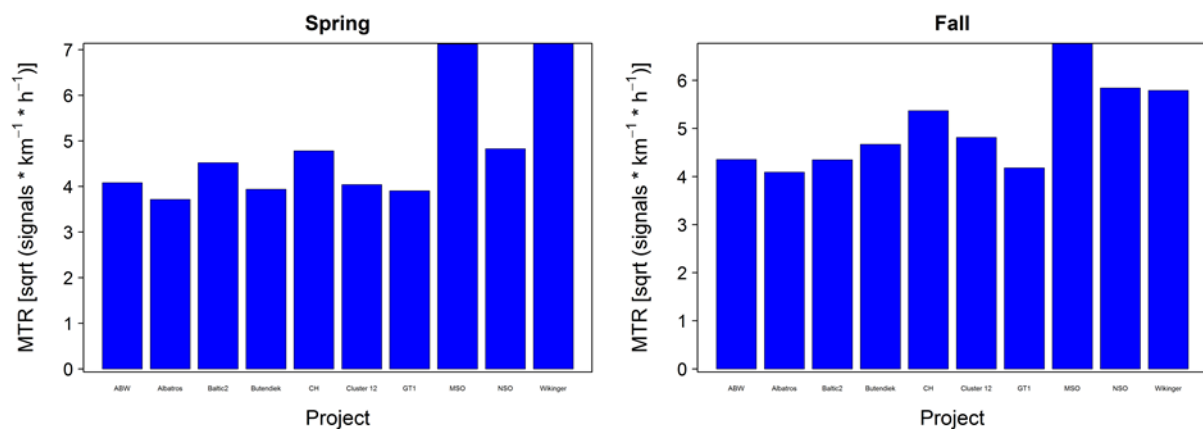


Figure A 19 Partial dependence plots of the factor “project” for RF models on migration intensities (MTR up to 200 m). Results for spring and fall migration are shown in left and right panels, respectively.

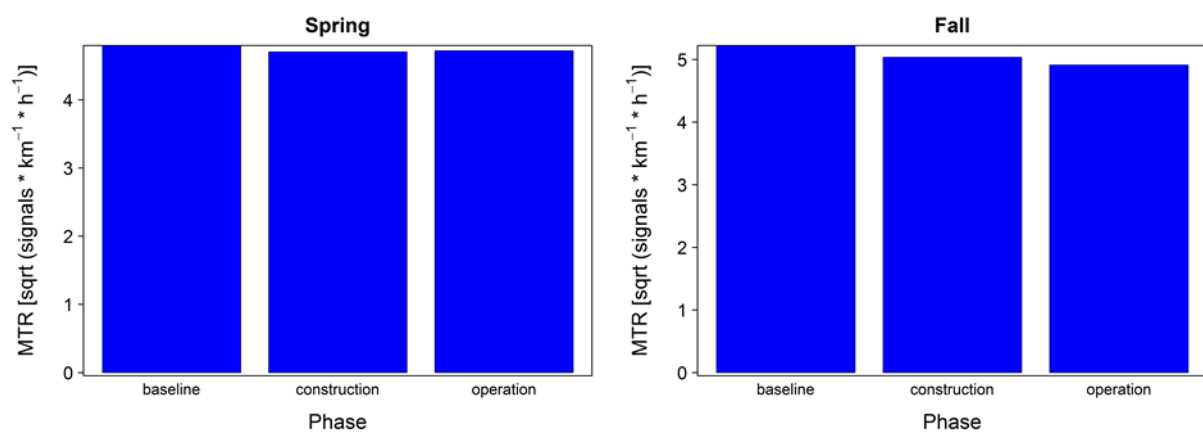


Figure A 20 Partial dependence plots of the factor “phase” for RF models on migration intensities (MTR up to 200 m). Results for spring and fall migration are shown in left and right panels, respectively.

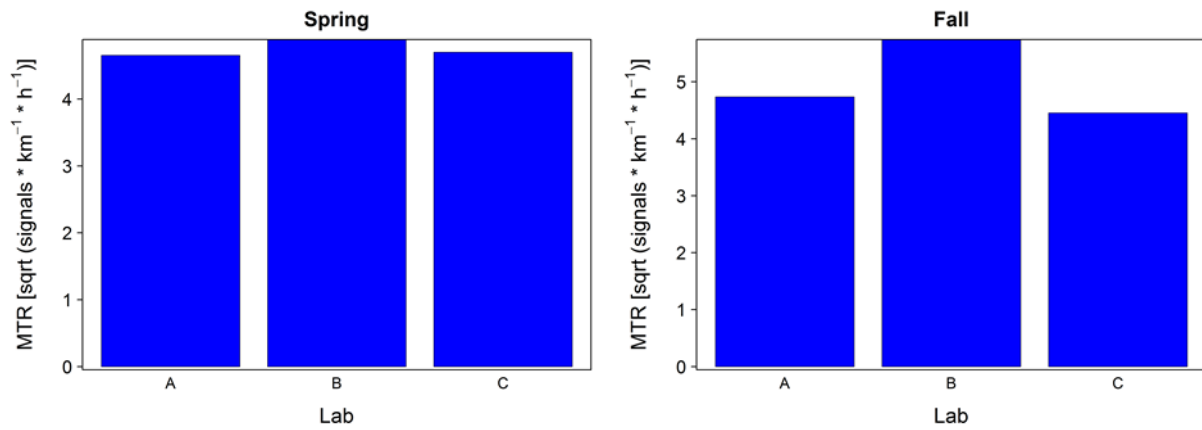


Figure A 21 Partial dependence plots of the factor “lab” for RF models on migration intensities (MTR up to 200 m). Results for spring and fall migration are shown in left and right panels, respectively.

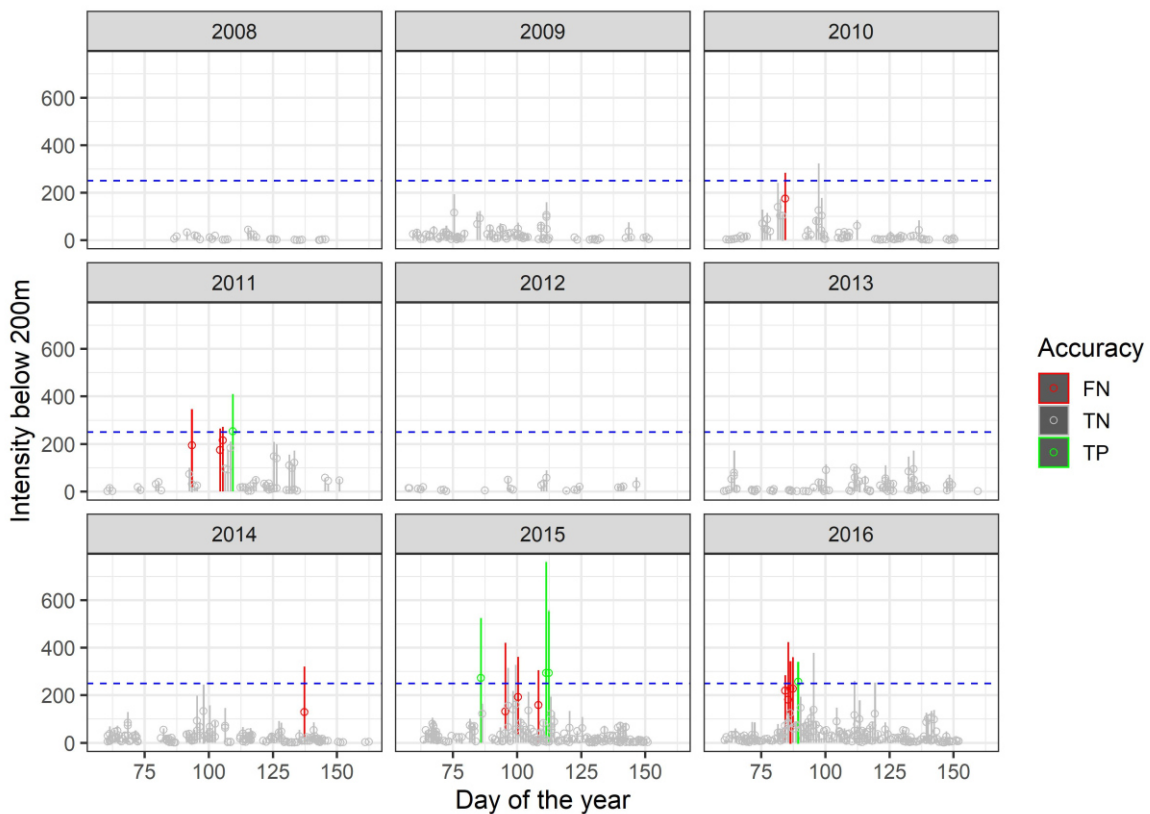


Figure A 22 Observed and predicted migration intensities (MTR) in spring for all study years with bars indicating the observed and open symbols the predicted values. In addition, the performance of the model in predicting nights with high migration intensities (>250 MTR) is indicated (FN = false negatives, TN = true negatives, TP = true positives). The dashed blue line represents the threshold for observed and predicted values (250 MTR).

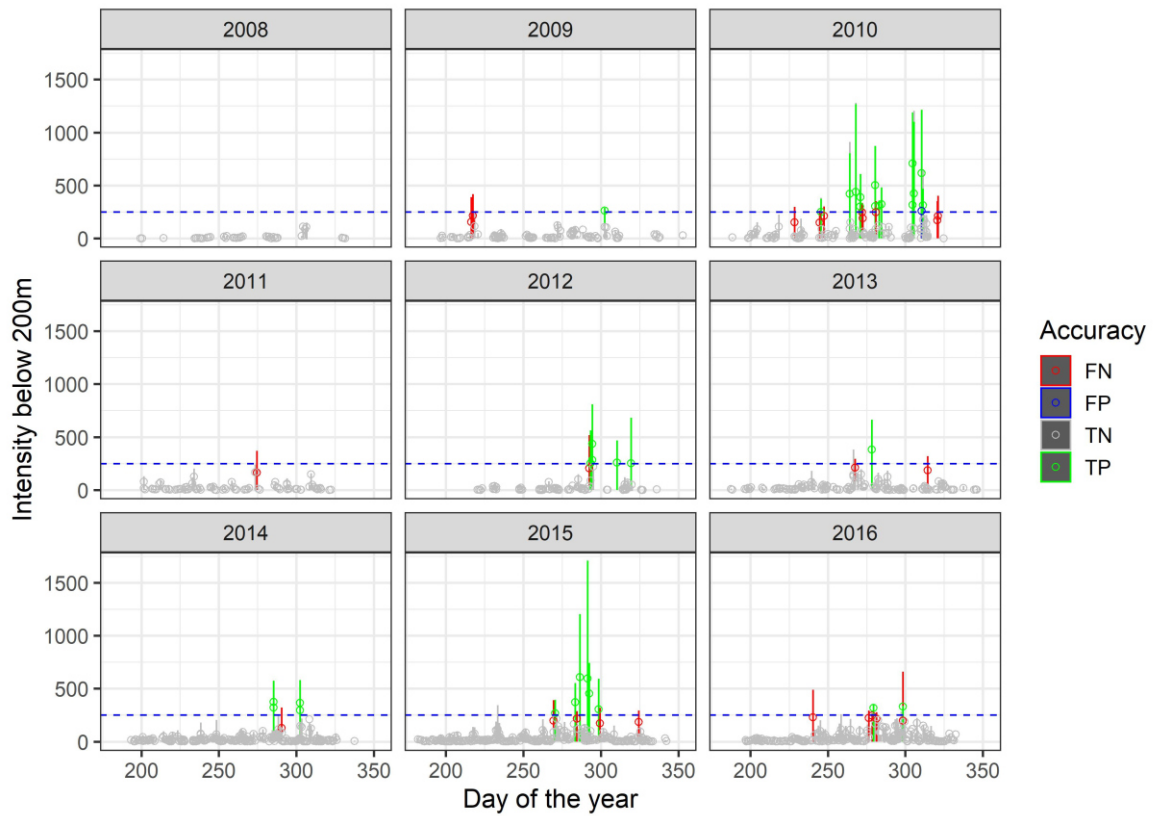


Figure A 23 Observed and predicted migration intensities (MTR) in fall for all study years with bars indicating the observed and open symbols the predicted values. In addition, the performance of the model in predicting nights with high migration intensities (>250 MTR) is indicated (FN = false negatives, FP = false positives, TN = true negatives, TP = true positives). The dashed blue line represents the threshold for observed and predicted values (250 MTR).

A.2 Coincidence of high migration intensities and unfavorable weather

Tab. A 1 *Coincidence of high migration intensities and unfavorable weather based on radar data from platforms only. Given is the number and percentage of hours in which migration intensity was above three different thresholds for “high migration intensities” and in which three different levels of unfavorable weather conditions prevailed.*

	MTR >250	MTR >500	MTR >750
All weather conditions			
Hours below threshold	3,517	3,638	3,678
Hours above threshold	198	77	37
% above threshold	5.33	2.07	1.00
weather: TWC <=-7 OR humidity >=95			
Hours above threshold	3	1	0
% above threshold	0.08	0.03	0.0
weather: TWC <0 AND humidity >90			
Hours above threshold	7	4	1
% above threshold	0.19	0.11	0.03
weather: TWC<=-5 AND humidity >=95			
Hours above threshold	2	0	0
% above threshold	0.05	0.00	0.00

A.3 Collision risk models

Tab. A 2 *Number of night hours per month used in the Collision Risk Models. Night hours were calculated based on latitude 54.4°N and Civil Twilight as the start and end point of the night. Night hours for July contain only the nights from the 15th of July onwards (see chap.3.2.4 for details).*

March	April	May	July	August	September	October	November
338.7	258.3	197.3	103.3	241.3	302.7	380.8	424.6

Tab. A 3 *Offshore wind farms in the German North and Baltic Sea for which collision risk models were constructed. The number of turbines, hub height and rotor radius is given for each wind farm.*

Region	Area	Wind farm	Number of turbines	Hub height [m]	Rotor radius [m]
North Sea	N-2	alpha ventus	12	91	60.5
North Sea	N-2	Merkur	66	102	75
North Sea	N-2	Borkum Riffgrund 1	78	87	60
North Sea	N-2	Borkum Riffgrund 2	56	104.5	82
North Sea	N-2	Trianel I	40	92	58
North Sea	N-2	Trianel II	32	104.5	76
North Sea	N-3	Gode Wind 1 and 2	97	110	77
North Sea	N-3	Nordsee One	54	90	63
North Sea	N-4	ABW	80	90	60
North Sea	N-4	MSO	80	89	60
North Sea	N-4	NSO	48	97	63
North Sea	N-5	Butendiek	80	91	60
North Sea	N-5	DanTysk	80	88	60

Region	Area	Wind farm	Number of turbines	Hub height [m]	Rotor radius [m]
North Sea	N-5	Sandbank	72	94.6	65
North Sea	N-6	BARD	80	90	61
North Sea	N-6	Deutsche Bucht	33	107.5	82
North Sea	N-6	Veja Mate	67	103.3	77
North Sea	N-8	GTI	80	92	58
North Sea	N-8	Hohe See	71	105	77
North Sea	N-8	Albatros	16	105	77
Baltic Sea	O-1	Arkona	60	102	77
Baltic Sea	O-1	Wikinger	70	97.5	67.5
Baltic Sea	O-3	Baltic 2	80	78.3	60

Tab. A 4 Total number of collisions and collisions per turbine for different thresholds of migration traffic rates (MTR) separately for the North and Baltic Sea. In addition the proportion of collisions that occur when MTR was above different thresholds, the proportion of time and the absolute number of hours that MTRs were above thresholds is given.

MTR threshold	Avoidance rate	Total number of collisions	Collisions per turbine	% collisions	% time above threshold	Hours per year above threshold
North Sea						
>100	0.956	20,067	16.3 ±1.7 [3.4 - 28.3]	71.3 ±2.4 [35.6 - 81.5]	10.3 ±0.8 [2.9 - 16.8]	231.4 ±17.5 [65.9 - 377.0]
	0.980	9,121	7.4 ±0.8 [1.6 - 12.9]			
	0.990	4,561	3.7 ±0.4 [0.8 - 6.4]			
>250	0.956	13,540	11.0 ±1.4 [1.1 - 21.0]	48.0 ±2.9 [11.9 - 62.3]	3.8 ±0.4 [0.5 - 7.3]	84.4 ±8.4 [10.8 - 163.4]
	0.980	6,155	5.0 ±0.6 [0.5 - 9.6]			
	0.990	3,077	2.5 ±0.3 [0.3 - 4.8]			
>500	0.956	8,113	6.6 ±1.1 [0.0 - 14.8]	28.8 ±3.0 [0.0 - 43.9]	1.3 ±0.2 [0.0 - 3.2]	30.3 ±4.3 [0.0 - 72.5]
	0.980	3,688	3.0 ±0.5 [0.0 - 6.7]			
	0.990	1,844	1.5 ±0.2 [0.0 - 3.4]			
>750	0.956	5,491	4.5 ±0.8 [0.0 - 11.1]	19.6 ±2.6 [0.0 - 32.9]	0.7 ±0.1 [0.0 - 1.8]	15.0 ±2.6 [0.0 - 40.9]
	0.980	2,496	2.0 ±0.4 [0.0 - 5.0]			
	0.990	1,248	1.0 ±0.2 [0.0 - 2.5]			
Baltic Sea						
>100	0.956	5,070	25.5 ±6.8 [10.4 - 38.8]	74.3 ±3.6 [63.3 - 76.4]	17.2 ±3.3 [9.1 - 21.3]	386.7 ±74.3 [204.8 - 477.7]
	0.980	2,305	11.6 ±3.1 [4.7 - 17.6]			
	0.990	1,152	5.8 ±1.5 [2.4 - 8.8]			
>250	0.956	3,030	15.3 ±4.3 [5.7 - 23.6]	44.5 ±3.2 [34.7 - 46.4]	5.8 ±1.4 [2.5 - 7.5]	130.5 ±30.4 [56.0 - 167.8]
	0.980	1,377	6.9 ±1.9 [2.6 - 10.7]			

MTR threshold	Avoidance rate	Total number of collisions	Collisions per turbine	% collisions	% time above threshold	Hours per year above threshold
	0.990	689	3.5 ±1.0 [1.3 - 5.4]			
>500	0.956	1,344	6.8 ±1.8 [2.7 - 10.3]	19.7 ±1.1 [16.4 - 20.3]	1.5 ±0.4 [0.6 - 2.0]	34.5 ±8.9 [12.7 - 45.4]
	0.980	611	3.1 ±1.9 [1.2 - 4.7]			
	0.990	305	1.5 ±0.4 [0.6 - 2.4]			
>750	0.956	709	3.5 ±0.7 [2.0 - 5.0]	10.3 ±0.7 [9.6 - 12.3]	0.6 ±0.1 [0.3 - 0.7]	13.1 ±2.7 [6.5 - 16.5]
	0.980	322	1.6 ±0.2 [0.9 - 2.3]			
	0.990	161	0.8 ±0.2 [0.5 - 1.1]			